POLITECNICO DI TORINO

Dipartimento di Ingegneria Meccanica e Aerospaziale (DIMEAS)

Corso di Laurea di 2° Livello

in Ingegneria MECCANICA

(Percorso FABBRICAZIONE ADDITIVA)

Tesi di Laurea Magistrale

Design and mechanical characterisation of lattice structures for additive manufacturing

Relatori

Prof. Luca Iuliano

Ing. Manuela Galati

Ing. Flaviana Calignano

Candidato

Stefano Bramante

Aprile 2022

Acknowledgments

I would like to thank my parents for their wise advice and loving support. You have always been close to me, helping me in times of need and encouraging me to always give my best. The main merit of my commitment in the university career is due to your teachings. In addition, I would like to thank my tutors, Dr. Galati Manuela and Eng. D. Calignano Flaviana for their valuable guidance throughout my thesis completion studies. Also, a special thanks to my friend and colleague Bruson Danilo who contributed to the setting of the simulation model, defined at the end of this thesis work.

Contents

List of Figures

List of Tables

List of Equations

1. Abstract

Along two decades, wide research has been carried out within the characterisation of the mechanical properties of cellular or lattice structures made by additive manufacturing. Being one of the most complex geometries, lattice structures have been extensively studied in compression condition. However, tensile characterization is rarely addressed because of the difficulties related to the definition of a suitable design. The present study aims to expand the knowledge about these structures produced with metallic powders, evaluating their tensile behaviour. Two different customised lattices structures are designed. The specimen is designed according to the BS EN ISO 6892 – 1 standard and using a graded geometry from full solid bulk to the lattice within the strain gauge length. Specific samples are designed and produced using both electron beam (EB-PBF) and laser powder bed fusion (L-PBF) technology and the different materials Ti6Al4V and AlSi10Mg, respectively. Moreover, the L-PBF structures are printed with two different building orientations and four different internal struts angulation, to evaluate the influence of defects such as porosity and dross formation. Finally, to perform a more complete characterization, four batches of specimens intended for compression have been produced with two different scanning technique of EB-PBF, using the same lattice designs adopted for tensile tests. The main mechanical properties are compared with the Ashby and Gibson's model. The experiments show that L-PBF-manufactured samples were subjected to a stress concentration near the transition area that cannot be removed, even when stress relief is performed. As a results, these specimens have almost no plastic deformation. Instead, EB-PBF-manufactured tensile samples meet the expectations, providing a localised failure within the gauge length and showing also interesting mechanical properties. The experimental data obtained are used to implement a simulation model created with Ansys Mechanical APDL.

1. Sommario

Nel corso di due decenni è stata condotta un'ampia ricerca nell'ambito della caratterizzazione delle proprietà meccaniche di strutture cellulari o reticolari realizzate mediante produzione additiva. Essendo alcune delle geometrie più complesse realizzabili, le strutture reticolari sono state ampiamente studiate in condizioni di compressione. Tuttavia, la caratterizzazione a trazione viene raramente affrontata a causa delle difficoltà legate alla definizione di una geometria idonea. Il presente studio si propone di ampliare le conoscenze su queste strutture prodotte con polveri metalliche, valutandone il comportamento a trazione. Sono state progettate due diverse strutture reticolari personalizzate. Il provino è progettato secondo lo standard BS EN ISO 6892 – 1 e utilizza una geometria graduata dalla parte solida completamente piena estremale alla zona lattice centrale del tratto utile del provino. Campioni specifici sono stati progettati e prodotti utilizzando sia la tecnologia del fascio di elettroni (EB-PBF) che quella della fusione laser a letto di polvere (L-PBF) e due diversi materiali, rispettivamente Ti6Al4V e AlSi10Mg. Inoltre, le strutture L-PBF sono stampate con due diversi orientamenti di stampa e quattro diverse angolazioni delle struts interne, per valutare l'influenza di difetti come porosità e formazione di scorie. Per effettuare una caratterizzazione più completa, sono stati prodotti quattro lotti di provini destinati alla compressione con due diverse tecniche di scansione di EB-PBF, utilizzando gli stessi disegni dei lattice adottati per le prove di trazione. Le principali proprietà meccaniche vengono infine confrontate con il modello Ashby e Gibson. Gli esperimenti mostrano che i campioni prodotti con L-PBF sono stati sottoposti a una concentrazione di stress vicino all'area di transizione che non può essere rimossa, anche se viene eseguita una operazione di distensione e rimozione degli stress residui. Di conseguenza, questi campioni non hanno quasi nessuna deformazione plastica. Invece, i campioni di trazione fabbricati con EB-PBF soddisfano le aspettative, fornendo un cedimento localizzato all'interno del tratto utile misurabile e mostrando anche interessanti proprietà meccaniche. I dati sperimentali ottenuti sono stati utilizzati per implementare un modello di simulazione realizzato con Ansys Mechanical APDL.

2. Literature Review

The following chapter of scientific literature review is the starting point of this thesis. The main previous research about lattice structure was studied, especially those regarding their importance in relation to their properties and possible applications. The analyses were addressed to highlight the mechanical characteristics of these structures and how they can vary according to the relative density, the type of cell and the dimensions. The goal is to assess the considerations common to all research material and therefore of general validity, as well as eventually highlight the problems encountered during their characterization. Furthermore, I tried to find a solution for defining a more accurate and rigorous method to evaluate the mechanical properties. It is important to specify that currently it does not exist any standard defined by the scientific community about the characterization of the mechanical behaviour of lattice structures, especially for the tensile one.

2.1 Cellular Solids

Cellular solids are reticular structures consisting of a set of struts or surfaces interconnected with each other, which form the sides or faces of an elementary cell [1]. In nature there are examples of these types of structure, such as the hexagonal cells of beehives.

Thanks to their interesting characteristics, they have been studied for decades in engineering and other branches of science. The main studied factors that can affect the mechanical properties are the following: cell size and geometry, type of connections present, relative density, material used, construction methodology, relative density [2].

Cellular solids structures can be classified according to the spatial arrangement of the cells into stochastic and non-stochastic [3]. Figure 1 shows a schematic classification.

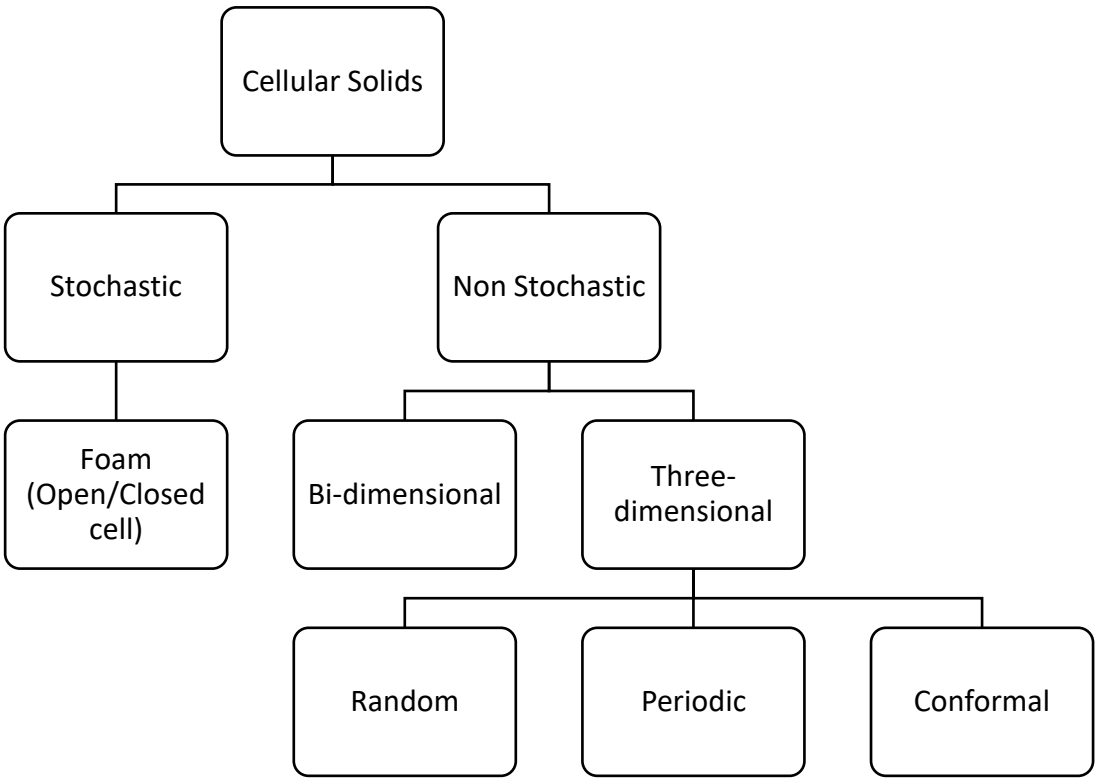

Figure 1: Cellular Solids classification

The first category includes foams, with random distribution of the cells, due to the production process: gas is inserted inside a molten material and during solidification the gas is trapped, arranging itself in an irregular manner within the volume. The cells can be open or closed. These materials often exhibit excellent thermal or acoustic insulation properties.

The second category can be divided into two-dimensional or three-dimensional structures. To the former belongs the hexagonal honeycomb structures. Instead, the latter are further classified into three types based on the arrangement of the cells: random, periodic, and conformal. The first type is represented by elementary cells with variable shapes and sizes, commonly associated with the name "Voronoi". The second typology is represented by cells arranged regularly in the volume, with a rigid pattern. In this case the external shape of the

structure does not define the internal volumetric arrangement and therefore the cells at the edges could be incomplete. The cells adopted can be made up of simple Platonic solids, of complex shapes defined through TPMS (Triply Periodic Minimal Surface) algorithms or of customized shapes according to specific conditions based on topological optimization algorithms. Figure 2 shows some possible types of elementary cells.

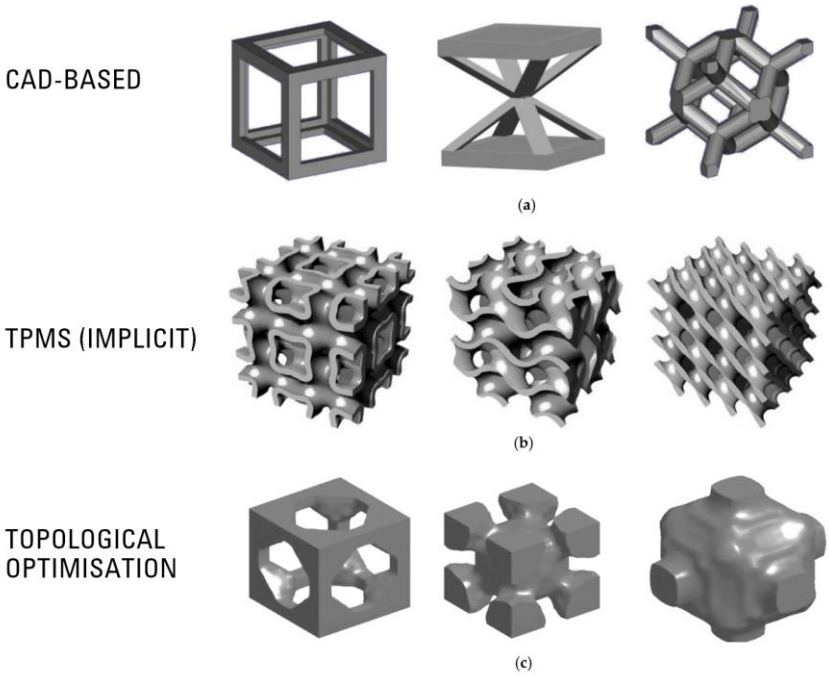

Figure 2: Different elementary cells [4]

Lastly, conformal typology is characterized by the deformation of the lattice inside the structure as a function of the external shape.

The periodic three-dimensional structures represent what are commonly referred to as the *3D Lattice Structures*.

Thanks to the many possibilities of diversification, three-dimensional cellular structures can have important properties: high surface / volume ratio (useful for high-performance heat exchangers), energy absorption capacity during shocks, osseointegration, acoustic insulation, lightness, uniform tension state.

2.1.1 Stress-strain model

The studies carried out showed a direct correlation between the properties of the lattice and its relative density ρ* [3], which is the ratio between the effective volume occupied by the lattice and the total volume of the solid that encloses it. By acting on the geometry of the lattice or on the production process, it is possible to modify the properties even at a point level.

The behaviour of the structures have been largely investigated under compressive loads, identifying two possible prevailing modes of behaviour, bending-dominated or stretch-dominated [3]. In the simplest cases it is possible to predict it, during a compression load application, by simply checking the degree of connectivity of the structure according to the Maxwell criterion[1].

In both modes it is possible to define three phases. If the prevailing behaviour is the stretch-dominated one, from the curve (see Fig. 3) a first elastic section is identified until yielding is reached, followed by a decrease in strength until the level of stress stabilizes for a wide range of deformation. In the final phase, the structure has completely collapsed on itself and can no longer compress. Therefore, there is a considerable increase in stress in the face of a low variation in strain. In this case, the lattice assumes properties more and more close to those of the bulk solid.

[1] Maxwell's stability criterion, formulated in 1864, defines a parameter M dependent on the connections of the cell nodes, such that when it varies with respect to the null value, it is possible to attribute a correlation with the degrees of freedom assumed by the structure itself. For $M < 0$ the cell is labile and has a prevalent bending behaviour when subjected to a load, for $M = 0$ it has a prevalent tensile behaviour, while for $M > 0$ the cell is over-constrained and presents internal stresses even if not subjected to any load.

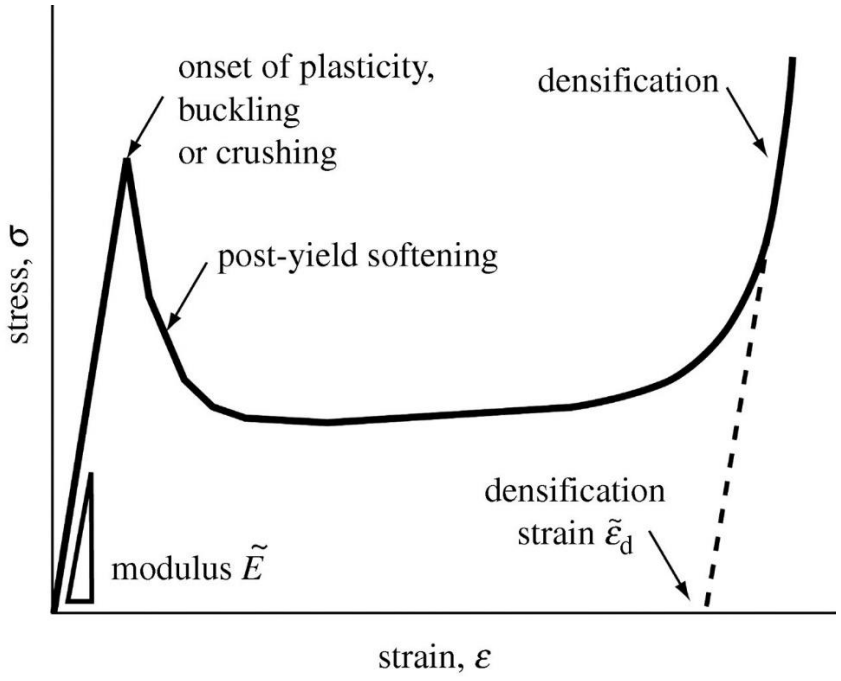

Figure 3: Lattice energy absorption under compression, stretch-dominated [3]

If the prevailing behaviour is bending-dominated (Fig. 4), the yielding occurs at a much lower value than in the previous case, then there is a long range at constant stress, called Plateau (this behaviour is often what engineers are looking for).

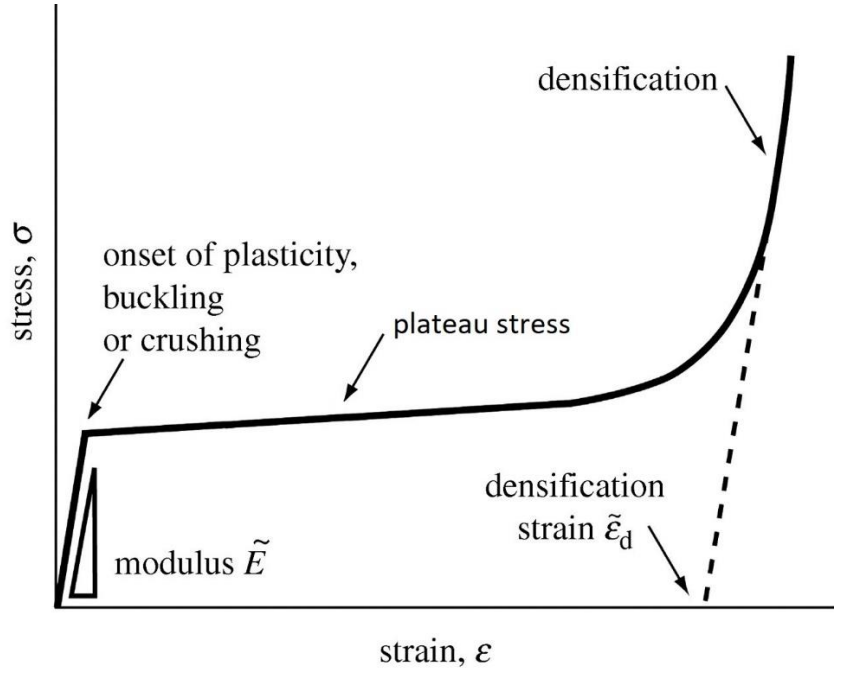

Figure 4: Lattice energy absorption under compression, bending-dominated [3]

The bending behaviour is typical of open cell or random structures, while the stretching behaviour is common for closed cell or periodic structures. The presence of the plateau phase is very useful if we consider the possibility of absorbing a large amount of energy at an almost constant load. The stress level at which the plateau settles depends on the relative density of the structure and on the rate of deformation. Therefore, the lower the relative density, the greater the plateau range at a lower stress value [1].

The model proposed by Gibson and Ashby was also compared with experimental data from tested lattice created through additive technologies such as Selective Laser Melting, emphasizing some discrepancies between the results predicted using the model and the actual properties. All of this, it is caused by several factors:

- The residual stresses induced by the powder melting process can produce deformations at lower stress levels than those obtained from the model [5]
- Precisely identifying the actual geometry of the struts is complicated, so it is not so easy to calculate stresses. Furthermore, some lattice can assume both linear and non-linear elastic behaviour under compression and this complicates the calculation of the elastic modulus [6]
- Some components often contain trapped or partially sintered powders that increase the overall volume but do not contribute to the increase in strength, distorting the property values obtained from the calculations [7]

Ultimately, the model remains approximately valid, at least regarding all the studies carried out in compression, as it still provides a good estimation (during initial design phase of a component) of the behaviour of the lattice, defining a direct positive power relationship between the structure properties and their corresponding relative density. However, regarding the properties that can be evaluated for tensile tests on reticular structures, it is not yet possible to correctly define the results or compare them with the Gibson-Ashby model, as most of the research carried out are based on compression-only experiments to identify mechanical properties. This is largely due to the fact that defining an experimental design of the specimens suitable for tensile testing is very difficult [8].

2.1.2 Manufacturability and limits

By means of additive manufacturing (AM) technologies, the production of lattice structures has certainly obtained an additional development with respect to the other traditional techniques. Although, it is important to specify that there exist limitations.

To fully understand the next paragraph, it is necessary to define the two manufacturing processes involved in this thesis. Both technologies work melting particles of a powder bed, the main differences are the heat sources used. In L-PBF[2] a laser is used, while in EB-PBF[3] an electron beam is used. The powders are melted layer by layer, proceeding along the vertical direction: after a powder layer is completed, a new one is spread above, and it is rolled on to continue the process. The L-PBF process takes place inside a closed chamber, usually filled with an inert gas such as N_2 or Ar. In addition, the build chamber is pressurized. To minimize the cooling rate, if desired, it is possible to use a substrate plate heating (200-500°C). Otherwise, in EB-PBF the powder bed is kept at high temperatures (>870K) and long cooling times are required after the completion of the build job. With this last process, higher surface roughness is obtained [9].

This type of structure requires the presence of supports based on the orientation of the component in the machine, that are useful for promoting heat dissipation during the construction process, as well as playing a purely structural role. Furthermore, supports are necessary to avoid the collapse of overhanging surfaces [10]. Supports presence can only be avoided for fully self-supporting models, which are designed to be built with only a few specific orientations. During the design phase, it is necessary to consider the difficulties induced by the removal of the supports, such as excessive deformation of the component. In addition, the pieces must be separated from the printing plate, generally by means of wire EDM, since

[2] L-PBF: Laser Powder Bed Fusion
[3] EB-PBF: Electron Beam Powder Bed Fusion

the use of mechanical processes could induce a break during the cutting phase, especially in the case of fragile structures such as lattice ones.

The characteristics of the process dictate the need to remove un-melted powders from the print volume. Removal can be completely manual with the aid of simple brushes or more commonly combined with the use of vacuum cleaners. In addition, a subsequent surface treatment may be necessary for surfaces that have a functional role [11]. Lattice structures generally tend to trap a large amount of powder, therefore it will be mandatory to use shot blasting machines, by means of which particles and air are shot at high pressure to release the powders from the component. During this phase, care must be taken to avoid damage to the finer struts.

Depending on the production technology adopted, it will be advisable to perform a stress relieving treatment of the components to reduce residual stresses, as these could cause distortion or even fracture of the very thin struts.

All manufacturing and process limitations must be considered when designing the components. One problem to consider is the difference in actual volume between the CAD model and a printed lattice structure, especially where there are elements with very small thickness. The studies carried out by Suard [12] show a correlation between the effective diameter of the thin elements and their orientation, the distribution of porosity and the process parameters. According to these studies, it is possible to create a model for the evaluation of the component properties more detailed, by defining an equivalent diameter (shown in Fig. 5) that considers the elasticity and variability of the dimensions.

During the design phase, you should be aware about the inherent limitations of the process adopted: that is because not all types of lattices can be built with any additive technique. It is necessary to consider the minimum angles between the various elements of the cells, as well as their distance to avoid the melting of an excess of unwanted powder. In relation to what kind of machine is used, it is possible to obtain a different level of detail and create thin struts. It is important to consider this, for the definition of the shape and the size of the elementary cells.

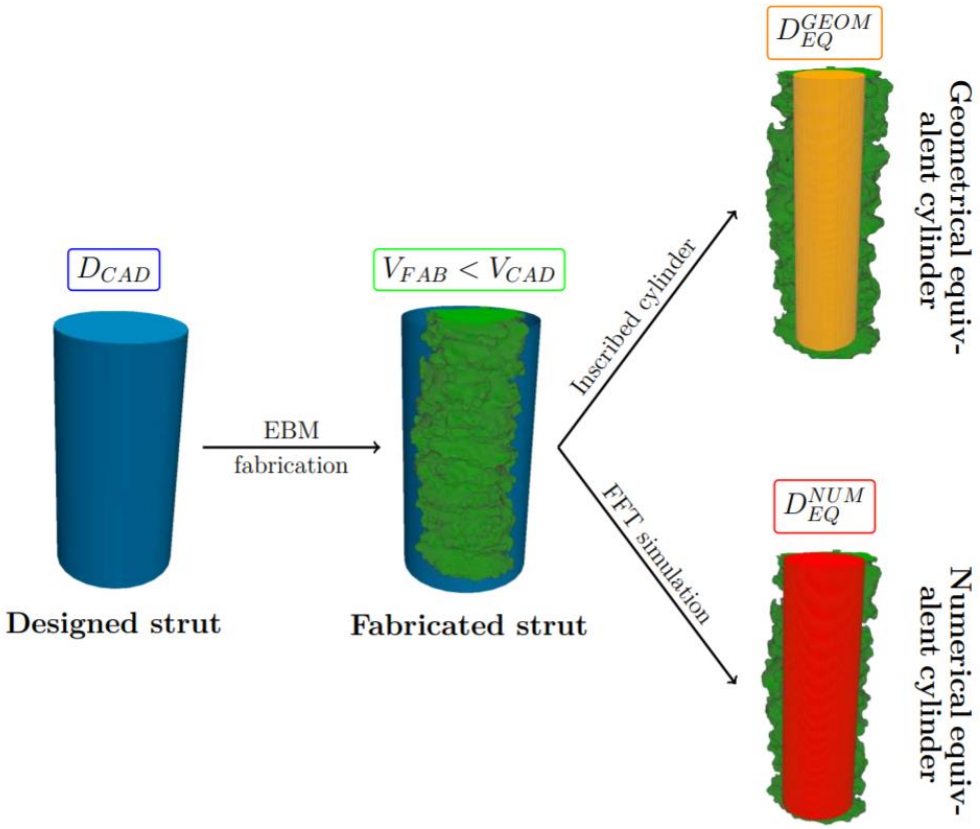

Figure 5: Equivalent diameter evaluation [12]

2.2 Compression studies

As above mentioned, compression tests are the most used to characterize lattice structures [13], since in most of the applications, such as biomedical [8], they are subjected to this type of load. In that case, the compression behaviour emulates the load on the prosthesis due to the weight of the human body [14]. Additionally, the loads induced by the human body are cyclic and therefore attention has been dedicated also to the fatigue life of the designed structures [15].

For the compression tests, ISO 13314 is the reference standard. However, this standard is applicable only to ductile trabecular materials (porosity greater than 50%) characterized by a behaviour with the presence of the plateau region. The cross section of the specimen used can be circular or even rectangular [16]. Each specimen size must be at least 10 times larger

than the pore size and not less than 10 mm; the ratio between the length of the specimen and the characteristic dimension of the cross section must range between 1 and 2. The pore size must be monitored and measured in the cross section.

In the literature research studies many different lattice structures have been analysed such as: octet-truss [12], body-centered cubic[17], truncated octahedron [17], hexagon [17], FCC [22], FCCz [23], hollow spherical [17], gyroid [29], primitive [35], diamond [20], etc. In Figure 6 is reported an example of different cell types analysed in the same research: these samples have the same external measures and they have been printing along the same direction, which certainly limits the comprehension of how different cell geometries can affect mechanical properties in an orthotropic view. In literature, both L-PBF [17][18] and EB-PBF [12][19] technologies have been investigated. That also involved the use of different material such as titanium alloys [19][20][21][30][34], aluminium [17][22][23], steel [18][24][25][26][29] and chromium[27][33].

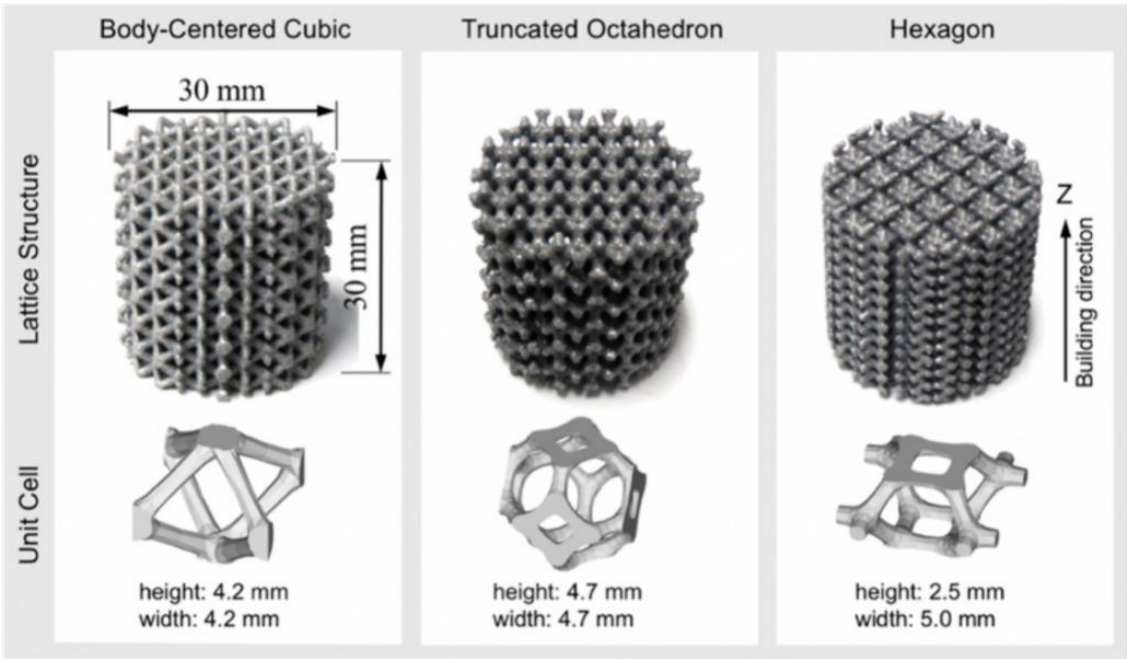

Figure 6: Different lattice specimens [17]

Studies were also focused on the process optimisation [28] and the effect of the dimensions of the elementary cell[26]. Table 1 resumes the mainly results reported in literature.

Table 1: Data collected for compression test of lattice samples

Ref.	Material	Cell	Process Design	Test Parameters	Output	Values
[20]	Ti-6Al-4V	Diamond	Sample orientations HIP (920 °C, 1000 bar, 2h)	30 kN load cell Constant displacement rate 0.9 mm/min	Quasi-elastic gradient (GPa) First maximum stress (MPa) Energy absorption (30% strain) (MJ/m^3)	3.2 - 5.4 GPa 91.2 - 133.9 MPa 5.4 - 27.4 MJ/m^3
[21]	Ti-6Al-4V	Regular Irregular Random	Heat treatment Randomization Void sizes Strut sizes	Displacemen rate 2 mm/min	E (GPa) Offset compressive strength (MPa)	1 - 16 GPa 70 - 420 MPa
[30]	Ti-6Al-4V	Piller Textile	Heat treatment (650 °C, 2h) Cells sizes	200 kN load cell Constant Speed 0.5 mm/min	Compressive peak stress (MPa) Compressive collapse stress (MPa)	130 - 310 MPa 18 - 80 MPa
[34]	Ti-6Al-4V	Gyroid Primitive	Graded	100 kN load cell Strain rate 2 mm/min	E (MPa) Yield strength (MPa) Peak strength (MPa) Energy absorption (MJ/m^3)	1188 - 1699 MPa 29.8 - 62.1 MPa 33.1 - 77.1 MPa 31 - 54 MJ/m^3
[17]	AlSi10Mg	BCC	Graded Heat Treatment (520°C, 1h; quench; 160°C, 6h)	50 kN load cell Displacement rate 0.03 mm/s	E (GPa) Energy absorption (MJ/m^3)	0.64 GPa 5.7 - 6.3 MJ/m^3
[22]	Al-Si10-Mg	FCC	Struts sizes	5 kN load cell Speed 0.001 mm/s	E (GPa) Yield Strength (MPa) Ultimate compressive strength (MPa)	0.5 -1.77 GPa 3.2 - 7.5 MPa 5.3 - 13.3 MPa
[23]	Al-Si12-Mg	BCC FCC BCCz FCCz FBCCz		Strain rate 10^-3 s^-1	E (MPa) Strength (MPa) Volumetric energy absorption up to compressive strength (MJ/m^3)	130 - 950 MPa 4 - 20 MPa 0.03 - 0.14 MJ/m^3
[24]	316L	FCC Bertex cube Edge-centered cube	Porosities Topological optimization	100 kN load cell Constant speed 1 mm/min	E (MPa)	240 - 3000 MPa
[25]	316L	Hexagon - honeycomb	Cell sizes	Interrupted loading	Effective E (GPa)	1.6 - 8.6 GPa
[26]	316L	Tetrakaidekahedron Diamond BCC	Process parameters Strut sizes Volume Fractions	Deformation rate / speed of loading 6 mm/min	E (MPa) Yield strength (MPa)	20 - 1810 MPa 1.66 - 81 MPa
[18]	316L	FCCz Hollow spherical	Heat treatment (900° C , 1 h)	400 kN load cell Constant strain rate 10^-3 s^-1	E (GPa) Specific energy absorption after 40% strain (J/g)	6.8 - 11 GPa 12.1 - 26 J/g
[29]	316L	Gyroid	Cell orientations	20 kN load cell Constant speed 0.4 mm/min	E (MPa) Yield strangth (MPa)	250 - 300 MPa 14 - 15.5 MPa
[27]	CoCr (Praxair)	Circular Crossing-rod		Strain rate 10^-3 s^-1	E (GPa) Yield Strength (MPa) Ultimate compressive strength (MPa)	33 - 34 GPa 70 - 110 MPa 235 - 365 MPa
[33]	316L CoCr	Simple cubic Crossing-rod		100 kN load cell Strain rate 10^-3 s^-1	Equivalent strength (MPa) Stifness modulus (GPa)	25 - 175 MPa 8 - 55 GPa

- The geometry of the cell affects the characteristics of the component, for example the face-centered cubic cell with vertical struts (FCCZ) has a higher resistance and elastic modulus than the hollow spherical one. This makes the first type undoubtedly superior from the structural point of view [17]
- Face-centered or body-centered cubic cells with vertical struts are absolutely those with the highest resistance and modulus values [18]
- The definition of the cell geometry by means of topological optimization often allows to obtain higher resistances [23]
- For some type of cell, the orientation according to a specific direction generates better mechanical properties, this is the case of the use of the gyroid with orientations of 0 degrees° and 90 degrees° [24]
- The process parameters affect the mechanical characteristics (see Fig. 7) of the lattice, in fact a higher laser power generally corresponds to a higher resistance [25]

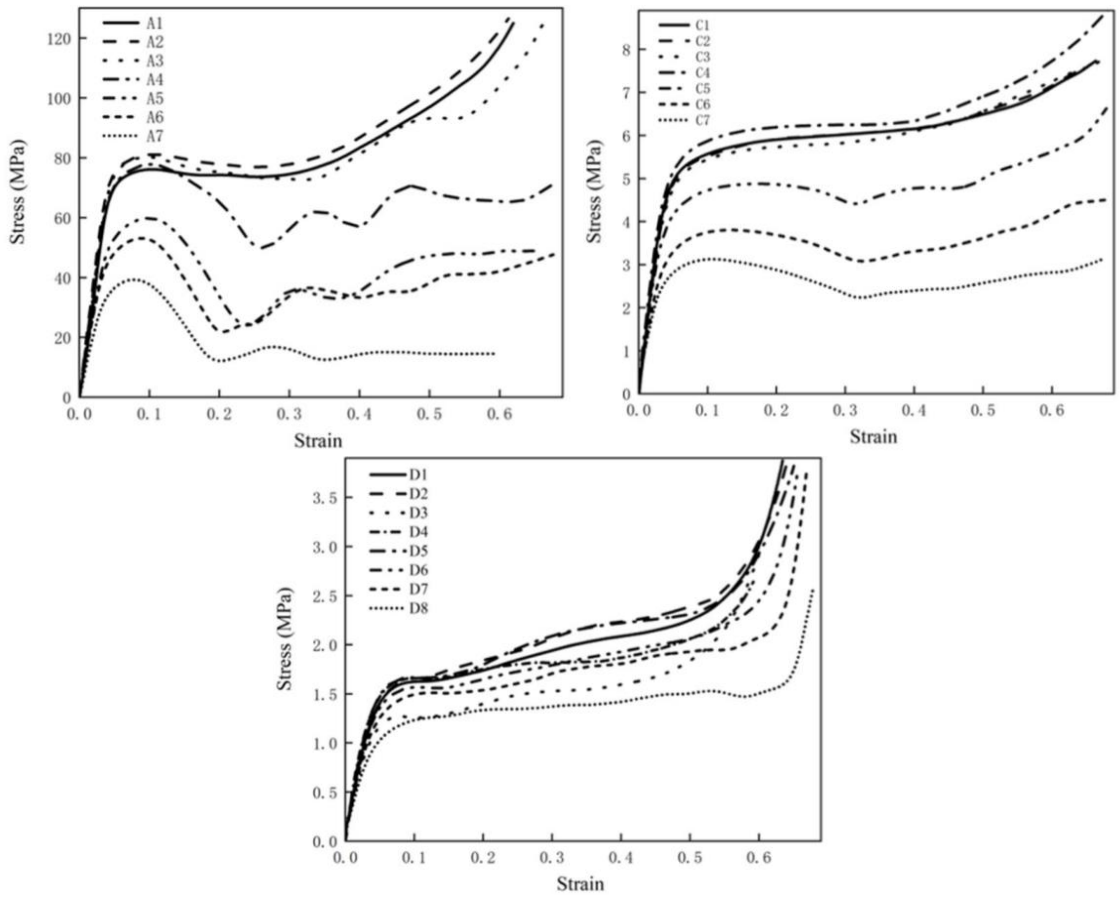

Figure 7: Stress-strain curves of different lattice specimens produced using different process parameters [25]

- An increase in relative density led to better mechanical performances [29]

- A larger cell size generates a decrease in compression load and effective modulus [30]
- L-PBF processes involve complications such as unwanted porosity, defect formation, dross formation and partially sintered powders, as well as residual stresses. Some heat treatments can partially reduce these problems, but generally the resistance of the component is reduced and the ductility increases[17], while in the case of chemical processes (chemical milling/etching) the mechanical properties are not affected [31]
- Graded lattice structures have a greater energy absorption capacity [32], furthermore plateau range is slightly reduced but its stress value is higher

In general, the used load cells ranged from 5 to 400 kN, indicating that the mechanical properties can vary significantly according to materials, geometries, relative density and printing orientations. The moving crossbar speed is kept generally low to obtain a low strain rate as described by the ISO 13314 standard. It is possible to highlight an increasing trend of the Young's modulus, the Ultimate Compressive Strength and the absorbed energy with the corresponding increase of the density. This behaviour is in line with the prediction of Gibson-Ashby model, but a modification of the exponent of the power law is necessary to correctly express the compressive behaviour of lattice structures [19].

As already stated above, in case of lattice subjected to compression, the emerging main feature is the absorption of energy, which makes this an excellent structure for impact application.

2.3 Tensile studies

International standards for tensile tests of cellular and porous structures are still missing. Some of the test parameters, such as the low crossbar speed, are easily set by taking the Iso 13314 standard as an example, but the main problems remain the specimen geometry and the deformation measurement. Since the transition between the cellular and the full-solid sections is not defined, the test results can be obtained with varying degrees of reliability. Due to the limited data, the static behaviour is generally studied taking into account only the two principal manufacturing orientations (i.e. parallel and orthogonal to the building platform)[33]. Lattice structures, having many cavities, make it difficult to use extensometers, whether they are contact or laser/video. The tensile properties, as well as the compressive ones, are strongly affected by the variation of the main factors that define the lattice geometry: cell size and type, printing orientation and post-processing. Each of these factors are discussed separately below.

2.3.1 Cell geometry

Many cell geometries have been studied and subjected to tensile tests, leading to several results:

- Koehnen et al. [18]performed on the same two geometries (FCCz and hollow spherical) both compression and tensile tests. The results are similar, since FCCz shows always higher performances. The tensile behaviour is investigated with the help of DIC analysis, revealing strain localization at the nodes perpendicular to the tensile direction (see Fig. 8). For the hollow spherical one, the strains are homogeneously distributed over multiple series of nodes with different distance from the centre. This leads to a global weakening of the specimen. On the contrary, for FCCz specimen, only the centered row of nodes is extremely stressed.

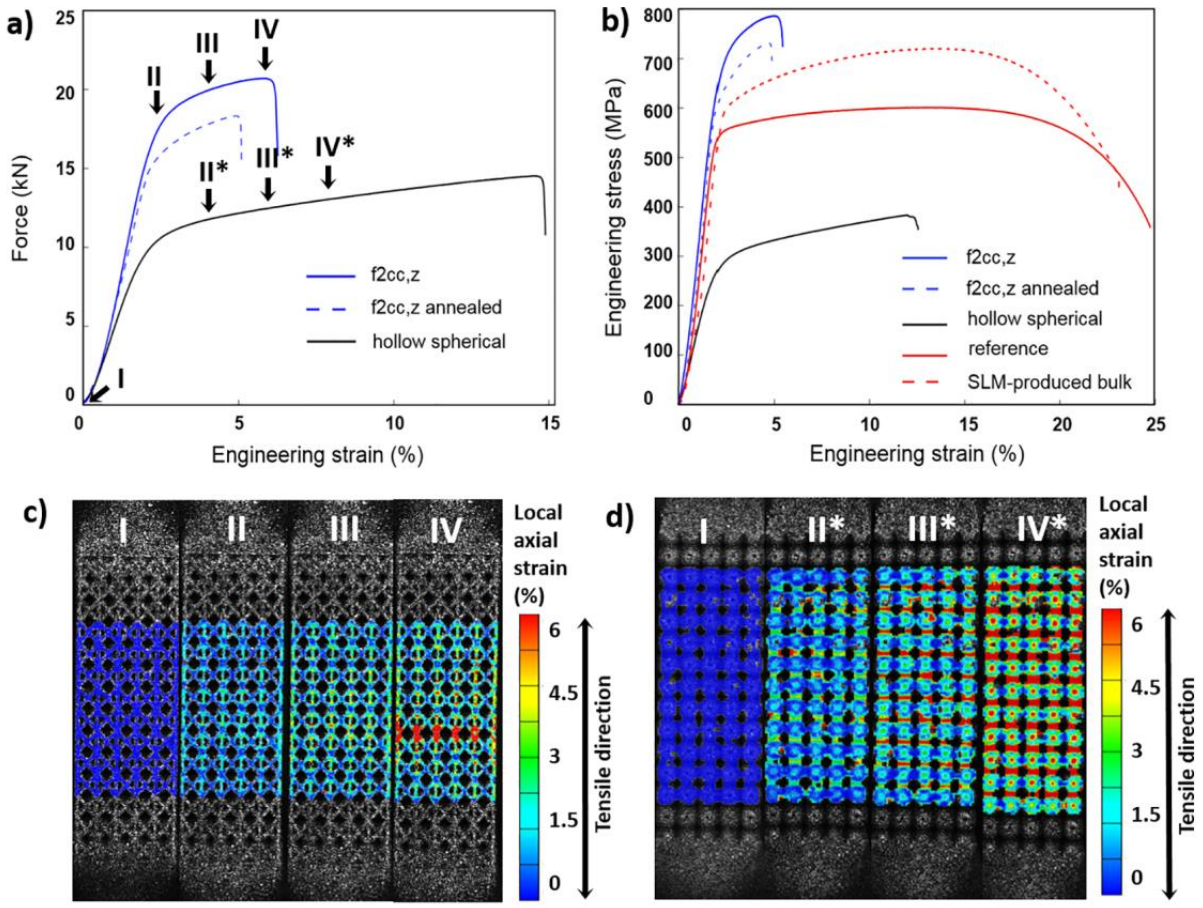

Figure 8: Tensile test curves and DIC analysis [17]

- Lutey et al. [34] compared the BCC, the simple cubic and the crossing rod geometries. They observed that under tensile load the latter showed the highest strength and stiffness
- Kessler et al. [35] also reported a comparison between truss structure, octahedral and BCC geometries, leading to higher tensile strength for the first
- Hajinys et al. [36] compared four different structures (simple cubic, BCC, tetragon vertex and tetragon edge), each one with three different strut diameter (0.5, 0.7 and 1 mm) and evaluate the stiffness of them. The tetragon edge geometry shows the highest ultimate tensile strength, at least two times superior then the others. With the increasing of the struts diameter, the necessary force needed to break the specimen increase too for every geometry

Following the above, surely it is possible to assert that several lattice geometries influence in different manner the mechanical properties of specimens that own the same external shape.

Generally, the geometry which performs better under compression load is the same as the one that has higher resistance for tensile tests.

2.3.2 Cell's parameters

Many authors evaluated the mechanical properties varying a combination of parameters such as the cell and the strut dimensions:

- Maskery et al. [37] examined the elastic modulus and UTS of lattice parts with different size of BCC cell but fixed density. Specimens with the smaller cell size shows the highest stiffness
- Alsalla H. [38] performed several tests on gyroid lattice specimens with three different cell size (2, 4 and 6 mm). With the increase of cell dimension, it is shown a decrease of relative density (from 98.75% to 90%) in addition to the obvious decrease of global density. The struts with the smallest size present less porosity. Stress-strain curves show higher UTS for smaller size but at the same time a lower elongation (see Fig. 9)

In the previous research, the influence of different struts size, maintaining unaltered the cell type, was not evaluated. This is probably because decreasing strut size commonly leads to worse mechanical properties, according to relative density - based theory. There is no reason to explore further.

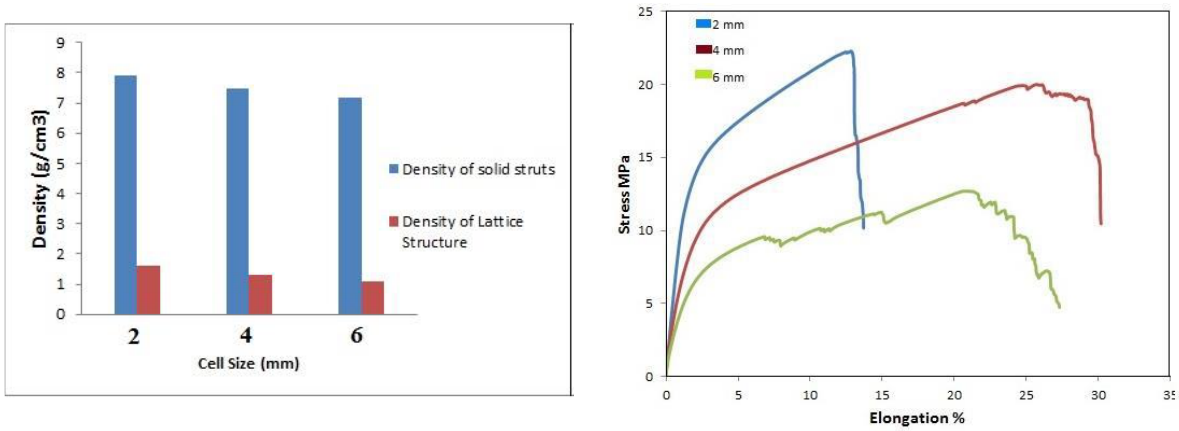

Figure 9: Density and stress values for different gyroid cell size [38]

2.3.3 Post processing

A few works studied how post-processing could modify tensile mechanical properties of specimens:

- Brenne et al. [39] highlighted that heat-treated samples presents higher tensile strength and can hold higher stresses even at early stages of deformation. With respect to the as-built condition, the annealing process improved a little the ductility of the sample as it is possible to see in Fig.10, regarding the absence of a steep decrease after highest force point

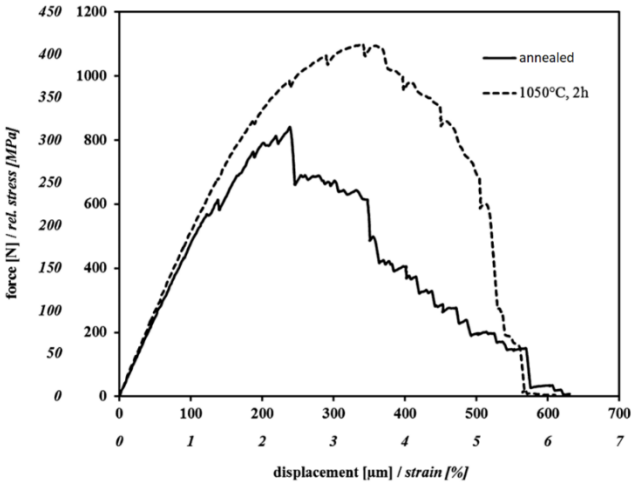

Figure 10: Deformation behaviour under tension of TI-6Al-4V lattice specimens before and after heat treatment [39]

Furthermore, the heat-treated condition (1050°C for 2 hours) enables the struts to improve their load carrying capacity by align them along the tensile direction. These results are common during test compression and four-point-bending test. The energy absorption, especially under the latter test, is improved. In case of cyclic loading, the fatigue life remarkably increases, and the site of failure can be predicted with the aid of DIC analysis (see Fig. 11).

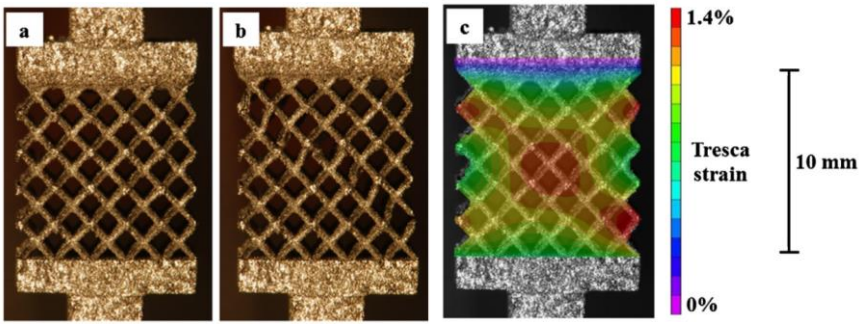

Figure 11: DIC analysis on tensile test [39]

- Kelly et al. [40] observed that surface treatments like rotopolishing and SILC cleaning could increase the Young's modulus and normalized the fatigue strength. Test were performed on Ti-6Al-4V samples with SLM, providing flexibility for medical bone implants application. The UTS directly increases with lower roughness, like is shown in Fig. 12

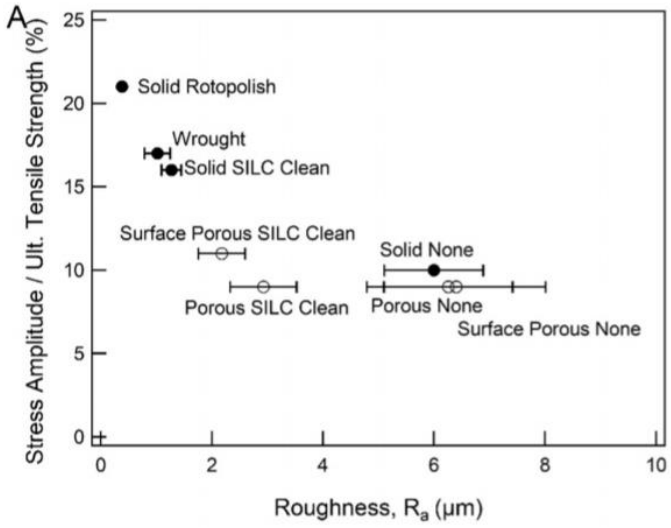

Figure 12: Fatigue strength normalized by UTS, compared to surface roughness [40]

2.3.4 Building orientation

Building orientation has been examined in many studies, nevertheless without any kind of consideration regarding every single possible arrangement in the printing volume. This is due to the fabrication process limits. It is not possible to print a specimen in every spatial orientation not even for a full-solid. This condition is even worse for lattice specimen.

Established this, several authors carried out tensile test for two ordinary orientations: horizontal (z-axis) and vertical (xy-plane).

- Alsalla et al. [41] examined scrupulously the influence of different orientations on density, Young's modulus and tensile strength. Several gyroid specimens were produced with fixed process parameters. The results point out that the vertical print direction leads to 1.5 times higher stress values, as shown in Fig. 13

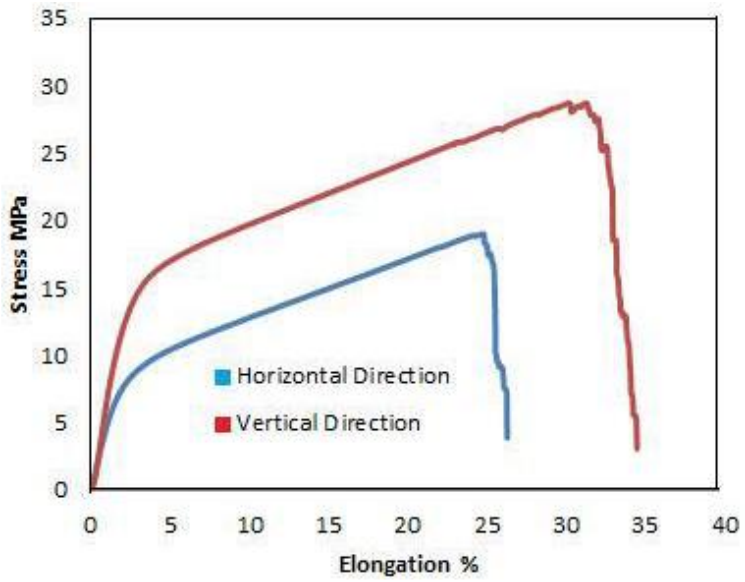

Figure 13: Stress-strain curves for different printing orientation [41]

- Barbas et al. [42] investigated on porous specimen (53% with pore size from 860 to 1500 µm) of Titanium alloy made by SLM. Under tensile tests, vertical printed samples presented higher stiffness and resistance

From literature, the vertical orientation samples seem to have best performances with respect to the horizontal one, but there is a lack of knowledge concerning all the other orientations. An interesting orientation to examine might be 45° because it shows higher resistance then vertical one for full-solid specimen [43].

2.3.5 Specimen geometry

Most researchers produced cylindrical specimens or parallelepipeds. No one ever tried to respect the external shape of other standards that can be reasonable similar, for example those relating to metals at room temperature.

Overall, research has followed a similar experimental method consisting of:

- The central section of the specimen has almost in any studies an overall area that is greater or equal to that of the extremities. In Fig. 14 it is possible to see some tested samples by Köhnen et al. [17] and Barbas et al. [42]. The main reason for this choice is the easiest way to use grips and extensometers of the respective tensile machines of the researchers

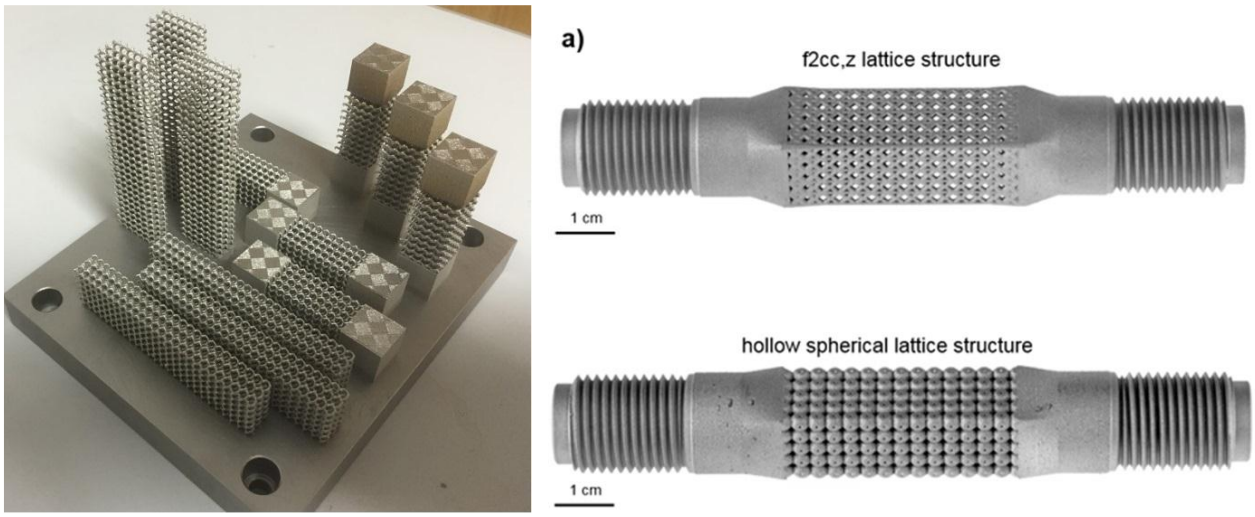

Figure 14: Tensile specimen geometry from literature [17] [42]

- In most of the research[37][38][40][41][42], the inner lattice area has a very limited length compared to that of the entire specimen. In two studies [44][45] this length is less than one forth of the overall specimen length.
- Maskery et al. [45] is the only one study that considered a Standard that could be used to make the tensile test results comparable to other with full-solid specimen. Following

the ISO 68921:2009, they designed two different BCC sample with 5 mm and 7 mm gauge width (see Fig. 15)

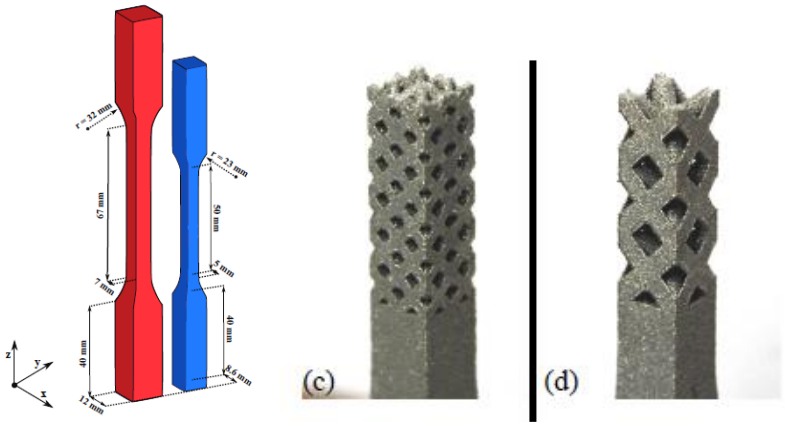

Figure 15: Different cell size for ISO 68921 [46]

For each width type, they produced different specimen with different cell size. The printing process parameters were optimized to avoid anisotropy factors that cannot be predicted. Besides this, the stress relieving was applied. Stress – strain curves are shown in Figure 16. The porosity does not present a significant variation for the two cell types.

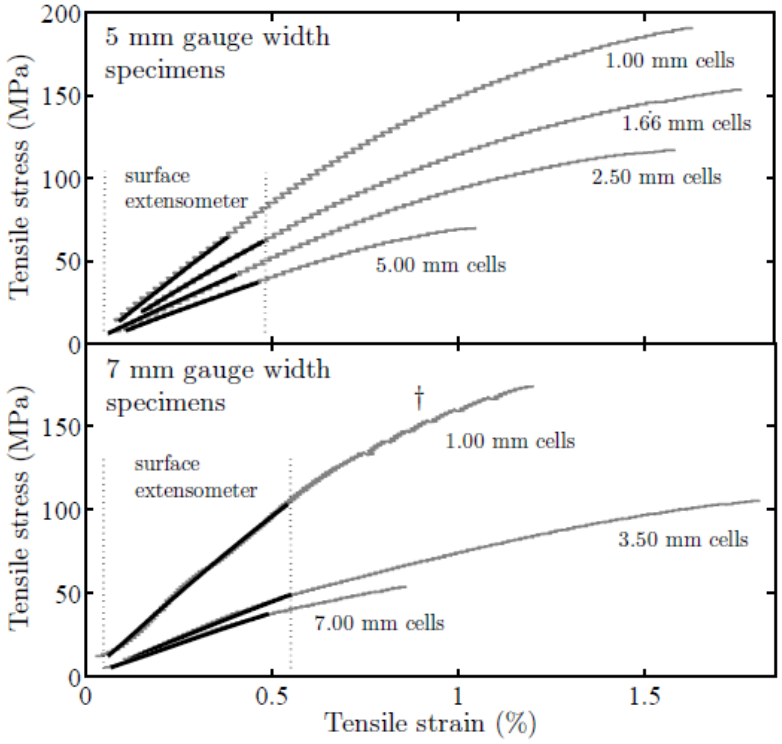

Figure 16: Stress-strain curves for BCC specimen [46]

Using this ISO standard leads to a fracture localization around the middle section of the useful area of the specimen, but this result depended only on the small width of this area. Substantially the results are driven and do not have much reliability: the thin struts geometry induces a great load distribution over a small cross-sectional area. The main failure mode is the initial fracture of an individual strut followed by the others in the same plane. The specimen section should be greater with a larger number of struts to be considered valid in relation to a wider case series. Furthermore, also in this study, the gauge length is very reduced (less than 1/3 of the overall length).

- In two studies [47][48] the lattice cell is so small that the effect of the relative density is confused with that of the porosity; for a better understanding a cross-section SEM image is reported in Fig. 17. In these cases, the specimens are externally covered with a solid layer of a few millimetres and the cell geometry is inaccurate. The mechanical properties follow the trend of the density variation in the same way they would do with a full-solid specimen with a ductile behaviour.
-

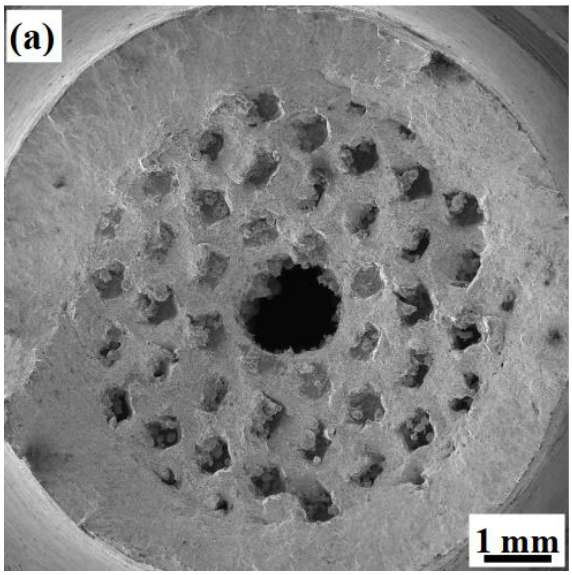

Figure 17: SEM image of a complete fracture morphology, Honeycomb lattice specimen [48]

- At the best of the author's knowledge, only Soul et al. research [49] focused on the fatigue behaviour of specimens with a diamond cell lattice of 45% relative density. Furthermore, this study reported the information obtained from different lattice

orientation depending on the cells spatial distribution and not on the printing direction. According to the orientation, different fracture modes are obtained

Thanks to several results it is possible to assert that the external shape plays a significant role in the definition of the mechanical properties. To be sure that the tensile tests are carried out correctly, it is important that the extremities areas of the specimen are firmly hooked to the machine grips. The geometry must allow for minimal misalignment during the tests, avoiding a misinterpretation of the results. These are not the only recommendations, as it will be discussed in the next paragraph.

2.3.6 Failure area

Almost each tensile test performed on various specimens by different researchers localized the failure of the samples near the transition area from full-solid to lattice structure at the extremes. In this region there is a drastic change of density and a significant concentration of stresses. Thus, thanks to the increase of the intensification factor that regards the actual cross-section, the failure occurs even if the specimen has not yet showed the elongation predicted from its ductility. This latter can be evaluated with a good approximation, by starting from its bulk material mechanical properties.

- Several authors [35][36][37][38][39][40][42] obtained failure at the extremes; this is a problem because it depends on the drastic change of relative density at the transition from the extremes to the inner lattice area where the section in no longer completely filled. In this way there is no possibilities to evaluate the actual properties of the lattice structure. This behaviour is not easily predictable using a simulation software because it is very difficult to validate the material model without any experimental data. The advisable procedure is to firstly detect the properties of a geometry close to the one desired, obtained from subsequent optimizations. Then, thanks to this knowledge, it will be easier to avoid the problem. Most of the specimen failure are similar to what is shown in Figure 18

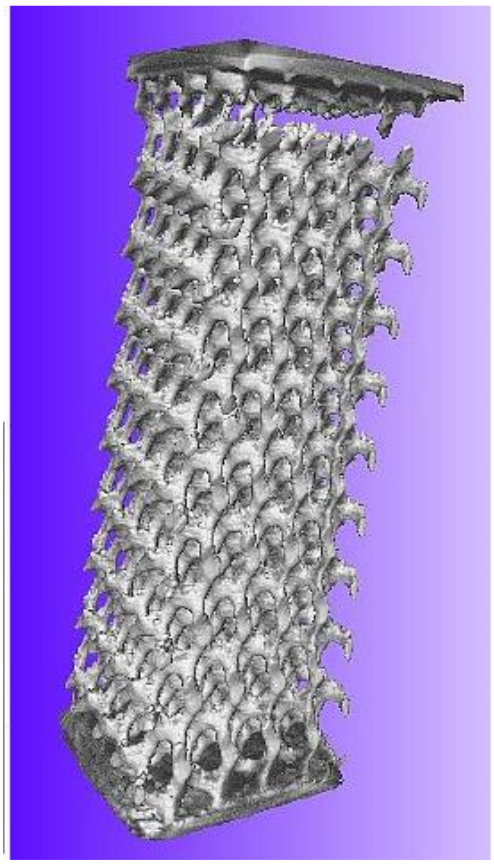

Figure 18: Gyroid specimen failure at the extremes [41]

- Drücker et al. [50] proposed an optimization in the load introduction geometry, defining a custom lattice structure with Python script that automatically generates the model. This geometry has the characteristic to gradually introduce load over the specimen. Relative density change from the extremes to the centre because of a variation of the struts diameter. A parametric model was defined inside Abaqus to be analysed with nonlinear FEM simulation. The material model was calibrated thanks to the properties evaluated from the experiments made on printed samples, tested for tensile, compression and single-edge-notch bending (SENB). A representation of the designed geometry is shown in Figure 19. The measurements for tensile test were performed with DIC, applying a white aerosol paint over the specimen, and recording the test with the cameras of GOM Aramis 4M system.

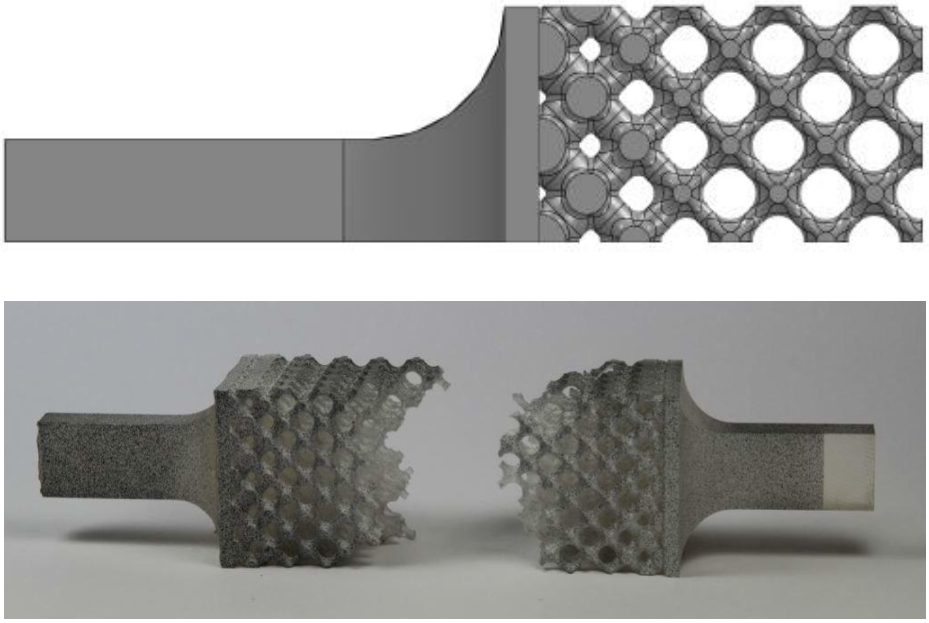

Figure 19: Geometry and failure of specimen with gradual increase of struts diameter [50]

This last research is particularly considered for this thesis work as it is the only one that tried to overcome the density transition problem, taking all the advantages of programming codes and a simulation software.

2.4 Literature review conclusion

The major findings of this literature review can be summarised as follows:

- There is no correct standard that can be used to achieve consistent results with respect to lattice feasible applications, but it is possible to create an ad-hoc geometry that fits a non-lattice standard, for example ISOs referring to metals at room temperature
- The mechanical properties mainly depend on several factors:
    - cell size: a lower cell size involves a higher stiffness
    - cell geometry: Gyroid, FCC and BCC are the most resistant geometries
    - building orientation: vertical orientation leads to better performances and fewer defects, but for technologies like SLM the specimen geometry must be suitable for this printing direction
    - post-processing: almost every post-processing treatment tend to weaken the specimens
    - specimen geometry: it must be designed a geometry to avoid stress intensification far from specimen centre

    In each cases the properties vary in according to global and relative density. An increase of the ultimate tensile strength always involves a decrease of maximum elongation

- The only accurate method to measure the deformations of complex lattice seems to be Direct Image Correlation, even if the complete measuring systems are expensive. In almost all cases it is not possible to use extensometers due to lattice geometry. The only remaining solution is to consider the displacement of the test machine crossbar with respect to the initial distance between the grips
- To perform tensile tests, it is desirable to avoid failure across density transition areas. The best method to achieve this result seem to be to gradually vary diameter of the struts. The smoother it is, the better the sample resist to load exploiting the whole lattice structure capacity.

3. Materials and method

3.1 Specimen design

In this chapter the procedure followed to obtain the best geometry to be analysed and manufactured, considering all the possible limits will be discussed. To create a model that can be easily modified, the 3D CAD software Solidworks by Dassault Systèmes was used. Thanks to it, it is possible to export files in STL format, that is the one read by printing machines. During the design phase process and printing space optimization was also considered.

3.1.1 Standard reference

The first step was the definition about which could be the optimal standard, since the aim of this thesis is to give results as unequivocal as possible. Furthermore, considering the geometries used in the previous research, with a limited gauge length and thus an easier way to obtain the failure in the inner area, it is important the make an improvement that will led to more technical analyses. At the end the selected one was the ISO 6892-1:2019 (see Fig. 20). Thanks to this choice, the specimen length of about 150 mm can fit correctly into the printing volume, and it was possible to insert more than one row of specimens, both vertical and horizontal. In this way, the printing space is optimized, and the waste of materials and time is minimized. Furthermore, this standard allowed to create a geometry which was neither too small nor too big. Considering the dimensions that the cells of a lattice could have had, this standard was optimal to be able to choose different types of structures that could adapt to it and let the geometry easily editable during the design phase.

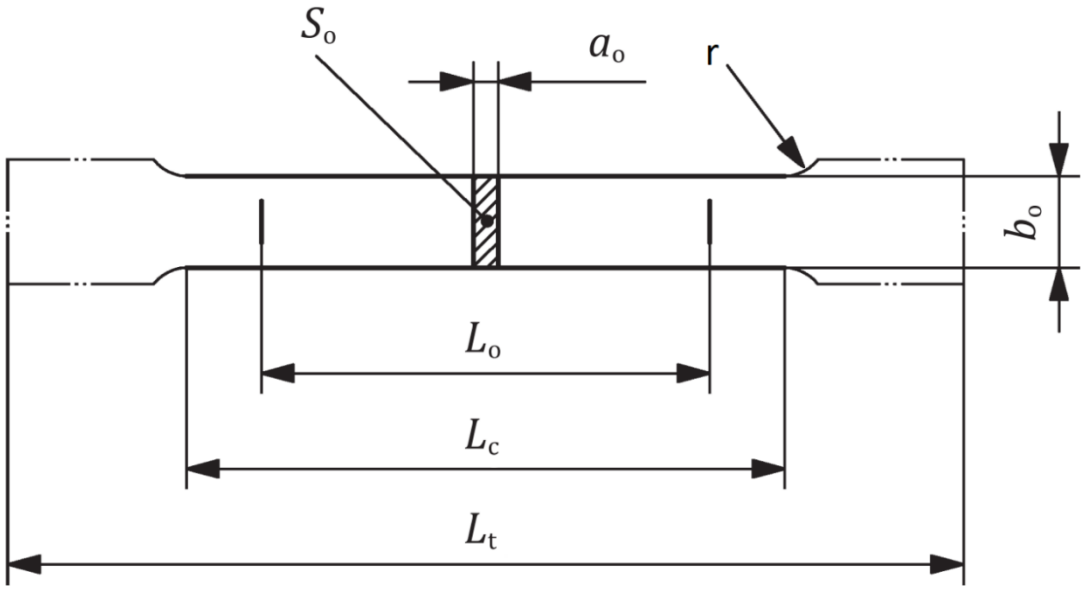

Figure 20: ISO 6892-1:2019 thin type specimen [51]

In Table 2 the measurements of the specimen are explained, the shown values are expressed in millimetres.

Table 2: Specimen dimensions

L_0	Preferred gauge length	50 ± 0.5
L_C	Length of narrow parallel-sided portions	75 ± 1
L_T	Overall length	150 ± 1.25
b_0	Width at narrow portion	12.5 ± 1
	Width at ends	18 ± 0.2
a_0	Preferred thickness	≤ 3
r	Radius	12.5 ± 0.5
	Initial distance between grips	87.5 ± 0.2

This specific standard is utilized for thin specimens, under 3 mm of thickness, but in this case, it would have been impossible to respect these limitations. To define a geometry, a multiple dimension of the preferred thickness was chosen for the lattice cell size, which is 6 mm. Other sizes were also initially considered, but at the end this one was the best to be working it, due to printing problem with thinner structures. Moreover, it allowed to design specimens with different internal struts angulation. All the motivations will be exposed in the next paragraphs.

3.1.2 Optimal design

The first assumption is that the specimen must contain a lattice structure at least inside the gauge length. Inside this area, it is desirable to obtain the failure because it is possible to record more accurate data if the extensometer is used.

For metal printing, especially for L-PBF, it is not so easy to reproduce any lattice geometry. During the design phase, it must be considered that in the production of parts with angles lower than 45°, the presence of supports is preferably required. The supports can counterbalance the recoater force and dissipate heat if necessary. With lower angles there is the risk of breaking some struts causing part failure or noticeably increasing the downskin surface roughness. This last phenomenon is known as dross formation. However, thanks to the optimization of some parameters, it is possible to avoid them, relying on the desired geometry. Viale et al. [52] studied the optimal set of parameters to obtain the best overhang surfaces quality for inclined specimens. A similar but simplified work has been done in this thesis, considering the inclined struts internal to the lattice structure.

Even with the use of optimal parameters, not every lattice type could be printed, for example some TPMS cells like Schwarz-P have shown a high probability to collapse during the print or immediately after when the specimens must be separated from the platform. Initially, the simplest lattice structures were considered, but the majority of them, based on cubic cell, presented horizontal struts, not printable without supports.

In this phase it is not important to choose the lattice type, because the first objective is to define the external geometry, but since it was still necessary to represent the lattice with the CAD instrument, some basic considerations have been conducted.

Referring to the scientific literature analysed in the previous chapter, the body-centered-cubic (BCC) unit cell seemed to be a proper choice. In literature, it shows often very high resistance [34][35][36][37] compared to the others, and it is easy to design. This choice is based on the following considerations:

- Lattice structures are generally weak, especially if there are a few rows of unit cells (it must be considered the middle of the tensile specimen)

- Avoiding supports is desirable, because their removal is always a complicated process and could cause parts breaking
- The best printing orientations are vertical and horizontal and producing an inclined specimen would lead to the increase of supports
- Since these specimens will be tested for tensile resistance, they must be as strong as possible

Once the lattice type was initially defined, the actual challenge was to create a geometry in which the failure can be localised in the gauge length, because of stresses intensification. In this first phase Solidworks Simulation Tool (Dynamic simulation) was used to obtain an initial approximation of the most stressed point localization. Various possible solutions have been evaluated and will be discussed below:

1. Firstly, it was thought to create a completely lattice structure:

   This specimen could present the advantage of having stresses uniformly distributed along the specimen through the struts, thanks to the absence of a full solid component. However, it presents three main problems:

   - Many lattice struts would be uncompleted near the fillet radius area, being in this way useless for the load transmission (see Fig. 21)

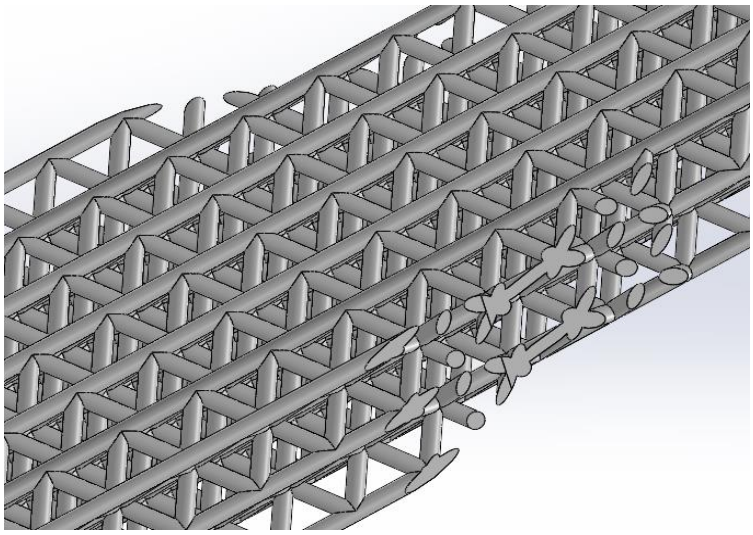

Figure 21: Fillet radius area

   - The external parts where the grips closes could collapse under the grips clamping force because they're weaker than a full solid part

- The absence of a flat surface at the extremes of the specimen could cause a sliding of the grips or a misalignment, invalidating the measured data

2. To solve the problems of the previous possible design, a solution was devised:
    - To avoid the presence of uncompleted struts, the fillet radius area could be replaced with a geometry that follows the unit cell. For example, struts at 45° for BCC cell
    - To avoid slippage or deformation at the extremes, support holes (one or two for each gripping side) could be introduced

    In Figure 22 it is presented an initial model for this design. Even in this case, there are some relevant problems:

    - This design absolutely don't agree whit the selected standard
    - The presence of the holes could increase the possibilities of an internal collapse out of the gauge length area, the one in which we desire to obtain the failure

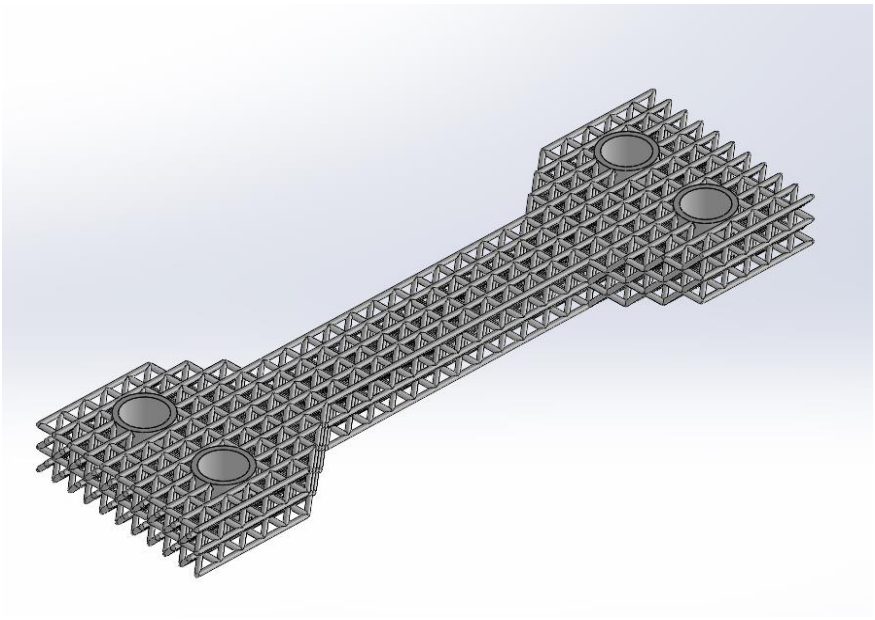

Figure 22: Initial possible design for tensile specimen

3. Another possibility was considered: create simple joining elements between the full solid area and the lattice in the centre of the specimen. A representation of this design is reported in Figure 23.a. Unfortunately, this design didn't allow to transmit uniformly the stresses near the fillet radius area, as it is possible to see in Figure 23.b, containing

the dynamic simulation carried out on the structure. The area immediately adjacent the joining element is extremely stressed and leads to failure.

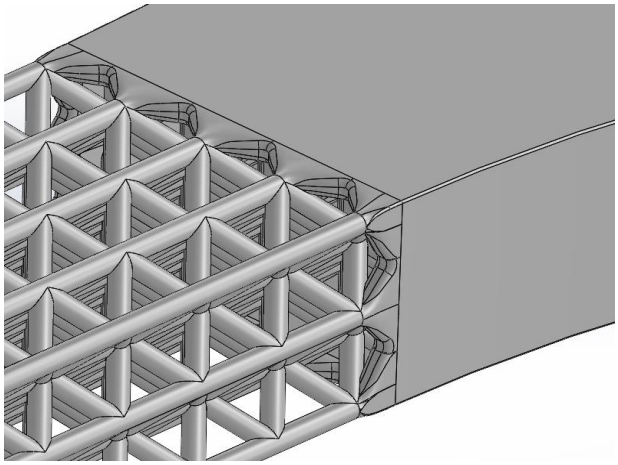

Figure 23.a: Specimen with joining elements

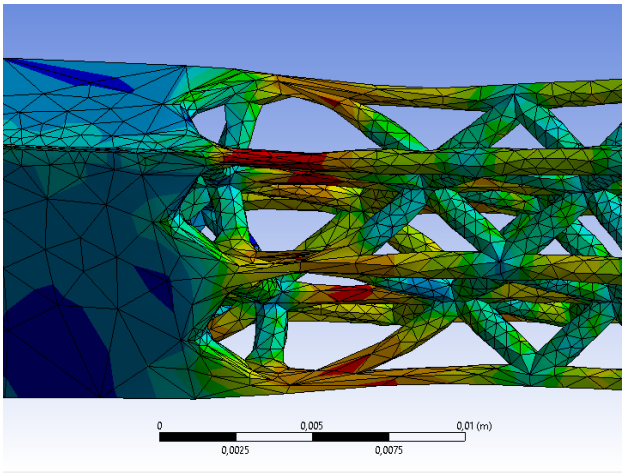

Figure 23.b: Dynamic simulation of the structure

4. Finally, considering the Drücker [35] work and the previous improvable models, an appropriate specimen design was created (see Fig. 24): the main idea is to generate a perfect density gradation from the extremes to the internal lattice, to reduce stresses near the transition area. A simple dynamic simulation returned positive results for this last design. The first adopted lattice was BCC, because of its previously discussed characteristics. As it is possible to see, the geometry differs from the selected ISO Standard, near the transition area. This modification was necessary to improve the resistance of the gradually increased struts diameter. Inside the gauge length there are no diameter variations.

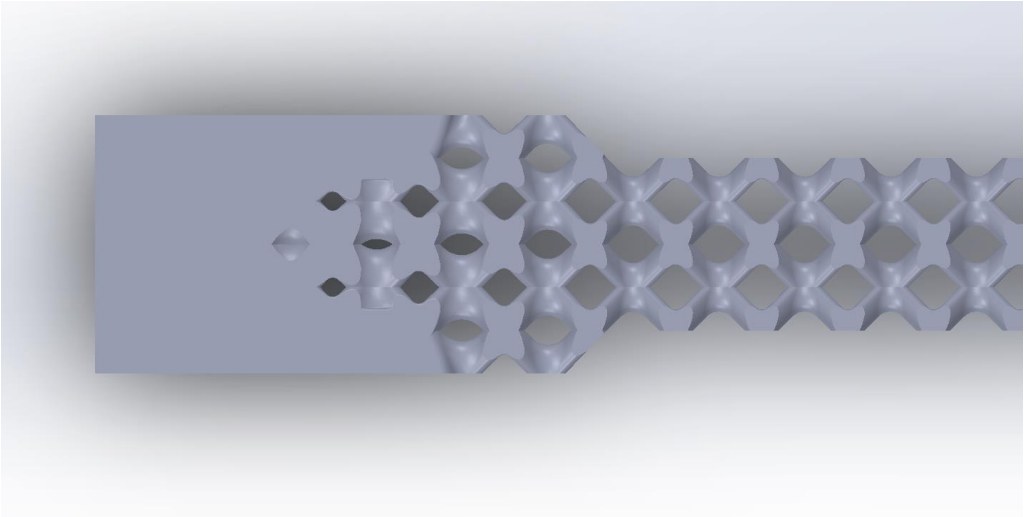

Figure 24: Graduated specimen design with BCC lattice

3.1.3 Cell Design

In this thesis work, the main objective is to fully characterize lattice structure, not only relatively to tensile behaviour, but also for compressive behaviour, to compare results with those present in literature. The Body-Cubic-Centered (BCC) unit cell was chosen as the starting point of the lattice structure design. The cell size is 6 mm with a truss width of 1.7 mm. The struts are arranged inside a cube, connecting the vertices along the four space diagonals intersecting each other in the centre of gravity, joined with a fillet radius of 0.4 mm along the Z direction. This modification is necessary to avoid supports. Therefore, the cell is symmetric only with respect to Z and Y planes. Each strut is inclined at 45°. In Fig. 25 the BCC cell unit is shown.

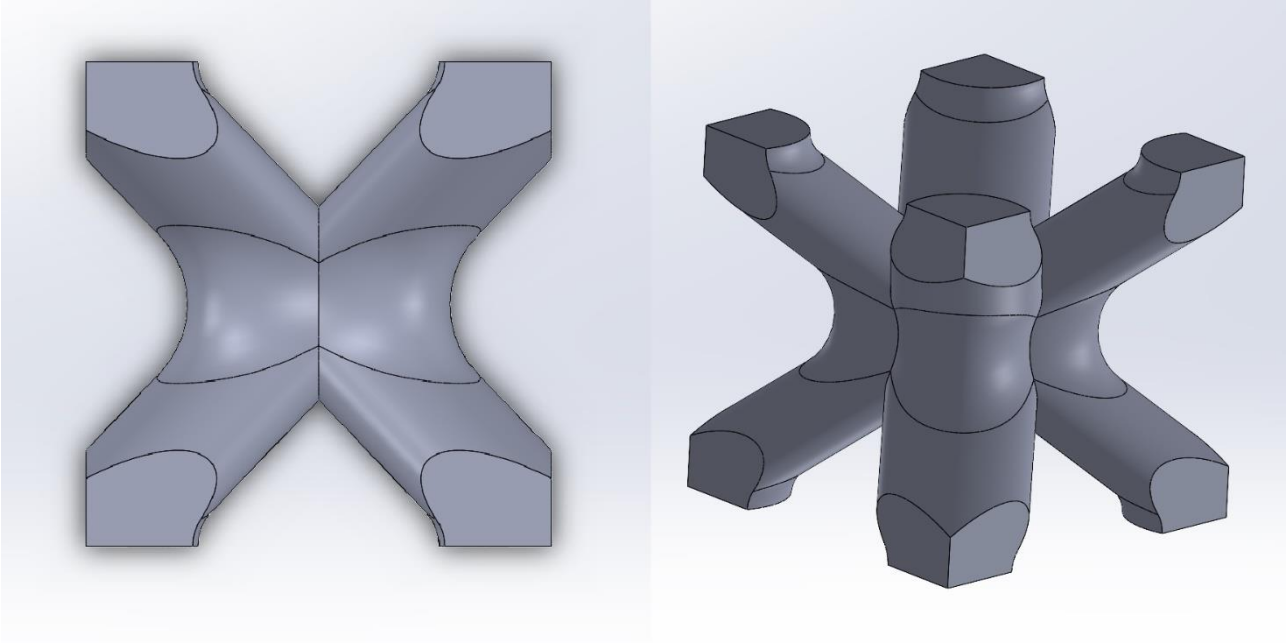

Figure 25: BCC unit cell: side view (left) and isometric view (right)

The cubic geometry of the unit cell has been kept unchanged to avoid losing the desired mechanical characteristics. However, this design choice entailed having to increase the specimen thickness. This was not the only one adaption made to the standard ISO 6892 for the BCC lattice structure: the reference specimen fillet radius area has been converted

considering the struts' diagonal planes not to be interrupted. The relative density gradient was obtained increasing gradually the struts' thickness inside the four cells located around the cross - section changing area. The struts' thickness has been increased continuously between adjacent cells, starting from the base value of 1.7 mm up to more than 4 mm, obtaining a completely fully dense cell towards the specimen extremities.

Another unit cell has been designed to avoid the fillet radius area modification of the standard reference specimen geometry. This elementary cell has been named DROP, since it has a drop shape cavity inside a parallelepiped volume. In this case, the geometry has been selected to accommodate a more convenient surface roughness, following the guidelines of optimal design for additive manufacturing. The cell height is 7.2 mm while the side of the square base is still 6 mm. The minimum width of 0.94 mm is in correspondence of the central area. The internal walls are inclined at 45°; in the next chapter we will refer to this angle when considering the internal struts. The cell volume has been reduced by subtracting a cylindrical column of 1.7 mm diameter passing in the centre of gravity along the Z direction. The relative density transition has been imposed with the same criteria over four cells around the cross-section change area. In Fig. 26 the DROP cell unit is shown.

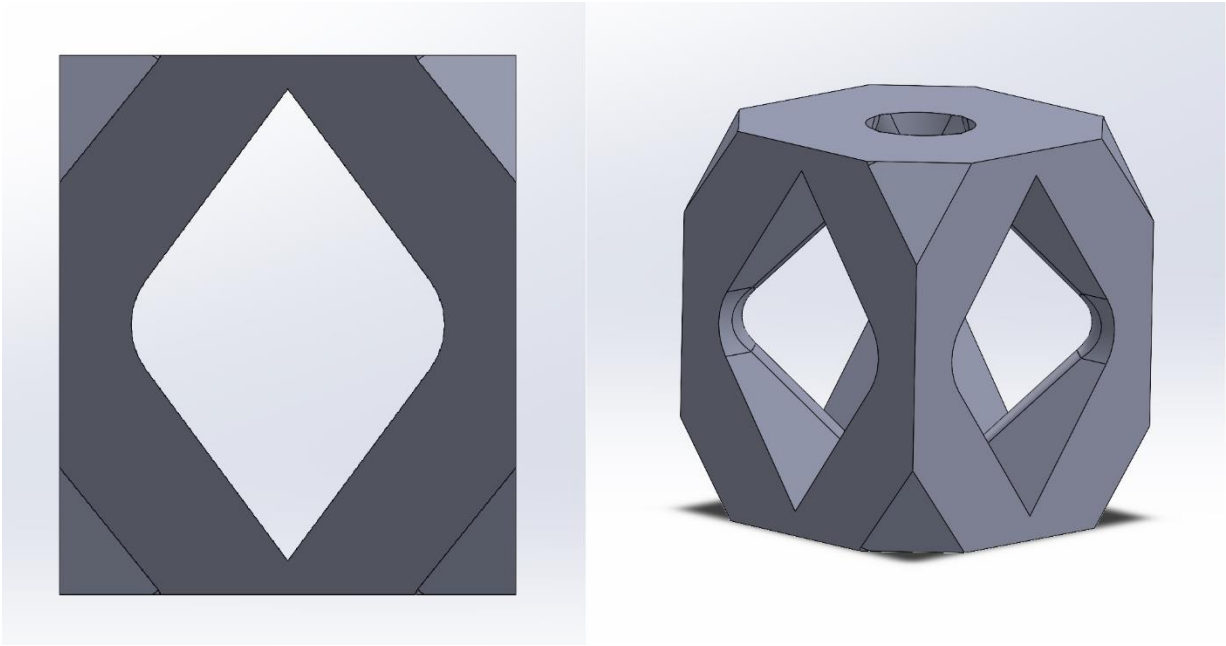

Figure 26: DROP unit cell: side view (left) and isometric view (right)

3.1.4 Tensile specimens

To characterize adequately the lattice structure behaviour through tensile tests, it was appropriate to create a set of different specimens. Two major types have been designed, with the respective lattice unit cells BCC and DROP. The first specimen has been already showed in a previous paragraph. The second specimen is shown in Figure 27.

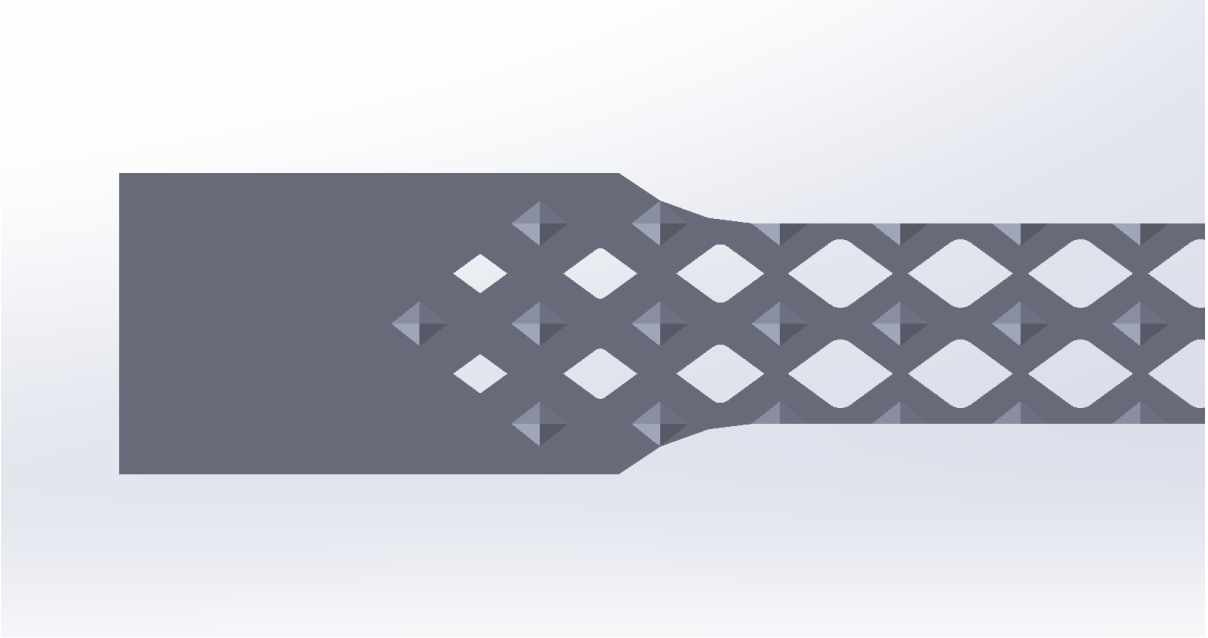

Figure 27: Graded specimen design with DROP lattice

In this case, the specimen was designed to keep the fillet radius area strictly respecting the ISO standard geometry. In this way, it is possible to evaluate the different behaviour at the transition area when the geometry is curved and when it is an angled bevel. These two types of lattices own an important feature: both can be printed vertically and horizontally, as they are self-supporting and do not need of any kind of external supports.

To be sure to have the most complete data collection as possible for tensile tests, the intention was to print the specimens both with EB-PBF end L-PBF machines.

- For SLM, a set of four specimen types with different internal angled - struts were designed. In this set, the internal struts are inclined by 30°, 35°, 40° and 45°. This diversification allowed us to obtain information on the printability of thin struts and on the incidence of defects, especially the dross-formation and the porosity. In Figure 28 (BCC) and 29 (DROP) the eight different specimens are shown.

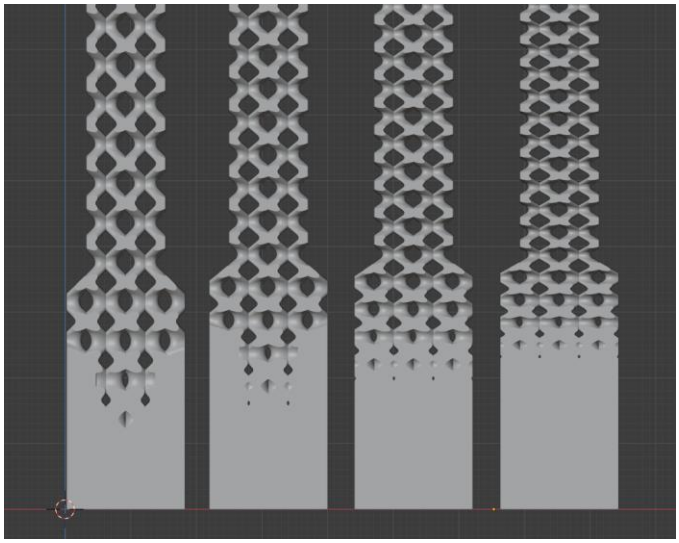

Figure 28: BCC different angled specimen designs

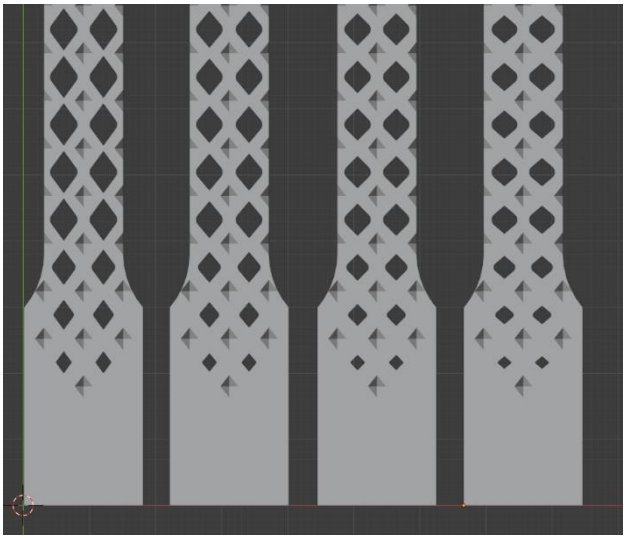

Figure 29: DROP different angled specimen designs

The intent was to print them both horizontally and vertically and highlight the differences. This also could be a test for the printability of different angled lattice structure that does not strictly follows the optimal design for additive recommendations.

- For EBM, only the two 45° specimens (the most stable and probably resistant) were selected to be vertically printed; no one was selected for horizontal printing. Later, it was chosen to print in addition a bulk ISO 6892 specimen, to validate some data which could be useful for creating a predictive simulation model. Figure 30 shows the ISO standard specimen design.

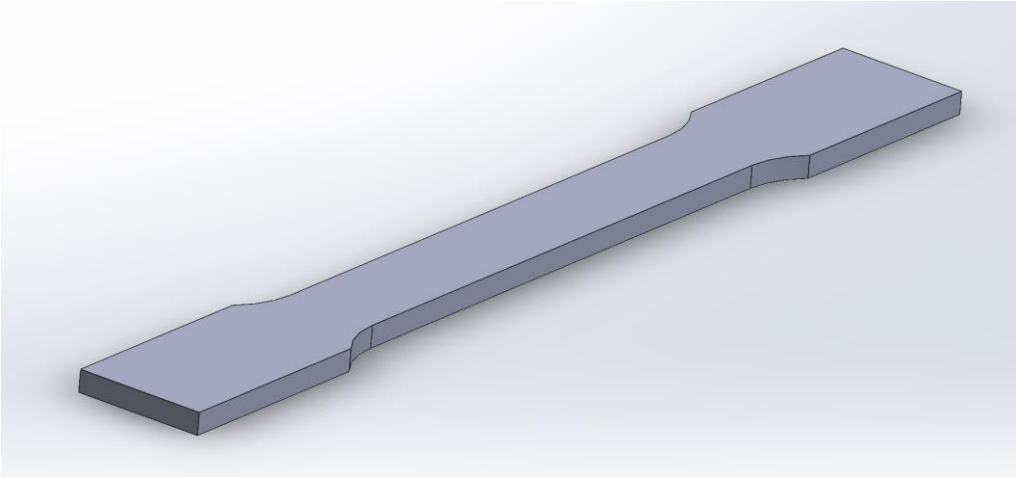

Figure 30: Bulk ISO 6892 specimen design

3.1.5 Compression specimens

In this study, since the variety of problems encountered with SLM printing, after discussed in the "Results" chapter, the compression specimens are designed only for EBM process.

The samples are developed with two different shapes for keeping the unit cell geometry unaltered:

- The BCC sample has a cubic shape (Fig. 31) with a side of 18 mm

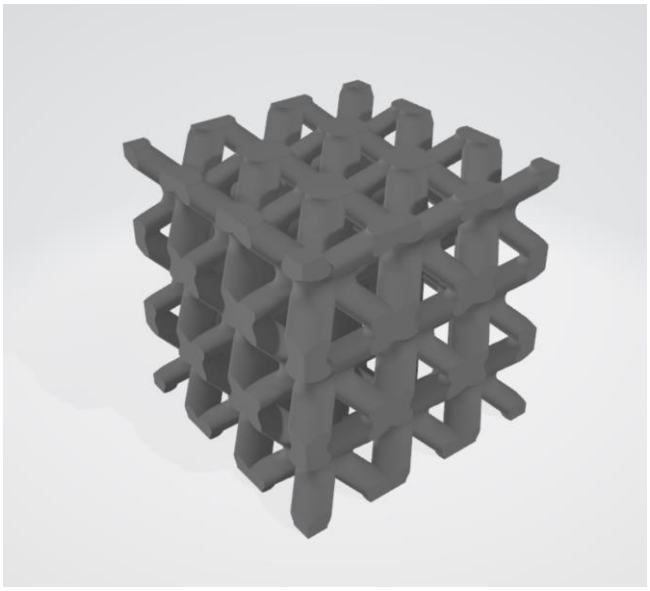

Figure 31: BCC compression sample

- The DROP sample has a lightly parallelepipedal shape (Fig. 32) with an external cross section of 18 x 18 mm and a height of 21 mm

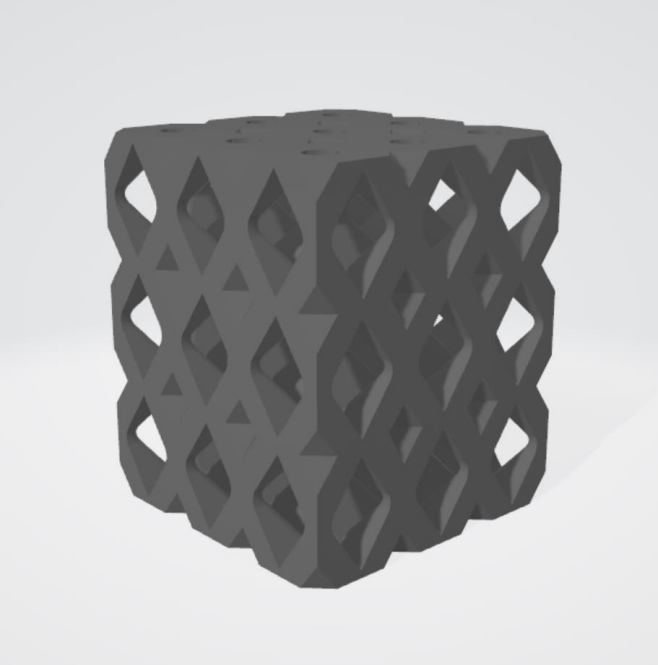

Figure 32: Drop compression sample

Given the fact that specimens will be printed in metal, the presence of bulk parts at the extremities is not necessary. The samples shape by its own provides a uniform distribution of the load during the compression test.

Unlike some previous research, in this study we do not vary the size of the struts diameter or the unit cell. All of this because this changing would be beyond the main objective of the thesis and moreover it would lead to conducting an enormous quantity of tests.

3.3 Manufacturing and testing

In this chapter, the production methods are explained in detail and the machines are briefly described. Thus, the reasons that have led to the choice of the materials and their own important characteristics are stated.

3.3.1 Materials

Initially, the intent was to use the same material, Ti-6Al-4V, for both printing technologies. In this manner a further comparison it was possible, nevertheless some problems have been highlighted and it was decided to opt for two different materials.

With SLM technology, there are many critical challenges associated with Ti64. Due to the high cooling rates, the microstructure of the as-built components is mainly composed by α' martensite [56]. Because of this, Ti64 parts processed with SLM often have high UTS but very poor ductility [57]. Furthermore, these components can present more microstructural defects, like porosity and balling, that affects the fatigue performances [58]. Moreover, the high-cooling process, can significantly influence the crack growth behaviour, creating fractures even on job, especially for thin structures [58].

For the reasons just enounced, the selected material for SLM printing was AlSi10Mg, which allows to have excellent properties and that it has already been tested multiple times in many previous research. Ti64 is used instead of EBM, as it is a hot chamber process, in which there are no residual stress problems. The powders used are those supplied by both machine manufacturers, respectively EOS and GE Additive. Below their data sheet are exposed in Table 3 and Table 4.

Table 3: Ti-6Al-4V Data sheet

Properties	Value
Yield Strength	950 MPa
UTS	1020 MPa
Elongation	14%
Reduction of Area	40%
Fatigue Strenght @600 MPa	> 10,000,000 cyc.
Rockwell Hardness	33 HRC
Modulus of Elasticity	120 GPa
Specific Density	approx. 4400 kg/m^3
Apparent Density	approx. 2500 kg/m^3
Meltin Point Range	1500°C to 1670 °C
Boiling Point	3287°C
Appearence	Silver-Grey

Table 4: Al-Si-10Mg Data sheet

Properties	Value
In Horizontal Direction (XY):	
Tensile Strength	460 ± 20 MPa
Yield Strength	270 ± 10 MPa
Modulus of Elasticity	75 ± 10 MPa
Elongation	(9 ± 2) %
In Vertical Direction (Z):	
Tensile Strength	460 ± 20 MPa
Yield Strength	240 ± 10 MPa
Modulus of Elasticity	70 ± 10 MPa
Elongation	(6 ± 2) %
Brinell Hardness	5.37 ± 0.27
Fatigue Strength in Z	approx 97 ± 7 MPa

3.3.2 Production

To guarantee the most explanatory analysis and gaining a collection with enough data, for each different design, a set of five replicas is produced. No heat treatment is performed. As said previously, the SLM specimens are fabricated vertically and horizontally. There were some problems during the printing of BCC specimens, which are discussed later, in the final chapter. Due to the impossibility of print them, only the DROP specimens with different struts angle are printed. All the replicas are produced using the minimum number of supports required, i.e., only at the platform. A stress relieving process is performed to minimize the residual stresses and subsequently they are removed from the platform with wire EDM process. This procedure, obviously, made the horizontal specimens more warped (See Figure 33).

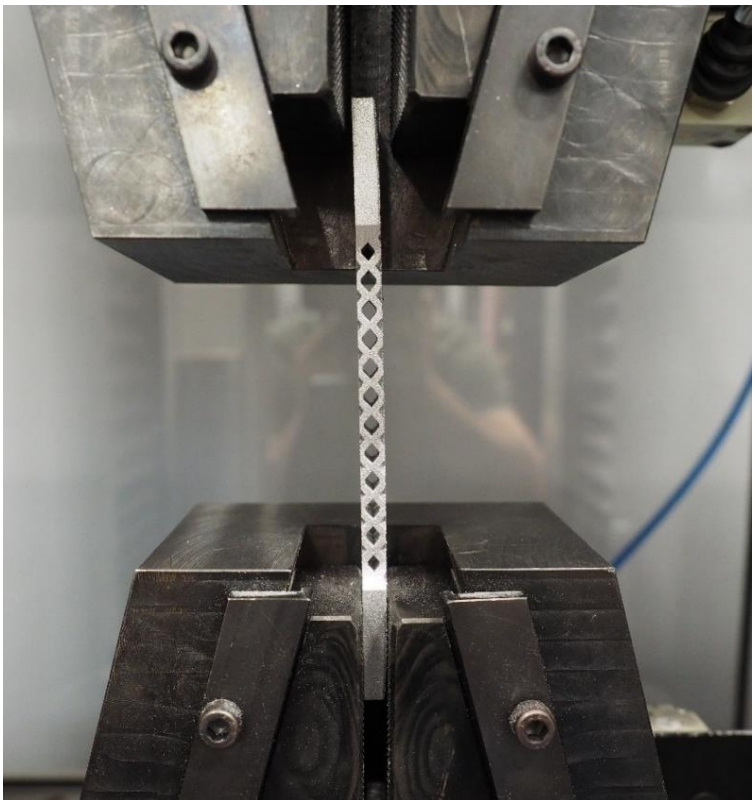

Figure 33: warped specimen produced with SLM horizontally

For EBM, in addition to the 45° BCC and DROP specimens, a Bulk specimen is produced following the ISO 6892 standard definition. All three types are printed only along z-axis. There is no need to use wire EDM in this case. For both machines, the build job is prepared using Materialise Magics, arranging the specimens with the most possible uniform distribution and considering the temperature gradient that could be formed during the job. When it was possible, the samples are located symmetrically with respect to all axes and to the centre of the platform.

For SLM the specimens are produced in multiple jobs because of printing problems and despite this, the printing of five samples failed. In Figure 34 the set of 45° sample is shown to notice the print quality.

For EBM only two jobs are performed, one for the tensile specimens and the other for the compression ones. No printing problem is encountered for the first job. All the compression specimens are printed with two different scanning technique, to which until now, we will refer as NET and MELT. The first technique is characterized by the passage of the electron beam only on the contour lines. These ones consist of concentric lines that starting from the external

contour of the geometry sliced and spaced apart by a length equal to the hatch distance. By doing so, it might be possible that the beam did not completely hit the whole selected section. The MELT technique, instead, allows the beam to cover the internal area in addition to the contours. The DROP compression samples obtained with MELT technique present some defects, and some broken struts, the others were intact.

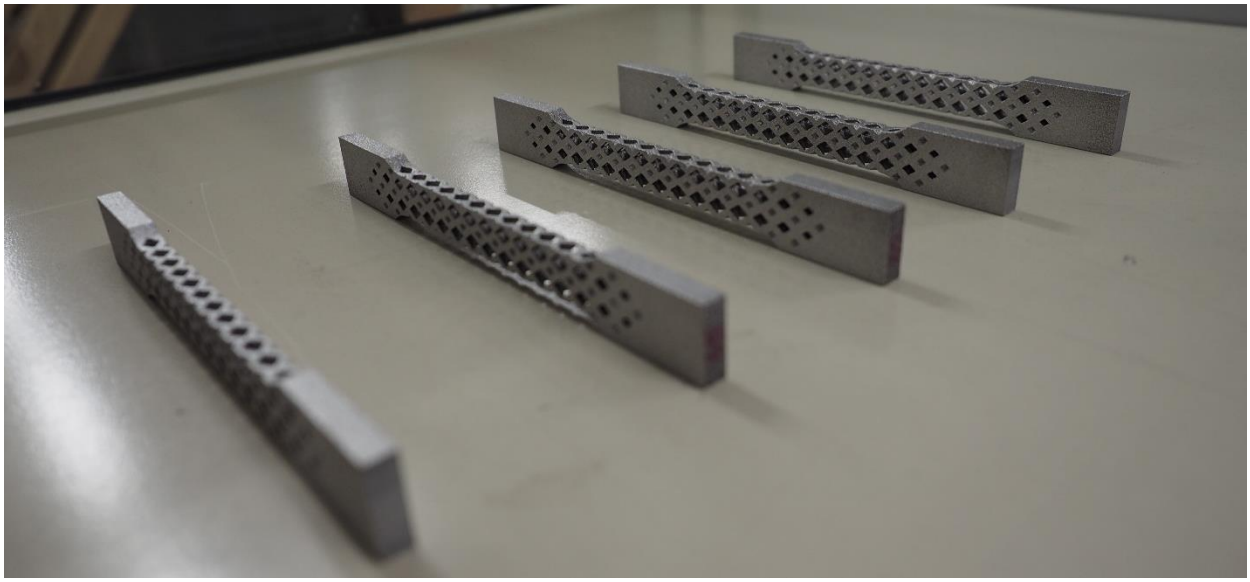

Figure 34: 45° struts angled Drop specimens obtain with SLM

3.3.3 Machines and testing

The experimental work took place in the *IAM@POLITO* laboratories at "Politecnico di Torino". Numerous additive machineries are supplied here. For this thesis, two main machines have been used:

- EOS GmbH, EOSINT M270 Metal, based on DMLS technology (LPBF process). Ideal for direct, cost – effective production of high-quality metal products [53]. It has a printing volume of 250 mm x 250 mm x 250 mm with a 200W Yb-fibre laser

- GE Additive, Arcam A2X, based on EBM process. It is well suited for high productivity with a multibeam technology and large build volume of 200 mm x 200 mm x 380 mm [54]. This metal printer uses a 3 kW electron beam.

For the characterization of the specimens for tensile and compression behaviour, EASYDUR AURA 10T machine is used [55]. This is an Italian universal testing machine, useful for tensile, compression, flexion, and shear tests. It uses EASYQS software, that is direct and easily interpretable, leading a maximum load of 100 kN. The machines are shown in Fig. 35.

Figure 35: Machines used for the thesis; from left: EOSINT M270, ARCAM A2X, EASYDUR AURA 10T

3.3.3.1 Tensile tests

Axial tensile test was performed at room temperature with a strain velocity of 2 mm/min, up to the complete failure of the specimens. For all SLM samples, the extensometer is not used, and the elongation is simply recorded considering the displacement of the upper crosshead with respect to the other at the bottom. In this case, the reference length is set to 97.26 mm, which is the initial narrower distance between the closed grippers. For EBM samples, the extensometer is used, and the gauge length is set to 50 mm. The load and the elongation data are acquired with a rate of 500 Hz by the machine software and a text file containing all the data was exported for each test. For evaluating the stress – strain curves, the minimum nominal cross section is considered, calculated with the CAD software. In this work, this area

is named S_0, the initial reference distance is called L_0, the load is renamed as F, the measured displacement is δ and the equations used to calculate stresses (σ) and strains (ε) are reported below:

$$\sigma = \frac{F}{S_0} \tag{1}$$

$$\varepsilon = \frac{\delta}{L_0} \tag{2}$$

As already described above, the lattice structures have never been fully characterized by traction. For this reason, considering the few examples present in the literature, due to the fragility of the thin struts, presumably the curve will not present an evident yielding point. Probably the curve will have a very similar trend to that shown below in the Figure 36.

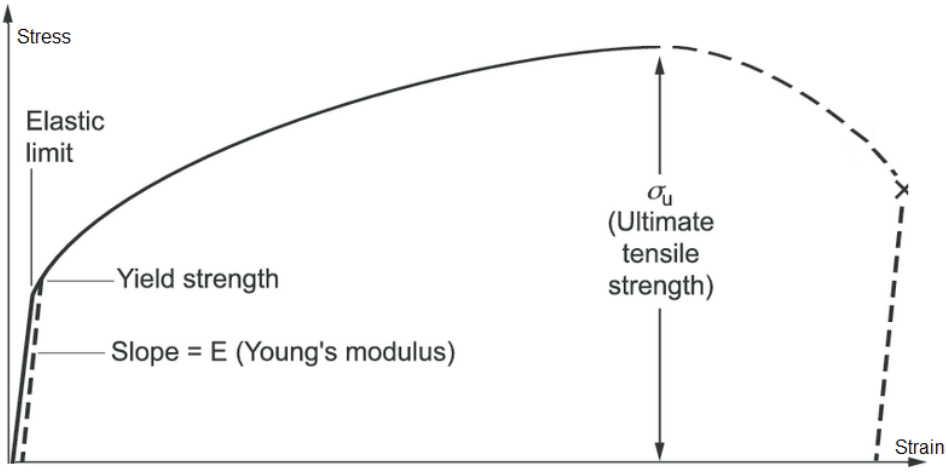

Figure 36: common stress – strain curve [61]

The maximum recorded stress represents the UTS, and the maximum strain is the elongation at failure A% of the structure. To evaluate the tensile Young Modulus the Equation 3 is used:

$$E = \frac{\delta_2 - \delta_1}{\varepsilon_2 - \varepsilon_1} \tag{3}$$

For this equation, two points must be selected inside the linear elastic region of the curve. If possible, the yield stress will be evaluated considering the RP02, referring to the ISO standard.

3.3.3.2 Compression tests

Compression tests have been performed at room temperature with a speed rate of 2 mm/min which are stopped only when densification is clearly noticeable. Gibson and Ashby [1] already studied the compressive behaviour of cellular solids, observing a recurring trend characterized by three main stages, which are already described in detail in the Review chapter. The compressive trend is shown in Figure 37.

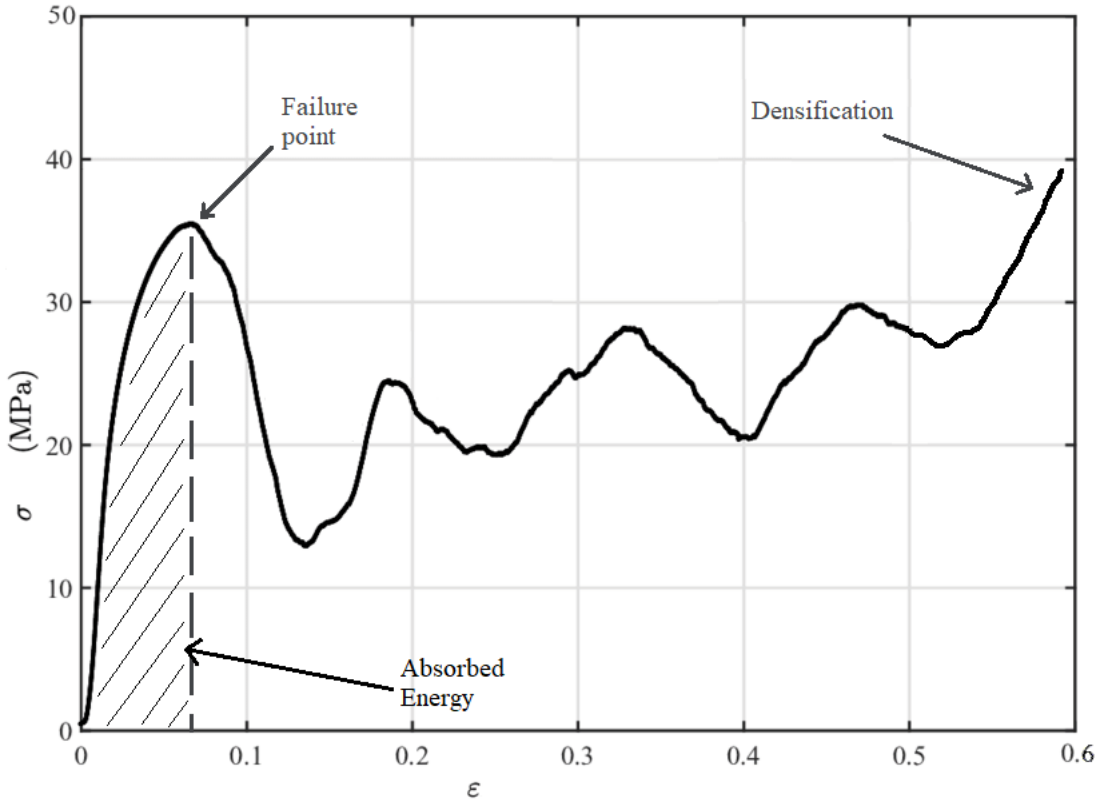

Figure 37: scheme of a compressive trend of a lattice structure from experimental results [62]

It is possible to highlight which is the effective failure point of the structure. The first failure point corresponds to the UCS* of the lattice, where the strain reaches his elongation at failure A%*. In the definition of the used abbreviations, the asterisk indicates the reference to the first point of failure. After this point, a series of increases and decreases in strength follow one another, while the structure compresses on itself until the densification finally occurs. For the evaluation about stresses and strains, the Equations 4 and 5 are used:

$$\sigma = \frac{F}{S_0} \tag{4}$$

$$\varepsilon = \frac{\delta}{L_0} \tag{5}$$

The area subtended until the UCS* by the curve represents the absorbed energy per volume unit. To calculate the absorbed energy W*, the integral formula reported in Equation 6 is used:

$$W^* = \int_0^{A\%^*} \delta \, d\varepsilon \, V^* \tag{6}$$

In this latter equation, the value of V^* represents the volume of the structure, which is easily obtained dividing the mass of the samples for the density of the material. Moreover, the nominal volume of the structure can be obtained thanks to the CAD software. In the same manner as the tensile test, the Elastic Modulus E^* is evaluated with the Equation 7:

$$E^* = \frac{\delta_2 - \delta_1}{\varepsilon_2 - \varepsilon_1} \tag{7}$$

3.4 Simulation model calibration

Besides the experimental observations also finite element analyses (FEA) are conducted to investigate the deformation behaviour of the tensile specimens in detail. This work was done for the EBM samples since they are all printed in one job with the same parameters and conditions, including the BULK batch. The FEA is performed using Ansys Workbench Mechanical APDL. Many studies in literature [63][64][65][66] highlighted how the elastic modulus can vary of less than 1% with respect to different printing orientations. Since the EBM specimens were all printed in the same spatial direction, the BULK specimens data were used for the generation of the TI-6Al-4V material model with isotropic elasticity. First, the average property curve of the five tested replicas are obtained by using interpolation on MATLAB. To create the model, the true stress together with the true strain results have been calculated. To simulate the gripping phenomenon and the tensile load, many reference nodes of the planes around the full-solid extremities are used to apply the boundary conditions, corresponding to the actual grips location. A scheme of the model is reported below in Figure 38, where the yellow planes incorporate all the nodes with a displacement vector and the blue ones corresponds to the fixed support.

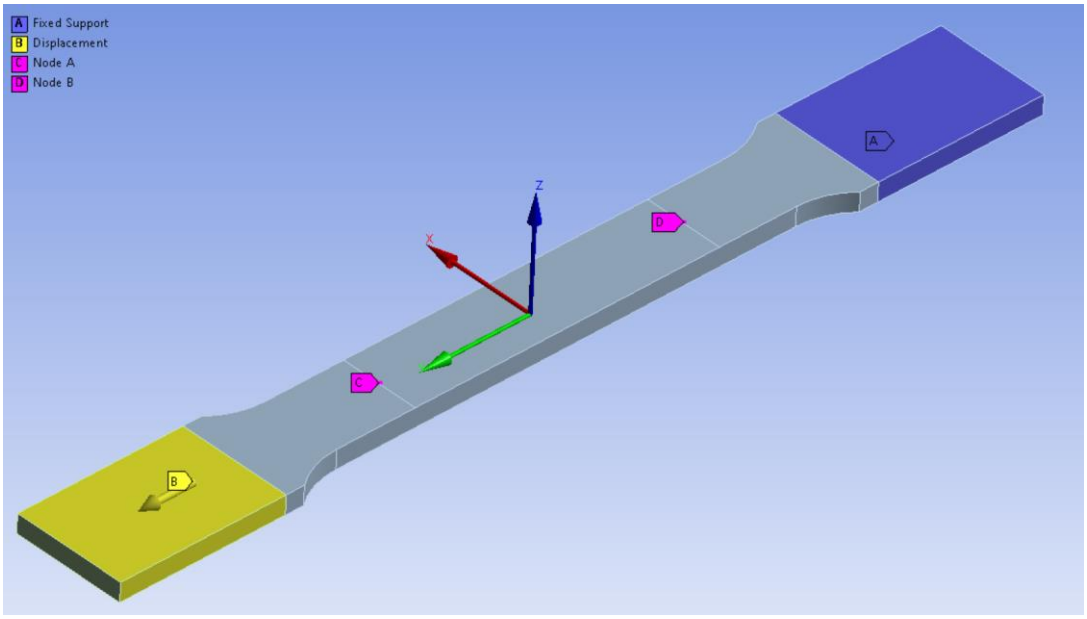

Figure 38: BULK specimen simulation model with applied constraints

Moreover, two nodes 50 mm apart are selected symmetrically from the centre of the specimen to simulate the measurement of the extensometer. The simulation done on the bulk specimen itself served to calibrate the model and to obtain data to define the multilinear isotropic hardening layout. To obtain a perfect match between the simulated curve and the experimental one, three iterations were performed: the curve points obtained from the first simulation were interpolated with the actual experimental curve and then with the following simulations consecutively, obtaining in that way a correct representation of the mechanical properties. In Figure 39 is reported the final multilinear hardening model of the material.

	A
1	Temperature (C)
2	20
*	

	B	C
1	Plastic Strain (mm mm^-1)	Stress (MPa)
2	0	349,39
3	6E-05	398,54
4	0,00013	447,47
5	0,000209	495,15
6	0,000292	542,26
7	0,000383	588,21
8	0,000491	631,83
9	0,000628	671,32
10	0,000819	703,23
11	0,001081	725,3
12	0,001401	739,08
13	0,001759	747,66
14	0,002137	753,47
15	0,002525	757,76
16	0,002919	761,19
17	0,003318	764,02
18	0,003719	766,46
19	0,004122	768,6
20	0,004526	770,56
21	0,00493	772,48
22	0,005336	774,07
23	0,005743	775,62
24	0,006149	777,13
25	0,006557	778,51
26	0,006964	779,85
27	0,007372	781,16

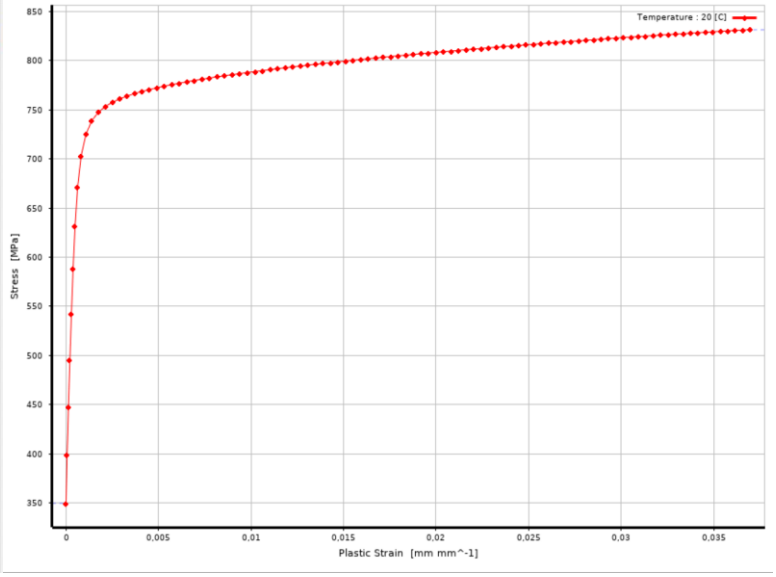

Figure 39: Multilinear isotropic model data for Ti64

The calibrated material model is than applied to the lattice structure models. To reduce the simulation time, planar symmetries were imposed on BCC and DROP specimens geometry. The simulation is performed by exploiting the Static Structural analysis system of Ansys Workbench, setting a rigid constraint at one end of the specimen and a linear displacement vector on the opposite side (the displacement increase linearly with the simulation time). A mesh of tetrahedral elements is generated, by using an aggressive mechanical quality check and an adaptive sizing command, to ensure the avoidance of mesh errors in the transition zone, since it is the most critical one. The mesh dimension for the BULK specimen has a maximum size of 7 mm as the geometry does not have portions thinner than this measure.

Contrariwise, the lattice specimens have many thin struts, and it was considered appropriate to use a mesh size at least equal to half of the strut if possible. For the BCC structure a mesh of a 0.6 maximum dimension was selected. Figure 40 shows a portion of the specimen model with the generated mesh.

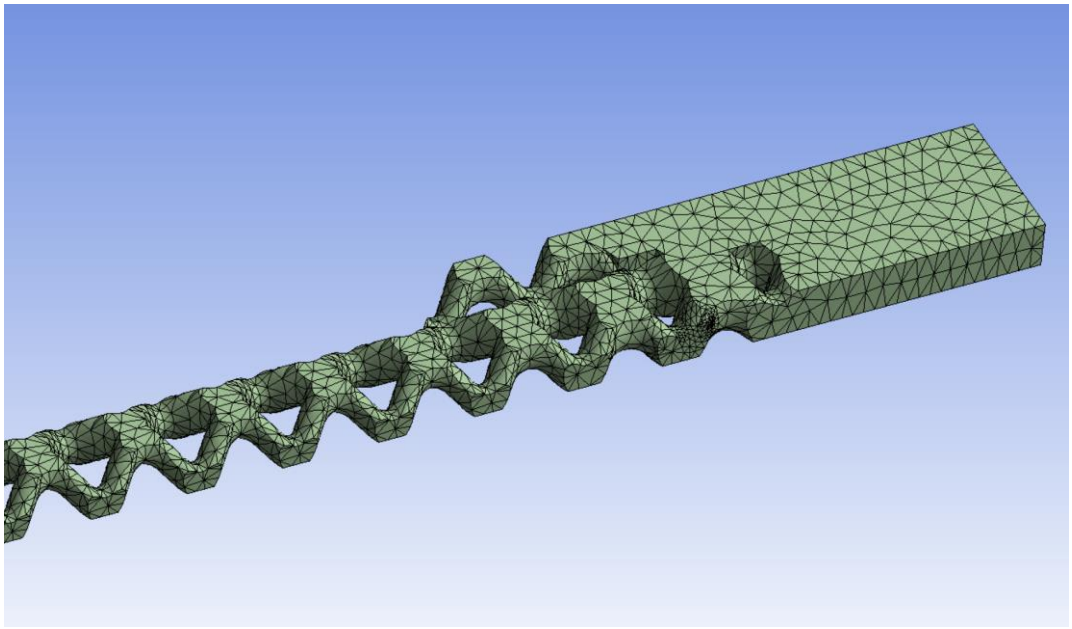

Figure 40: BCC specimen model meshed body

Below in Figure 41 is reported a scheme of the applied symmetry and conditions on the BCC structure model.

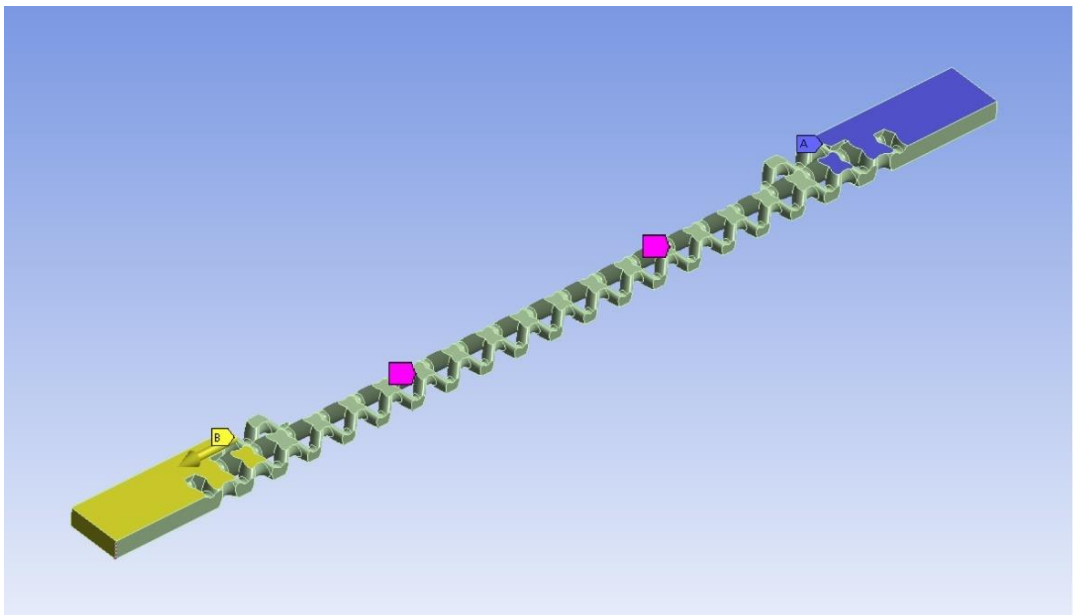

Figure 41: BCC simulation model with constraints applied

For the DROP specimen model, considering some particularly thin points of the structure, an adaptive mesh with a maximum dimension of 0.25 mm was generated, to obtain more accurate results without making the calculation process too heavy and avoiding spending many hours to carry out the simulation. An image representing the mesh of this specimen model is reported below in Figure 42.

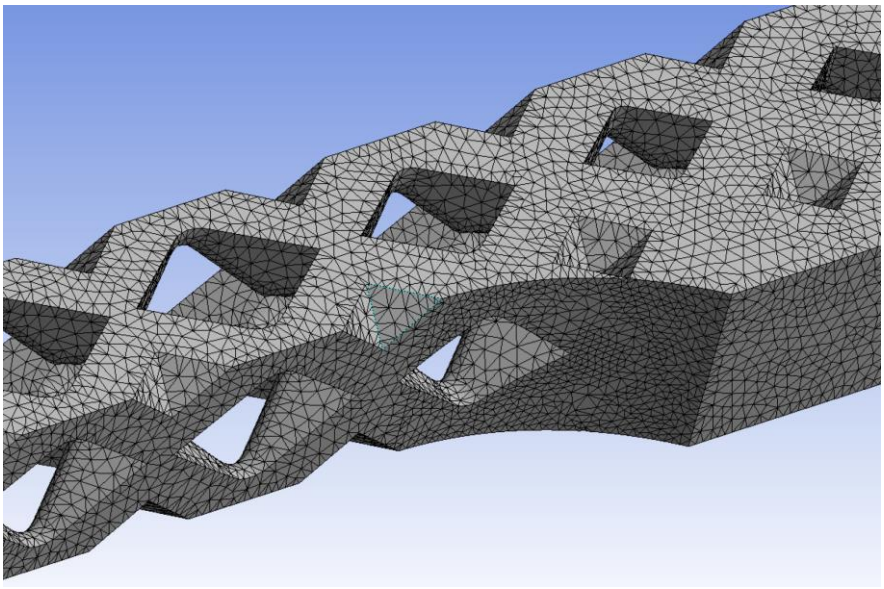

Figure 42: DROP specimen model meshed body

The analysis is set on quasi – static behaviour to get more accurate results. Since the material model is time – independent, the explicit dynamic solver is used to improve computational efficiency and additionally the mass scaling option is enabled. From the simulation results it was possible to extrapolate the displacement (in millimetres) of the simulate extensometer nodes and the average reaction force of the nodes belonging to the faces subjected to constraints. The adaptive mesh refinement was set to obtain the mesh and output convergence together. The mesh convergence option allow the software to automatically modify the mesh size of the most critical area making iterative simulations until it gets the best output values. The max refinement loops and depth were set to three iterations. Thus, a "convergence" tab was applied to the equivalent stress allowing a maximum value change of 2%. All the obtained data are processed thanks to MATLAB software to derive the simulated force – displacement curve, comparable with the experimental ones, without the influence of the effective cross – section measurement.

4. Results and discussion

In this chapter, all the obtained data from testing procedures are exposed and analysed. As already mentioned, not all specimens have been tested, because some of them broke during the printing process or during the removal procedure. In the next paragraphs all the problem--related causes and the choices done during the evaluation of the data are explained in detail.

4.1 Tensile mechanical behaviour of EBM specimens

The tensile specimens produced with EBM did not need a stress relief treatment, hence they are tested in as-build condition. As previously discussed, there are no previous tensile studies on lattice performed according to a standard, so the results differ enormously between one research to another. Despite these discrepancies, the general observed trend is similar to that of any other ductile metal full-dense specimen.

The first step is to analyse the replicas data obtained for every specimen type batch. The following graphs show the acquired load – displacement values, without any further reworking. Stress and strain values will be shown subsequently, considering the calculation procedure explained in Chapter 3.

- The BULK specimen curves are reported below in Fig. 43. Both in the elastic and the plastic region, the curves overlap without significant discrepancies. However, it can be noted that the value of the displacement at break varies within a 1 mm range, a rather high value, equal to 25-30% of the total measured extension.

This spread phenomenon can be explained by misalignment occurred during the test and considering the presence of small defects of some layers, detectable with the naked eye on the external surface, which may have affected the tensile resistance.

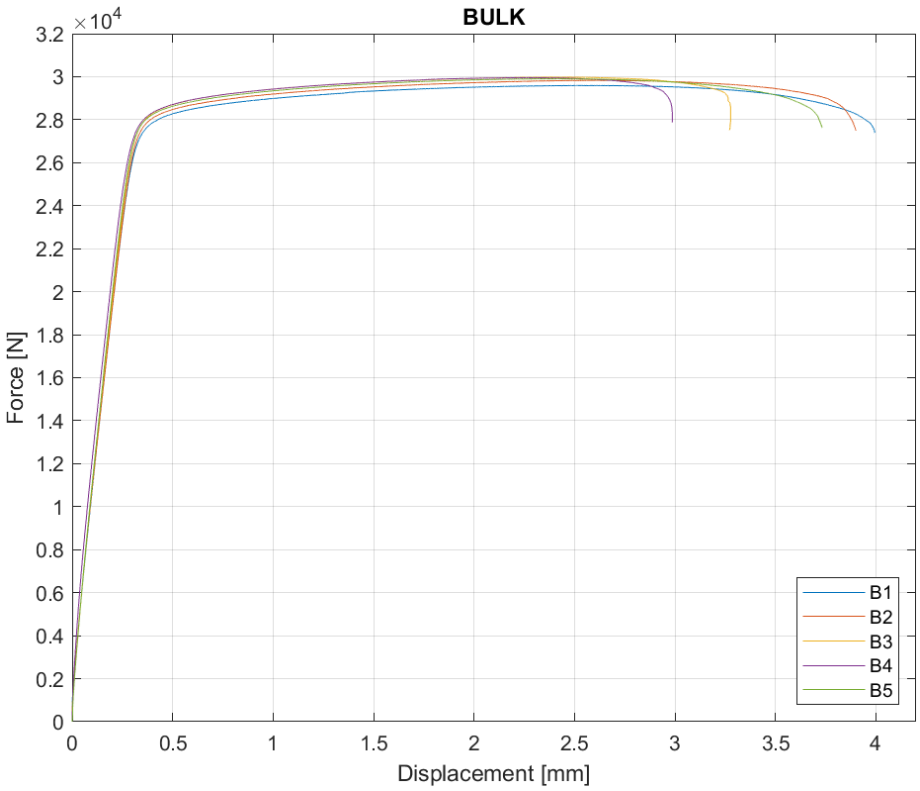

Figure 43: BULK specimen load – displacement curves

The BULK specimen presents mechanical characteristics that are not perfectly in agreement with those listed in the powder data sheet. The UTS and the RP02 turns out to be about 20% lower, with the average values of 796.17 ± 5.2 and 749.85 ± 5.84 correspondingly. This situation is perfectly explicable considering that the machine parameters set up for this job are not the same used by the company that released the property declaration table. For completeness, the images of the fractured specimens are shown below in Fig. 44.

Figure 44: fractured BULK specimens after tensile testing

- For what concern the experimental testing of the BCC lattice specimens, the acquired load – displacement plots are reported below in Fig. 45. Also in this case, the curves hare very similar to each other, overlapping almost completely and having almost the same mechanical characteristics. The only exception concerns the sample C3, which was subjected to a considerable slipping of one extremity. This specimen, in fact, was put in uniform tension only after the beginning of the test, at the point where the machine crossbar had already moved the other extremity by 0.3 mm. It can be seen from the corresponding plot that the curve becomes linear (elastic region) starting from that displacement value. Therefore, that specimen shows an overall displacement at break value greater than all the others. Regarding the other curves, the detectable non-uniformities among the displacement at break values agree with the variability of porosity, especially within the thinnest struts, and with the presence of small layers defects and misalignment during the tests.

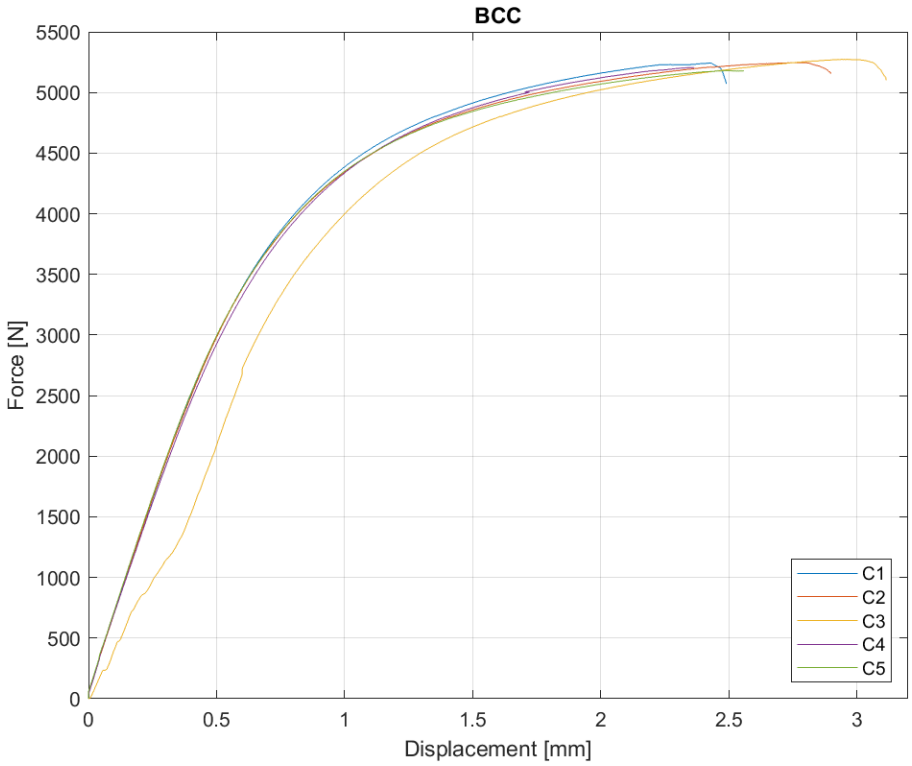

Figure 45: BCC specimen load – displacement curves

All the failures were located within the useful narrowed section portion. The failure always occurred along a plane perpendicular to the printing direction, at the points with the smallest cross - section values (equivalent to S_0 14.88 mm^2), as expected. One of the fractured specimens is shown In Fig. 46 with two different view angulations.

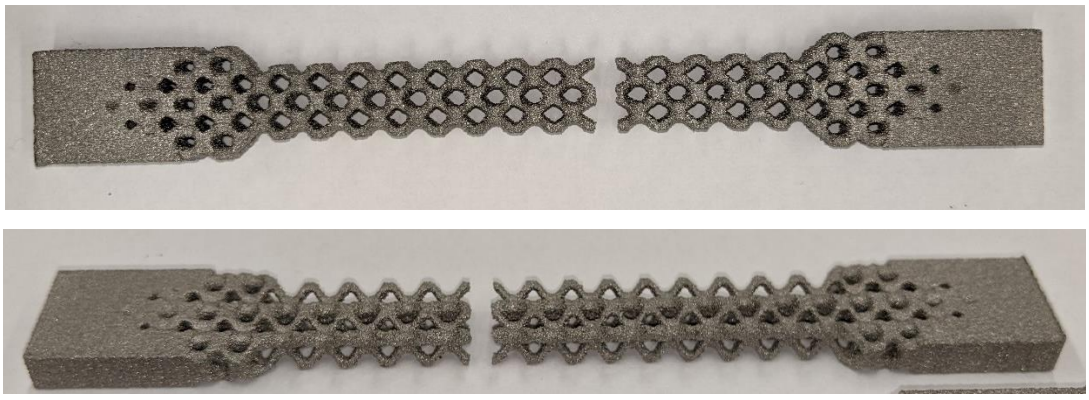

Figure 46: fractured BCC specimen after tensile testing

It is worth noting that looking at the struts, during the test, there was no evidence of shrinkage, however this evaluation is not so trivial since the small size considered: the BCC struts diameter measures 1.7 mm.

- The load – displacement curves obtained from the experimental testing of the DROP lattice specimens are reported below in Figure 47.

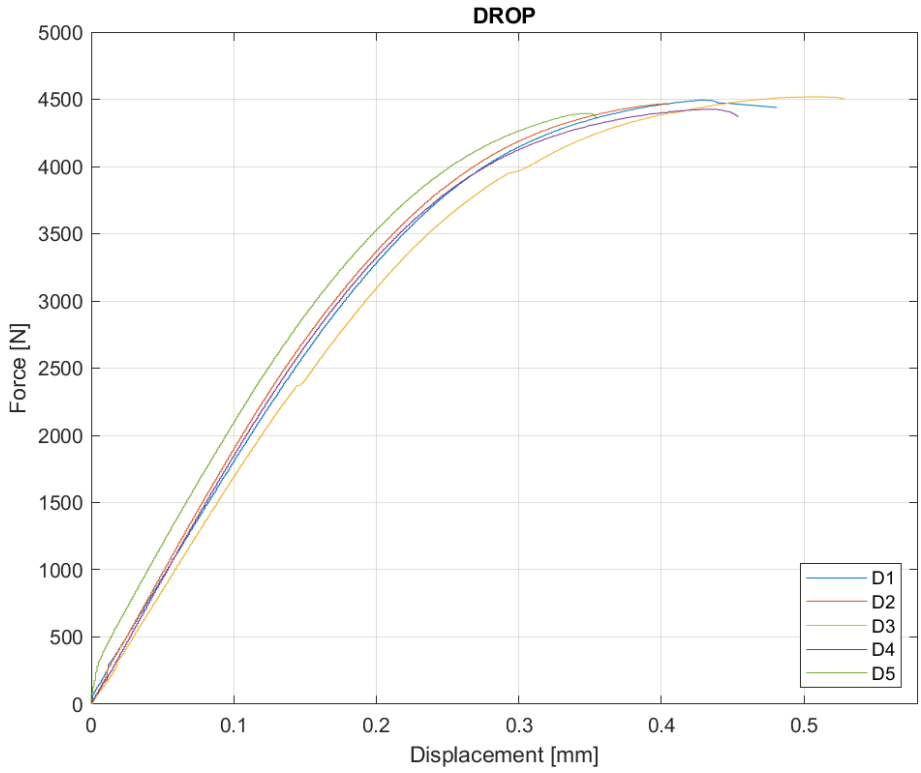

Figure 47: DROP specimen load – displacement curves

The curves do not show perfectly homogeneous behaviours, due to some misalignments. There are two specimens showing anomalies. The sample D3 underwent two misalignments which occurred during the test around the point corresponding to a displacement of 0.15 mm and 0.3 mm, in which it is possible to observe a curve side-shifted movement. This issue affected the maximum detected force value and the displacement at break value, greater than the others, but not excessively. The sample D5, instead, underwent a misalignment at the beginning of the test, distorting the starting point of the linear elastic region, leading to a lower displacement at break value. All the other detectable non-uniformities among the curves agree with the restrained variability of properties and small defects of different samples. The failure locations occurred within the useful narrowed section portion

only three times out of five, the others occurred close to the end of the density gradual variation area. Although the geometry of these specimens was studied ad hoc to cause a failure inside the gauge length, the influence of porosity and the concentration of micro-defects within the thinner struts of the transition area may have weakened them. Each fracture area presented a distribution along a plane perpendicular to the printing direction, at the points with the smallest cross - section values (equivalent to S_0 6.5 mm^2). The failure occurred immediately after reaching the maximum force value (and so the UTS). No evidence of struts shrinkage was detected, considering the complexity of observing such a small structure: the struts diameter measures less than 1 mm. One of the fractured specimens is shown In Fig. 48 with two different view angulations.

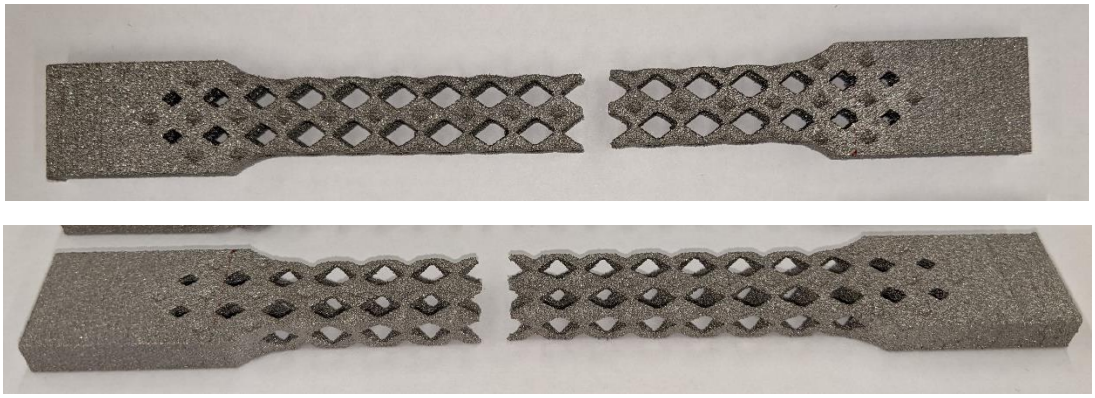

Figure 48: fractured DROP specimens after tensile testing

The second step is to analyse the behaviour of the two structures BCC and DROP and comparing their curves whit the Bulk specimen one.

Figure 49 shows the comparison of the three specimen types, including five replicas each, produced with EBM. In general, these specimens showed a great repeatability of the results. As it is possible to observe immediately, the properties are very different from each type. The young modulus of the BCC specimen is considerably lower than the Bulk one, unlike the DROP sample, which has a closer value. Contrariwise, the elongation at break of the BCC specimen is more than five times higher than the DROP one. These two aspects are very significant: the

lattice type may affect the elasticity of the structure in an extremely different manner, and although it is apparently more deformable, it does not necessarily have a higher elongation than the Bulk specimen. In this case, the brittleness of the material played a key role. The DROP specimen breaks almost without plastic deformation, but it has a tensile strength comparable to the Bulk one, while the BCC sample has about half the resistance. As it is possible to see looking at the curves, one BCC sample presents a different behaviour, due to a slippage.

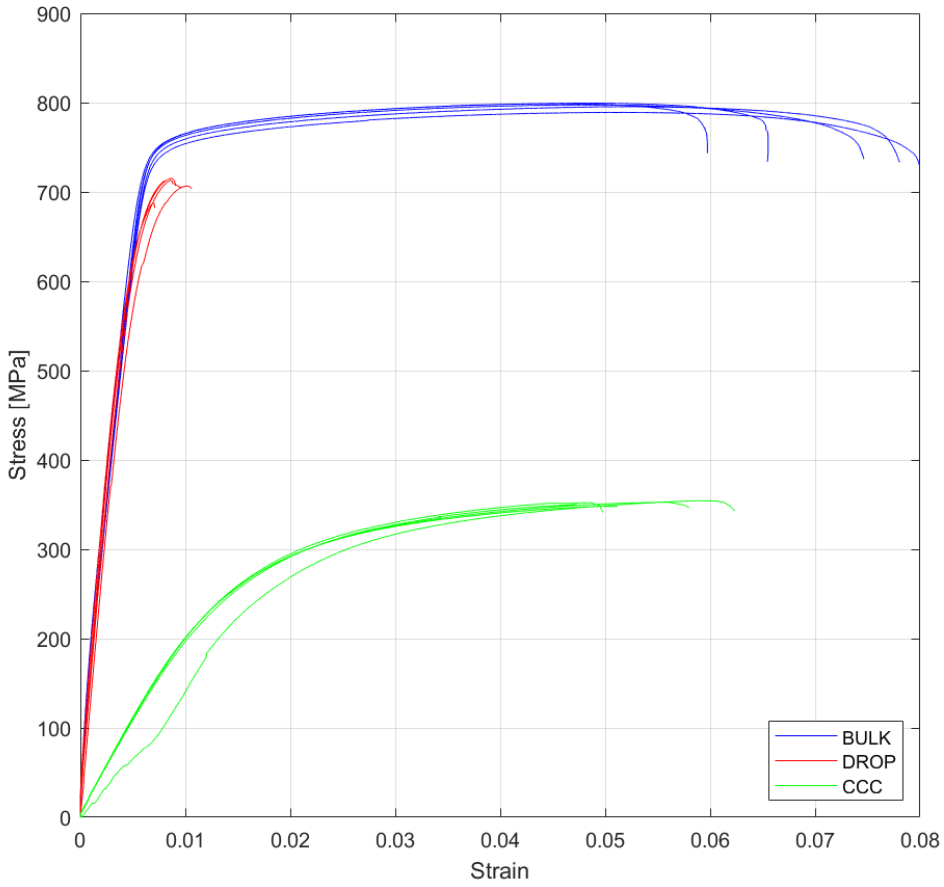

Figure 49: BCC, Drop and Bulk specimen EBM tensile curves

As specified in the paragraph 3.3.4, the main properties have been evaluated by considering the nominal minimum cross section S_0, calculated from the CAD file. Table 5 shows the average values of the mechanical properties for each specimen type.

Table 5: Average properties of each different EBM tensile specimen

Structure	RP02 [MPa]	UTS [MPa]	E [GPa]	A %	Porosity[4] [%]
BULK	749.85 ± 5.84	796.17 ± 5.2	127.7 ± 7.7	7.16 ± 1.01	-
DROP	686.61 ± 8.62	706.97 ± 14.1	140 ± 16.8	0.89 ± 0.75	53.84%
BCC	241.19 ± 2.06	351.49 ± 3.13	19.8 ± 4	5.37 ± 0.17	62.14%

In Table 5, the porosity is calculated considering the ratio between the nominal empty volume of the CAD model and the overall volume of the lattice unit cell.

It is worth noting that the young modulus of the DROP specimen has a higher value than the Bulk modulus, this might seem an unusual feature for a lattice sample. However, it must be reminded that all calculated values are based on the assumption that the equivalent cross-section is the absolute minimum one over the entire gauge length. However, the section value changes considerably according to the point of the specimen observed. If the maximum detectable value of the cross-section were used instead, it would be observed an elastic modulus lower than the BULK one. Neither choice can be considered right, but only a decision to keep in mind while reading the data. Considering the definition of the Young's Modulus, that is a measure of the resistance to elastic deformation, it can be stated that the lattice entire specimens have a lower resistance, in fact, they plastically deform faster. A further aspect of uncertainty concerns the interpolation of the curves, especially as regards the modulus between the BULK and the BCC specimens which have very close values (less than 10% difference).

The obtained data, unfortunately, based on only two types of unit cells, cannot be used to create a predictive linear or non-linear relationship as it was already done in the past for the compression behaviour [1]. The only possible consideration is that by increasing the overall porosity of a lattice structure, i.e., decreasing the relative density, leads to lower UTS. The behaviour in the elastic region strictly depends on the lattice design.

[4] This value is considered as the complementary of the relative density; it is not considered for the BULK specimens

4.2 Tensile mechanical behaviour of SLM specimens

In this case, the produced samples are differentiated in two ways:

- Vertically (Z-axis) or horizontally (XY-plane) printed. The first letter of the samples nomenclature on the graphs indicates the direction: V for vertical and H for horizontal ones
- Different angle of the lattice struts (30°, 35°, 40° or 45°). The number that indicates the struts angulation is reported after the first letter. Eventually a second number from 1 to 5 indicates each single specimen

As already mentioned, only the DROP specimens have been successfully printed and tested, with a total of 34 samples. Below are shown the curves for every batch of tested specimens in Figures from 50 to 57. The first four figures show the horizontal specimens, while the last four show the vertical ones.

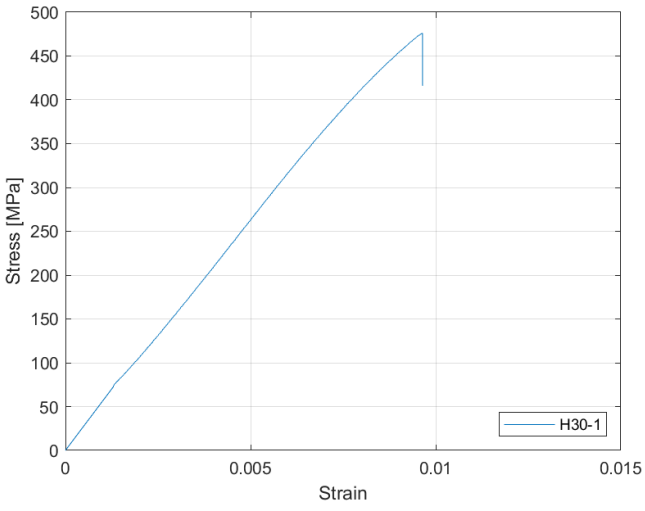

Figure 50: Stress-strain curve of SLM XY-plane 30-deg specimens

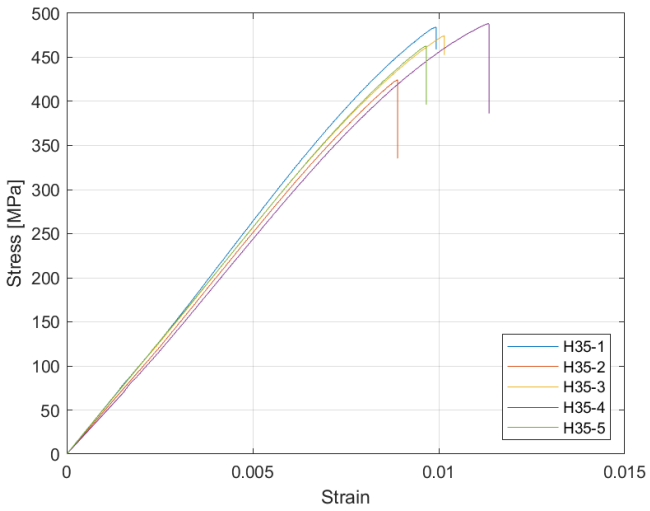

Figure 51: Stress-strain curve of SLM XY-plane 35-deg specimens

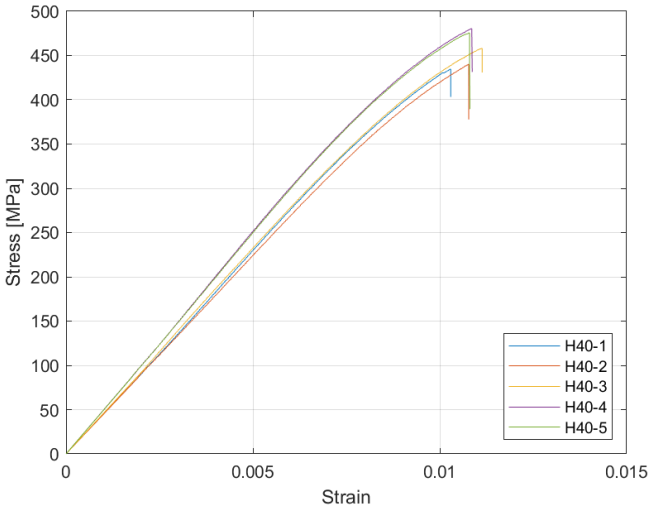

Figure 52: Stress-strain curve of SLM XY-plane 40-deg specimens

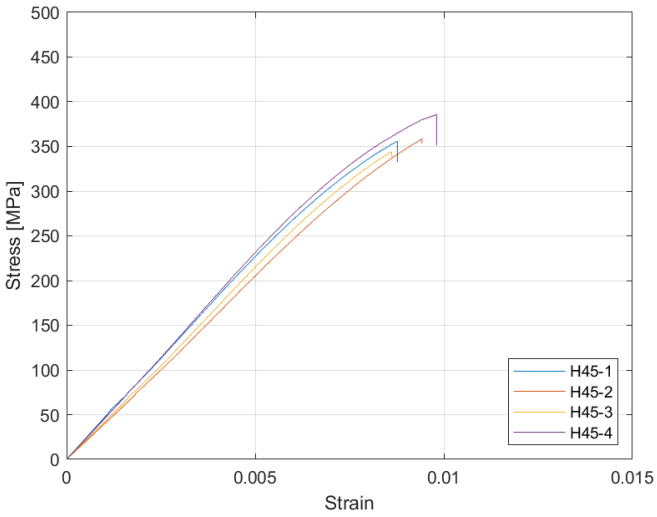

Figure 53: Stress-strain curve of SLM XY-plane 45-deg specimens

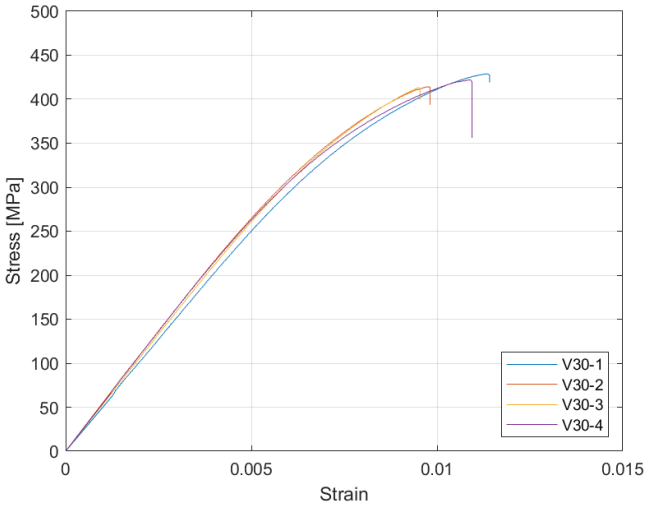

Figure 54: Stress-strain curve of SLM Z-axis 30-deg specimens

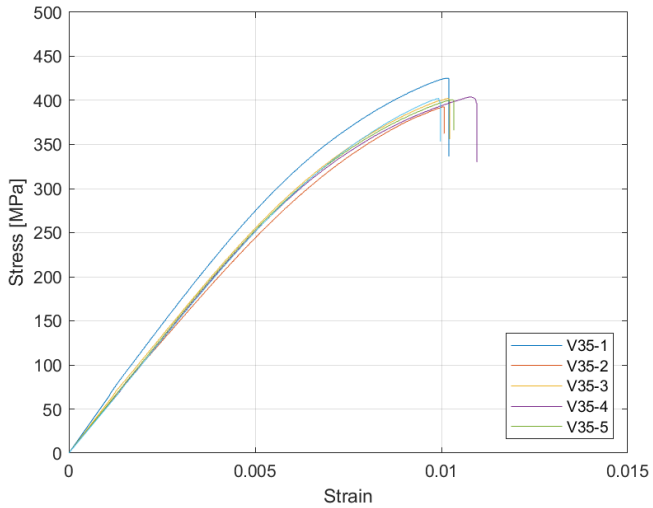

Figure 55: Stress-strain curve of SLM Z-axis 35-deg specimens

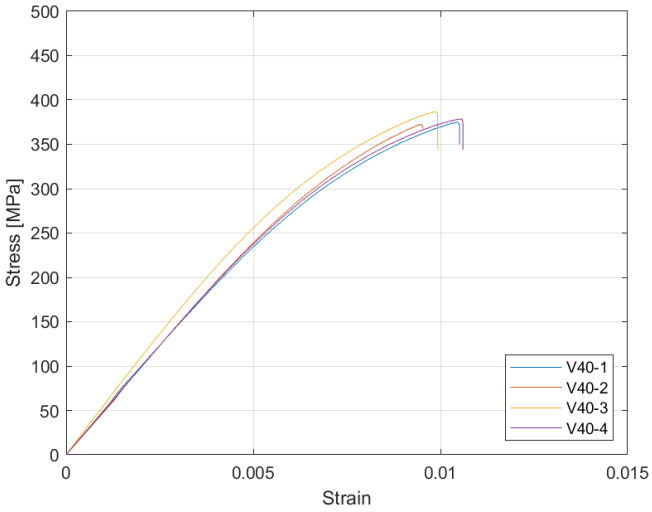

Figure 56: Stress-strain curve of SLM Z-axis 40-deg specimens

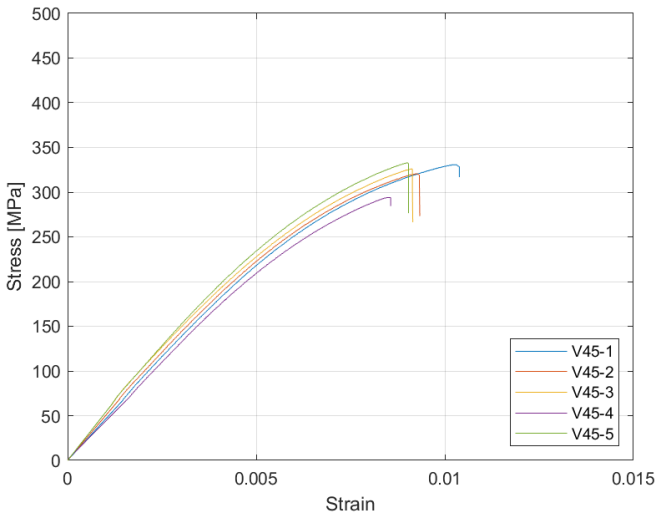

Figure 57: Stress-strain curve of SLM Z-axis 45-deg specimens

To better highlight the trend of these samples, in Figure 58 and 59 the average curves of every batch are shown.

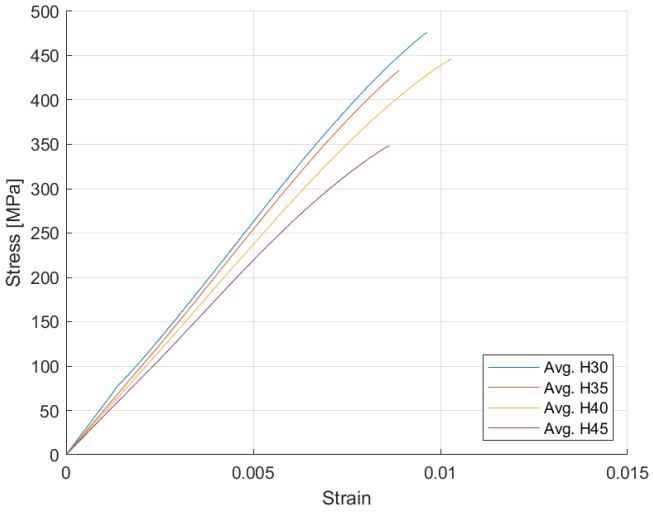

Figure 58: Stress-strain curve of SLM XY-plane specimens

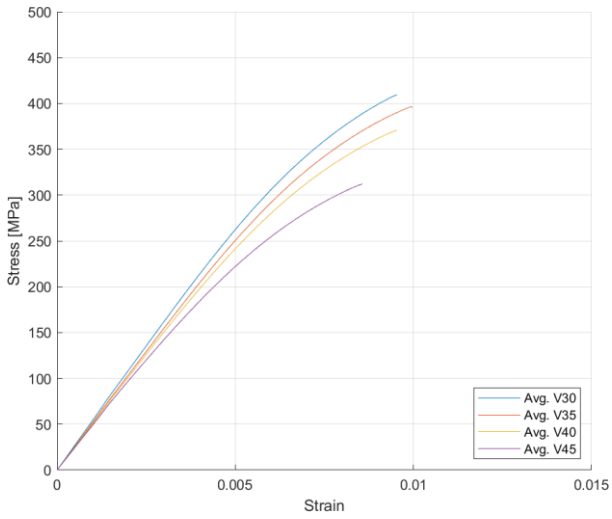

Figure 59: Stress-strain curve of SLM Z-axis specimens

These lattice structures, due to the manufacturing process, possess a transient zone where stresses concentrate even if a stress relief treatment is applied. Thus, the linear elastic region is prevalent. Moreover, the anisotropy of the mechanical behaviour can be evidenced:

- Plastic deformation is almost absent in XY-plane specimens. They broke as soon as they reached the UTS
- Z-axis printed samples presents lower stress values but almost the same average elongation at break
- UTS values are considerably dispersed when compared with those obtained with EBM process

Tensile test results for both vertically and horizontally printed samples are reported below in Table 6.

Table 6: Average tensile test results for SLM specimens

Structure	Z-AXIS			
	RP01 [MPA]	UTS [MPA]	E [GPa]	A%
30°	288.69 ± 8.15	420.69 ± 6.31	43.85 ± 2.41	1.04 ± 0.09
35°	270 ± 7.98	400.31 ± 5.47	42.08 ± 3.85	1.03 ± 0.05
40°	249.51 ± 7.59	372.82 ± 5.23	39.8 ± 0.96	1.01 ± 0.05
45°	235.65 ± 6.01	322.46 ± 13.14	37.14 ± 2.65	0.93 ± 0.09
Structure	XY-PLANE			
	RP01 [MPA]	UTS [MPA]	E [GPa]	A %
30°	MISSING	475.98	42.28	0.96
35°	MISSING	466.75 ± 23.12	41.76 ± 2.64	1.00 ± 0.12
40°	MISSING	457.72± 17.59	39.04 ± 1.79	1.08 ± 0.04
45°	MISSING	360.97 ± 21.03	36.17 ± 1.01	0.92 ± 0.06

It is important to highlight that the 30° XY-plane batch results have been evaluated on one single specimen as the others broke during the removal process. The plastic deformation region of the curves is so limited that it is impossible to calculate RP02. Hence, for the Z-axis batch, RP01 was calculated, while for the other batch not even this property was evaluable.

The mechanical properties depending on the different angle of the lattice struts can change significantly: the 30° struts allow to have better properties among all. In this case, for XY-plane samples, that have the higher strength values, the UTS is about the 87% of the Bulk one (specified on data sheet), and the elastic modulus about the 57%. The elongation at break for every sample is about 10 ÷ 15 % of the Bulk property.

For both SLM batches, the failure point is randomly distributed in the reduced section area, but most of the time outside the gauge length. In this case, the preliminary dynamic simulation

performed on the CAD model could not foresee this behaviour. The 45° XY-plane broken specimens are showed in Figure 60.

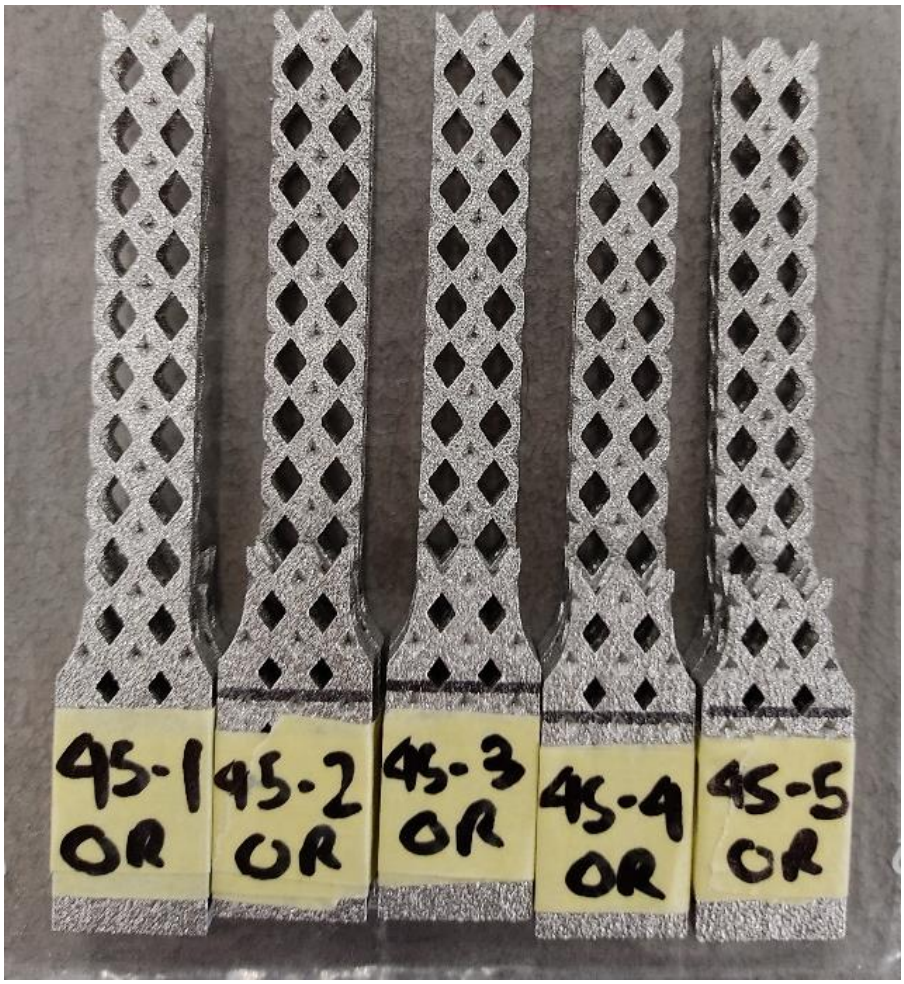

Figure 60: Broken 45° XY-plane SLM specimen

It is worth noting that for SLM process, it was impossible to print correctly all the BCC specimens, as they failed during the job itself or the removal procedure. All the BCC samples broke in the transition zone from full dense area to lattice area, even if a smooth density gradation was present. The DROP samples succeed to print but only after many attempts by varying the process parameters. In any case, with considerable difficulties during their removal. All the horizontally printed specimens were deformed during the removal assuming a curved shape. Four of the five horizontally printed 30°-struts specimens and one 40°-strut vertically printed specimen failed during the removal with wire EDM procedure. This problem has been carefully analysed: hardness tests have been performed on those failed specimens,

since there were doubts about their behaviour, related to residual stresses. The detected hardness values were compliant and not higher than expected after the annealing process, confirming a correct stress relieving. The most likely reason for the failures is that this specific graded design, due to the process characteristics, leads to a stress concentration near the transition zone, especially inside the lower cross-section area. This type of stresses cannot be individuated by carrying out a simple software simulation because they depend on the process parameters combination that can differ according to the technology, the machine used, and the geometry of the parts printed.

4.3 Compressive mechanical behaviour of EBM specimens

As discussed before, the compressive behaviour of a generic lattice structure is characterized by three main stages:

1) Elastic region: the stress increases until the first main collapse
2) Progressive collapse of the layers
3) Densification: the lattice assumes the same behaviour of the bulk material as it is too much compressed and loses his initial deformation properties

The trends obtained in the present work are not all perfectly in agreement with the compressive mechanism proposed by Gibson and Ashby [1] or with those observed in the literature. The Figure 61 shows the curves for every batch of tested specimens.

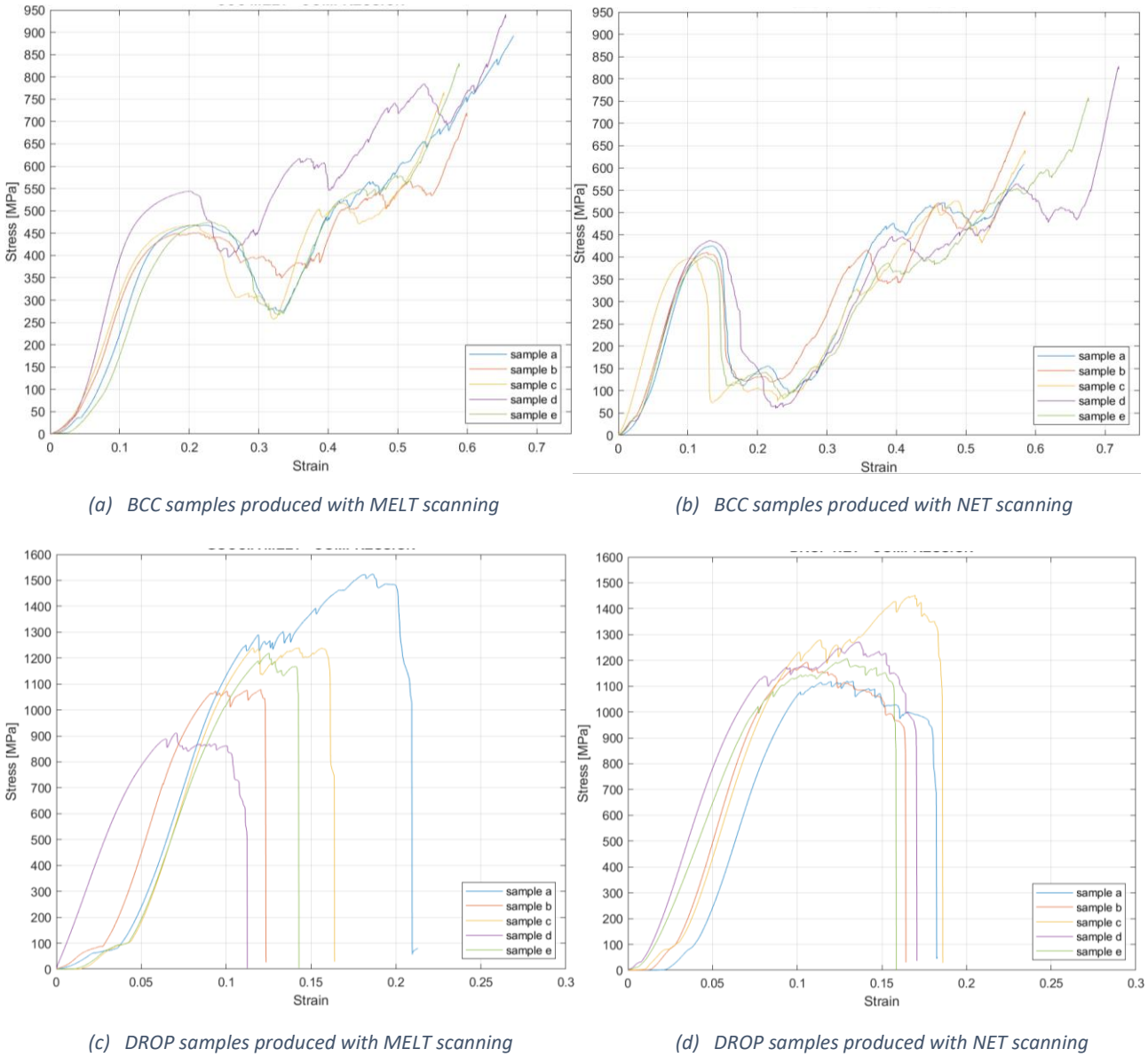

(a) BCC samples produced with MELT scanning

(b) BCC samples produced with NET scanning

(c) DROP samples produced with MELT scanning

(d) DROP samples produced with NET scanning

Figure 61: Stress – strain plot of compression test performed on EBM specimens

Figure 61 shows four different cases; the first two (cases a and b) represents the curves of the BCC specimen produced with two different scanning technique, MELT and NET, previously explained. The last two trends (cases c and d) show the experimental results of the DROP samples. As it is possible to see, only the trends of the BCC specimens are exactly as expected. This depends on the different failure mechanism of the two lattice types:

- The BCC lattice breaks gradually starting from the top where the load is applied; each plane of unit cells collapses on itself around the point where the cross-section is smaller. At the same time the entire structure slightly expands but manages to resist and does not present

the typical 45° failure. This behaviour is not attributable to auxetic properties, because the Poisson's ratio is positive. During the compression, some of the external thinner struts are projected outward at high speed. Figure 62 shows a schematic representation of the breaking mechanism.

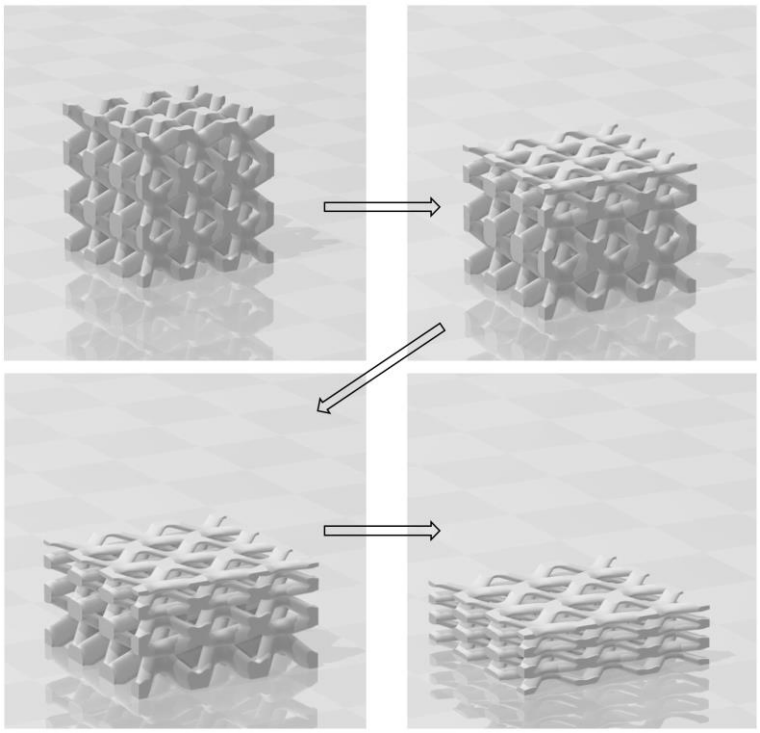

Figure 62: Failure behaviour of BCC compression specimen

- The DROP lattice breaks down in a completely different manner; when it reaches the first maximum stress point, the structure abruptly collapses sliding simultaneously along a horizontal direction. The upper part engages with the lower part interrupting the test. The joint is made possible due to the sample design. Figure 63 shows this failure mechanism.

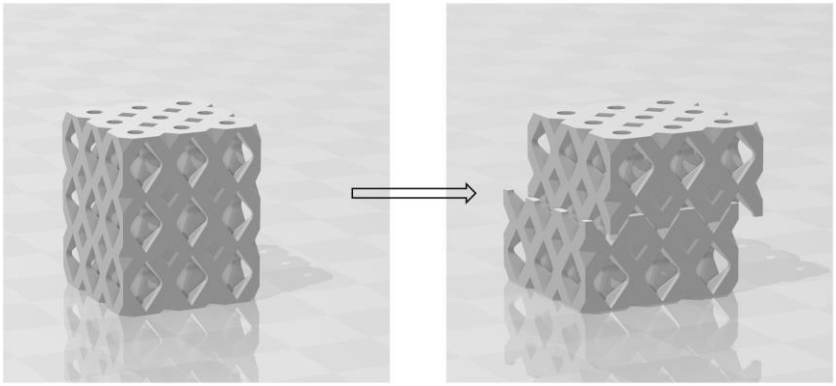

Figure 63: Failure behaviour of DROP compression specimen

The most important aspects regarding the compression test results are the following:

1) MELT scanning methodology leads to more dispersed results than NET
2) For BCC specimens the failure of the NET structure occurs at a stress 15% lower than the MELT one but at almost half of the strain
3) For the DROP specimens, the failure of the NET structure occurs at an average stress and strain 5 ÷ 15% higher than the MELT one
4) DROP samples are more than two times stronger than BCC and reach a similar elongation
5) The elastic modulus differs by approximately 5% between the two scanning methods. For the respective specimens, higher values are obtained with the NET method
6) The fractures of both specimens are on a plane and not at 45°. It must be considered that these lattices, compared to the classics tested in the literature, are coarse and along the unit cell there is a considerable cross – section variation (even an order of magnitude)

Each DROP compression specimens printed with MELT scanning technique presents at least one broken strut already in the as-built condition, as visible in Figure 64.

Figure 64: EBM MELT DROP compression specimen with broken struts

It is important to consider that, the points where the structure fractured are extremely thin and the program that controls the printing process, it may have problems trying to define their internal geometry for the beam passage on the section. The broken struts are randomly distributed, but always on the outer contour, where the beam made fewer passes and therefore did not have the opportunity to properly melt all the powder.

As said in the paragraph 3.3.3, the main properties of the samples have been evaluated considering the nominal minimum cross-section. The average properties values for each batch are listed in Table 7.

Table 7: Compression specimens average properties

Structure	UCS* [MPa]	E* [MPa]	A%*	W* [MJ]
BCC MELT	481.04 ± 46.3	4988 ± 1126	21.7 ± 2.21	1270 ± 112.16
BCC NET	414.17 ± 20.26	5255 ± 587	12.43 ± 1.71	605.3 ± 66.4
DROP MELT	1194.34 ± 306.2	18213 ± 2678	14.34 ± 4.94	3132 ± 1475
DROP NET	1248.1 ± 166.6	19040 ± 1748	16.53 ± 1.21	4232 ± 615

One important consideration can be made immediately, by simply looking at Table 7. The distribution is highly skewed. Table 8 shows the ratio between the standard deviation and the mean of the values for each batch. This ratio is reported as a percentage.

Table 8: Standard deviation above mean ratio for compression tests

BCC MELT	6.72%	**15.87%**	7.99%	6.68%
BCC NET	3.66%	7.25%	9.88%	7.93%
DROP MELT	**16.94%**	9.57%	**23.52%**	**34.57%**
DROP NET	9.04%	6.60%	4.83%	11.10%

It is worth noting that some data are very scattered (see the bold ones). Ultimately, for the compression data of the analysed batches, there is not a good repeatability.

From the results collected, it is impossible to define a behaviour predictive law, because the differentiation is too poor, but the four batch average values can be compared to the Gibson – Ashby model [1]. This model relates the relative strength and the relative modulus of a cellular structure with its relative density. The relations are made with the bulk material values. The model assumes the form of a positive power relationship with a coefficient "C" that depends on the different unit cells and an exponent "n" which depends on the other hand on the dominant behaviour of the lattice structure (bending or stretching) (See Equations 8 and 9).

$$\frac{\sigma^*}{\sigma_S} = C \left(\frac{\rho^*}{\rho_S}\right)^n \tag{8}$$

$$\frac{E^*}{E_S} = C \left(\frac{\rho^*}{\rho_S}\right)^n \tag{9}$$

Considering a bending dominated lattice structure, the proposed exponents "n" is 3/2 for the Equation 8 and 2 for the Equation 9. In this work, the properties of the bulk specimen are not tested, but the elastic compressive modulus E_S is reported in the material data sheet. The UCS_S is assumed to be equal to 1000 MPa. By doing so, it is possible to use both the equations. For the metallic cellular structure, the model predicts the coefficients "C" range of [0.1 – 4] and [0.1 – 1] respectively for the two relationships [67]. Figure 65 shows the bi-logarithmic diagrams in which the experimental results and the extreme limits of the proposed model are presented. In this diagram the power laws limits are the two straight lines.

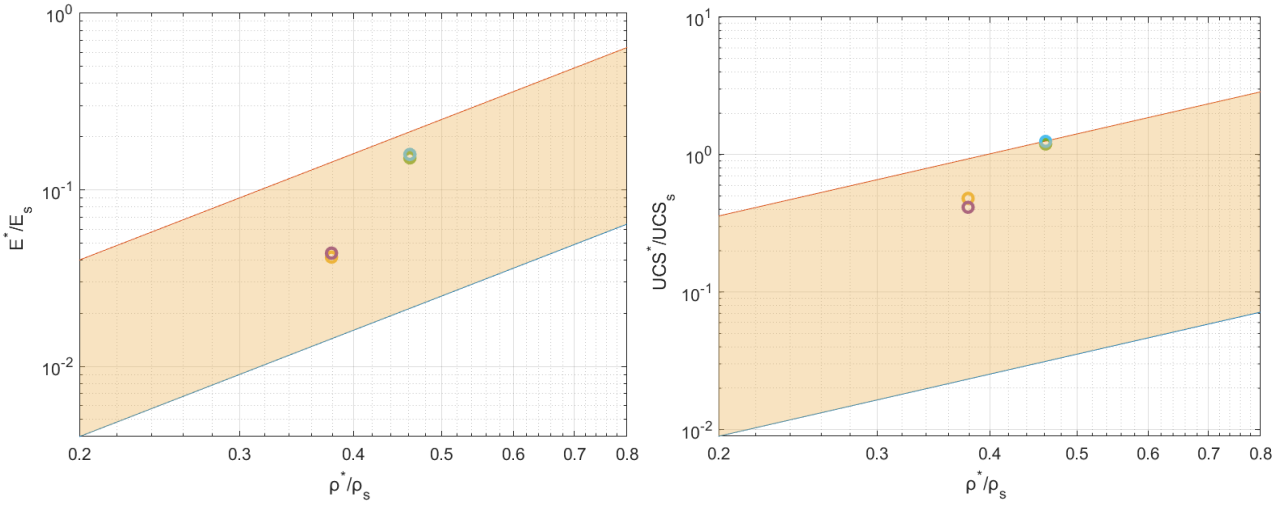

Figure 65: comparison of experimental data with the prediction of Gibson-Ashby model

As it is clearly visible, the results agree with the model, since the data points are located within the range, inside the coloured area. The two dots at the bottom represent the MELT and NET batches of the BCC specimens. The upper ones are the DROP samples results. The nominal relative density of the BCC sample is 37.86%, while the DROP one is 46.16%. Unfortunately, this work samples lattices are not comparable with those of other researchers, as they were created ad hoc.

4.4 EBM lattice compressive and tensile properties

The results obtained for the compressive specimens are more scattered than those obtained for the tensile ones. It is possible to compare the batches printed with the MELT scanning technique, for which the detected compressive properties show considerable fluctuations.

- The BCC lattice samples show an ultimate compressive strength higher than the ultimate tensile strength of by an average of 130 MPa, with a deviation almost 15 times higher. The Young's modulus from tensile test ranges between 16 and 24 GPa, while in quasi-static compression it ranges between 4 and 6 GPa, therefore being on average 5 times smaller.

- The DROP lattice samples show an ultimate compressive strength higher than the ultimate tensile strength of by an average of 490 MPa, with a deviation almost 21 times

higher. The Young's modulus from tensile test ranges between 123 and 157 GPa, while in quasi-static compression it ranges between 16 and 21 GPa, therefore being on average 7.5 times smaller

The obtained results for the specimens printed with the NET scanning technique are substantially similar. The trends experimentally observed generally agree with the literature results introduced by Raghavendra et al. [68]. The compressive strength of these lattice structures are superior to the tensile ones, while the resistance to elastic deformation under compressive quasi-static loads is smaller, inducing earlier a plastic behaviour.

4.5 EBM and SLM lattice tensile properties

Since the DROP specimen with 45° struts has been produced with both the printing technologies, a comparison can be made, even if the materials are different. The properties of the AlSi10Mg SLM specimens are significantly lower than those of the bulk material. The UTS and the Young's modulus of the Z-axis specimen are equal to 60% of the Bulk. For the Ti-6Al-4V EBM specimens, the properties are much higher in percentage: the UTS is approximately the 90% and the elastic modulus is even 17% higher. The peculiarity is that the elongation at break point in both cases is practically the same.

4.6 Simulation model results

The curves obtained by the simulation are reported below, compared to the experimental ones, shown in Figure 66 and Figure 67, representing the mechanical behaviour of BCC and DROP specimens.

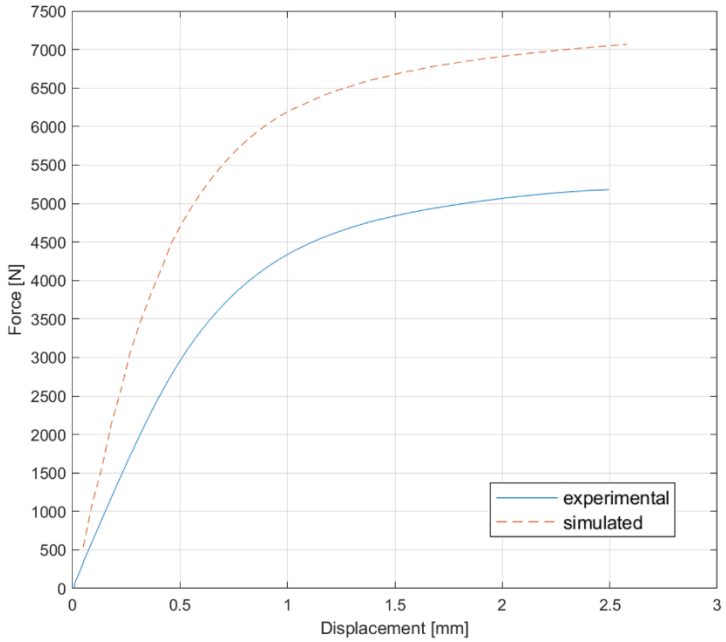

Figure 66: BCC simulated vs experimental Force – Displacement curve

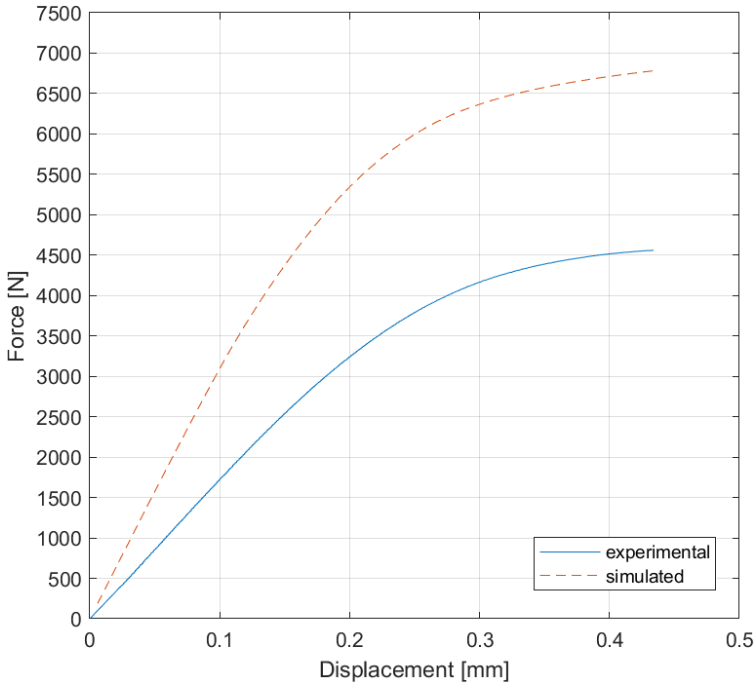

Figure 67: DROP simulated vs experimental Force – Displacement curve

The curves shown above are deliberately stopped at the minimum value among all the specimens' elongation at break. The average experimental curve is calculated only until the lowest breaking value among all the specimens, since beyond it would no longer represent an arithmetic mean of five curves.

From the depicted force – displacement curves in Figure 66 and 67, some considerations can be made:

- The different behaviour of the simulated BCC and DROP models can be highlighted, looking at the orange dashed curves. The two structures show a similar resistance trend, with a difference of approximately 275 N of the maximum force value. Noticeable higher displacement at break values are detected for the BCC model with respect to the DROP one: on average 2.5 mm and 0.44 mm, respectively. It is possible to recognize the linear elastic region of the two curves, with some approximation, due to the absence of a clear transition to the plastic behaviour: the BCC elastic region ends at about 0.2 mm, i.e. 8% of the overall displacement, while the DROP elastic region ends at about 0.1 mm, i.e. 23% of the overall displacement. Considering the area under the curve, since it is not a stress-strain curve, no considerations can be made for the toughness. Summarizing, the BCC model presents a lower extension of the elastic region with a greater elongation capacity and higher mechanical properties.
- It is possible to highlight that the general trends exhibited by the simulated model are the same showed by the actual specimens if we compare the two lattice structures, looking at the blue curves. The DROP specimen shows lower performances: it fails earlier with less than the 20% of the overall displacement of the BCC structure and it reaches approximately 620 N less (equal to 12%) of maximum force. The plastic behaviour for the BCC specimen is observed in correspondence of the 14% of the overall displacement, while for the DROP specimen shows it on 30%.
- Each lattice structure simulated results can be compared to the experimental data. Table 9 resumes the simulated and experimental more significant values, considering loads and displacements, instead of stresses and strains, avoiding reporting errors related to the cross-section measure.

Table 9: Main evaluated results from load-displacement curves - FEM simulation and experimental data comparison

Structure	Simulated	Experimental	Error [%]
Force at the end of the elastic region [N]			
DROP	3130	2667	14.8%
BCC	2330	2250	3.4%
Maximum force [N]			
DROP	6780	4560	32.7%
BCC	7055	5181	26.5%
Displacement at break [mm]			
DROP	0.4647	0.4448	4.8%
BCC	2.5828	2.686	3.9%

As it is possible to observe, the simulated behaviour has higher mechanical properties in general. Potentially there are some systematic errors that go beyond the performed FEA consistency. The main influencing factors are the following:

- The model does not consider any kind of presence of defects such as porosity, surface roughness, partially unmelted powders, actual struts diameter and macro deformations of the structure
- The simulation, however precise it may be, does not consider the effect that the EBM process has on a lattice component compared to a solid one. The local properties of the central structure of the specimen differ from those of the extremes. All of this because the thermal energy is uniformly distributed over a constant solid section, while its dissipation is not homogeneous on the lattice sections. These are characterized by the presence of numerous parts in which the powder must not be melted, but very close to each other

Considering that the bulk specimens have been produced in the same job of the lattice ones, it is reasonable to think that the material properties are very similar for all the three specimen types. Thus, reading the stress values obtained from the simulations, which does not consider the actual cross-section measure, we can compare the Bulk UTS with the stress values obtained from the simulations, knowing that the specimens broke immediately after reaching their maximum stress. In this way, the presumable force and displacement values at failure are cautiously obtained. Moreover, the evaluation of the results must consider the convergence of the simulation parameters. In particular, the simulation curve can be reasonably stopped at the point where maximum residual forces and maximum stresses both converge. Figures 68 and 69 shows the stress results from the FEA simulation.

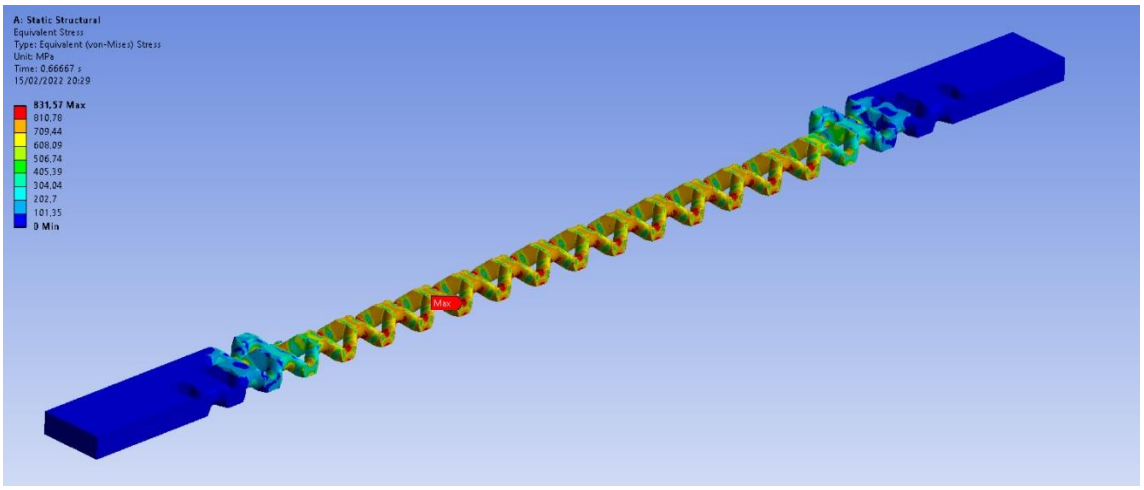

Figure 68: Failure localization for BCC specimen simulation (1/4 of the CAD model)

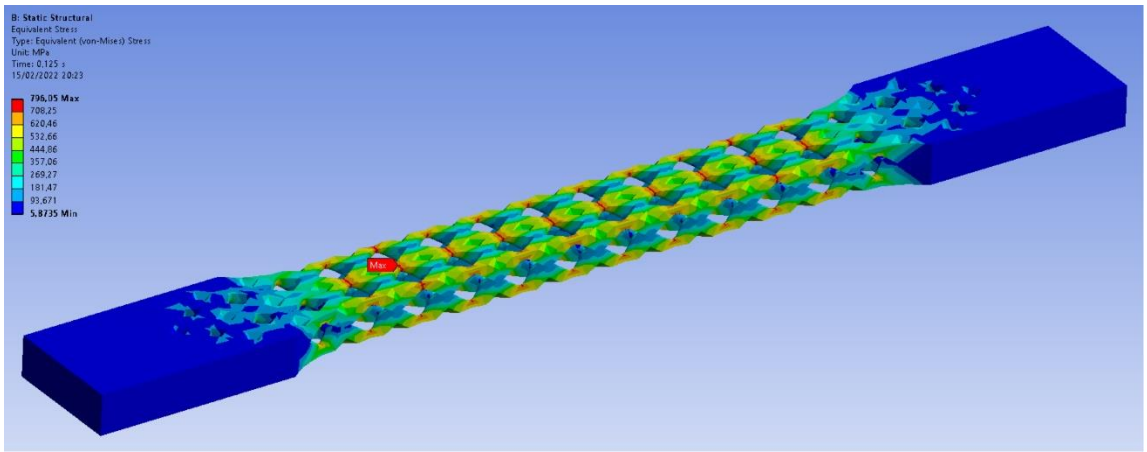

Figure 69: Failure localization for DROP specimen simulation

Figure 69 shows the simulation stress results for the DROP specimen. As it is possible to see the figure clearly indicates the most probable failure points, where the thinner struts have less than 1 mm of width. The maximum stresses is reached exactly in the fracture initial point obtained experimentally. Even the BCC specimen failure localization showed in Fig. 68 agrees with the experimental one. Furthermore, it is possible to extrapolate the displacement at break values for the two lattice simulations and compare them with the data obtained from the tensile tests (see Table 5). These results are obtained with an error of less than 5%, therefore they are very reliable.

5. Conclusion and future developments

In the present work the design, the production, and the testing of EBM and SLM suitable lattice specimens for the tensile characterization have been performed. The review of the literature highlights how well the previous studies have been conducted only in the compression conditions, while there is a deep lack of knowledge regarding the tensile properties. The present study focused on this specific characterization, overcoming the lattice design limits, and managing to follow an ISO standard. After the analysis of the results, several important observations can be made:

- In general, the gradual variation of the struts diameter is optimal for solving the problem of the induced weakness on the zone with the density transition. It must be considered that the specimen geometry has been created manually on Solidworks. A method to obtain a much more precise gradation could be to write a code interfacing with a programming language such as Python or C, interfacing with MATLAB or other software capable of extrapolating a valid geometry, i.e., an STL file
- In the case of the SLM specimens, a phenomenon of stress intensification was detected, which depends on the process itself and it cannot be overcome even by means of the stress relieving procedure. A possible solution could be to further decrease the space occupied by the completely solid part and on the other hand extending the transition zone
- The designed specimens are based on the BS EN ISO 6892 standard (E) almost entirely, with the exception of the thickness. The design created it might be replicated using other lattice geometry, so it is possible to assert that a standard definition for tensile characterization could be formulated and used in another research
- The effect of the different scanning technique, used during the printing process, it might lead to different mechanical properties

- According to the lattice geometry it is possible to obtain very diversified properties; for the EBM specimens, with high ultimate tensile stresses, little deformations are detected, while for the lower UTS values, close to 40 – 50 % of the bulk material, high deformations can be reached. This behaviour is very similar to the one produced by an heat treatment and it should be explored further
- The SLM manufactured specimens have been studied by varying the internal struts angles and the printing orientation; these different parameters can affect the tensile stress and the yield stress with a variation up to 25%, while the variability of the elongation at break is decidedly lower, with a maximum of 15%. This suggest that the last property mainly depends on the lattice geometry
- The specimens tested under compression show results that are in good agreement with the Ashby and Gibson model [1]
- All the specimens broke into the sections with the lower area value, which is the same used to derive the stress – strain curves, however it is not yet clear whether it is possible to refer to this area and obtain reliable UTS values. Further studies should be conducted on this problem, perhaps designing components with the same gradation of the specimens and evaluating their properties within a real application case
- Unfortunately, the obtained data are not sufficient to be able to hypothesize some type of predictive law in the tensile field like those already confirmed for the compression behaviour. In the future it would be interesting to create many more batches of specimens with different lattice geometries and different cell sizes
- A possible expansion of this work could foresee an analysis of the microstructures, the hardness and the surface roughness of the specimens produced. Eventually, these data could be parametrized for the creation of a more efficient simulation model, since the one based only on CAD files, presents significant discrepancies with respect to the experimental results, considering the force values. Instead, the displacement data obtained from the simulation present only less than 5% error in respect to the experimental values

References

[1] L. Gibson, M. F. Ashby, “Cellular Solids: Structure and Properties”, Cambridge University Press, 1999

[2] M. F. Ashby, A. G. Evans, H. N. G. Wadley, L. Gibson, J. W. Hutchinson, “Metal Foams: A Design Guide”, 2000

[3] M. F. Ashby, “The properties of foams and lattices”, Phil. Trans. R. Soc. A. 364, pp. 15–30, 2006

[4] Mahmoud, D.; Elbestawi, M.A. “Lattice Structures and Functionally Graded Materials Applications in Additive Manufacturing of Orthopedic Implants: A Review”, J. Manuf. Mater. Process. 2017, 1, 13

[5] C. Yan, et al., “Advanced lightweight 316L stainless steel cellular lattice structures fabricated via selective laser melting”, Mater. Des. 55 (2014), p. 533-541.

[6] X.Z. Zhang, et al., “Selective electron beam manufactured Ti-6Al-4V lattice structures for orthopedic implant applications: Current status and outstanding challenges”, Curr. Opinion Solid State Mater. Sci. 22 (3) (2018), p. 75-99.

[7] M. Yakout, M.A. Elbestawi, S.C. Veldhuis, “Density and mechanical properties in selective laser melting of Invar 36 and stainless steel 316L”, J. Mater. Process. Technol. 266 (2019), p. 397-420

[8] T. Maconachie, M. Leary, B. Lozanovski, X. Zhang, M. Qian, O. Faruque, M. Brandt, “SLM lattice structures: Properties, performance, applications and challenges”, Materials & Design, Volume 183, 2019

[9] Gokuldoss PK, Kolla S, Eckert J. Additive Manufacturing Processes: Selective Laser Melting, Electron Beam Melting and Binder Jetting-Selection Guidelines. Materials (Basel). 2017;10(6):672. Published 2017 Jun 19. doi:10.3390/ma10060672

[10] Vayre, B., F. Vignat, and F. Villeneuve 2012b. “Metallic additive manufacturing: state-of-the-art review and prospects”, Mechanics & Industry, 13(02):89–96

[11] Cooper, D. E., M. Stanford, K. A. Kibble, and G. J. Gibbons 2012. “Additive manufacturing for product improvement at red bull technology”, Materials & Design, 41:226–230

[12] M. Suard, 2015. “Characterization and optimization of lattice structures made by Electron Beam Melting”, PhD thesis, Univ. Grenoble Alpes

[13] M. Pisati, 2019, “Experimental characterization of the mechanical behaviour of lattice structures under monotonic load condition”, Master Degree Thesis, Politecnico di Torino

[14] Mullen L, Stamp RC, Brooks WK, Jones E, Sutcliffe CJ. Selective Laser Melting: a regular unit cell approach for the manufacture of porous, titanium, bone in-growth constructs, suitable for orthopedic applications. J Biomed Mater Res B Appl Biomater. 2009 May;89(2):325-334. doi: 10.1002/jbm.b.31219. PMID: 18837456

[15] Li F, Li J, Huang T, Kou H, Zhou L. Compression fatigue behavior and failure mechanism of porous titanium for biomedical applications. J Mech Behav Biomed Mater. 2017 Jan;65:814-823. doi: 10.1016/j.jmbbm.2016.09.035. Epub 2016 Sep 28. PMID: 27788474

[16] ISO 13314:2011 - Mechanical testing of metals — Ductility testing — Compression test for porous and cellular metals, https://www.iso.org/obp/ui/#iso:std:iso:13314:ed-1:v1:en

[17] Maskery I, Aboulkhair NT, Aremu AO et al (2016) “A mechanical property evaluation of graded density Al-Si10-Mg lattice structures manufactured by selective laser melting”, Mater Sci Eng A670:264–274

[18] Köhnen P, Haase C, Bültmann J, Ziegler S, Schleifenbaum JH, Bleck W (2018), “Mechanical properties and deformation behavior of additively manufactured lattice structures of stainless steel”, Mater

[19] Del Guercio, Giuseppe & Galati, Manuela & Saboori, Abdollah. (2021). Electron Beam Melting of Ti-6Al-4V Lattice Structures; Correlation between Post Heat Treatment and Mechanical Properties. 10.21203/rs.3.rs-248635/v1

[20] Cutolo A, Engelen B, Desmet W et al (2020) “Mechanical proper-ties of diamond lattice Ti – 6Al – 4V structures produced by laser powder bed fusion: on the effect of the load direction”, J Mech Behav Biomed Mater 104:103656. https://doi.org/10.1016/j.jmbbm.2020.103656

[21] Raghavendra S, Molinari A, Fontanari V, Luchin V, Zappini G, Benedetti M, Johansson F, Klarin J (2018) “Tensile and compres-sion properties of variously arranged porous Ti-6Al-4V additively manufactured structures via SLM”, Procedia Struct Integr 13:149 – 154. https://doi.org/10.1016/j.prostr.2018.12.025

[22] Y. Amani, S. Dancette, P. Delroisse, A. Simar, E. Maire, “Compression behavior of lattice structures produced by selective laser melting: X-ray tomography based experimental and finite element approaches”, Acta Mater., 159 (2018), pp. 395-407

[23] Leary M, Mazur M, Elambasseril J, McMillan M, Chirent T, Sun Y, Qian M, Easton M, Brandt M (2016) “Selective laser melting (SLM) of AlSi12Mg lattice structures”, Mater Des 98:344 – 357, https://doi.org/10.1016/j.matdes.2016.02.127

[24] Xiao Z, Yang Y, Xiao R, Bai Y, Song C, Wang D (2018) “Evaluation of topology-optimized lattice structures manufactured via selective laser melting”, Mater Des 143:27 – 3 https://doi.org/10.1016/j.matdes.2018.01.023

[25] Ibrahim Y, Li Z, Davies CM, Maharaj C, Dear JP, Hooper PA (2018) “Acoustic resonance testing of additive manufactured lattice structures”, Addit Manuf 24:566 – 576 https://doi.org/10.1016/j.addma.2018.10.034

[26] Zhong T, He K, Li H, Yang L (2019) "Mechanical properties of lightweight 316L stainless steel lattice structures fabricated by selective laser melting” Mater Des 181:108076. https://doi.org/10.1016/j.matdes.2019.108076

[27] Caravaggi P, Liverani E, Leardini A et al (2019), “CoCr porous scaffolds manufactured via selective laser melting in orthopedics: topographical, mechanical, and biological characterization”. J Biomed Mater Res Part B. https://doi.org/10.1002/jbm.b.34328

[28] Abele, Eberhard & Stoffregen, Hanns & Klimkeit, Klaus & Hoche, Holger & Oechsner, M.. (2014). Optimisation of Process Parameters for Lattice Structures. Rapid Prototyping Journal. 21. 117-127. 10.1108/RPJ-10-2012-0096

[29] Yan C, Hao L, Hussein A, Young P, Raymont D (2014) “Advanced lightweight 316L stainless steel cellular lattice structures fabricated via selective laser melting”, Mater Des 55:533–541

[30] Campanelli SL, Contuzzi N, Ludovico AD et al (2014) “Manufacturing and characterization of Ti6Al4V lattice components manufactured by selective laser melting”, Materials 7:4803–4822

[31] Van Hooreweder B, Lietaert K, Neirinck B et al (2017) “CoCr F75 scaffolds produced by additive manufacturing: influence of chemical etching on powder removal and mechanical performance”, JMech Behav Biomed Mater 68:216–223

[32] Zhao M, Zhang DZ, Liu F, Li Z, Ma Z, Ren Z (2020) “Mechanical and energy absorption characteristics of additively manufactured functionally graded sheet lattice structures with minimal surfaces”, Int J MechSci 167:105262

[33] Sven Drücker, Martina Schulze, Hendrik Ipsen, Laura Bandegani, Helge Hoch, Maximilian Kluge, Bodo Fiedler, “Experimental and numerical mechanical characterization of additively manufactured Ti6Al4V lattice structures considering progressive damage”, International Journal of Mechanical Sciences, Volume 189, 2021, 105986, ISSN 0020-7403, https://doi.org/10.1016/j.ijmecsci.2020.105986.

[34] Liverani, Erica & Lutey, Adrian & Fortunato, Alessandro & Ascari, Alessandro. (2017). Characterization of Lattice Structures for Additive Manufacturing of Lightweight Mechanical Components. V002T01A012. 10.1115/MSEC2017-2835

[35] Kessler, Julia & Balc, Nicolae & Gebhardt, Andreas & Abbas, Karim. (2017). Basic research on lattice structures focused on the reliance of the cross-sectional area and additional coatings. MATEC Web of Conferences. 94. 03008. 10.1051/matecconf/20179403008

[36] Hajnys, Jiri & Pagac, Marek & Zlamal, Tomas & Petru, Jana & Kousal, Lukáš. (2018). Stiffness of 316L stainless steel support structures proposed for the SLM process. MATEC Web of Conferences. 244. 01008. 10.1051/matecconf/201824401008

[37] Maskery, Aremu, Simonelli et al. (2014), The BCC unit cell for latticed SLM parts; mechanical properties as a function of cell size, 25th Solid Free Form Symposium, pp 688 – 701

[38] Alsalla, H. (2017). Enhancing Fracture Toughness of Ultrahigh Strength Aerospace Components made by Additive Manufacturing

[39] Brenne F, Niendorf T, Maier HJ (2013) Additively manufactured cellular structures: impact of microstructure and local strains on the monotonic and cyclic behavior under uniaxial and bending load. J Mater Process Technol 213:1558 – 1564

[40] Kelly CN, Evans NT, Irvin CW, Chapman SC, Gall K, Safranski DL (2019) The effect of surface topography and porosity on the tensile fatigue of 3D printed Ti-6Al-4V fabricated by selective laser melting. Mater Sci Eng C 98:726 – 736

[41] Alsalla, Hamza & Hao, Liang & Smith, Christopher. (2016). Fracture toughness and tensile strength of 316L stainless steel cellular lattice structures manufactured using the selective laser melting technique. Materials Science and Engineering: A. 669

[42] Barbas A, Bonnet A-S, Lipinski P, Pesci R, Dubois G (2012) Development and mechanical characterization of porous titanium bone substitutes. J Mech Behav Biomed Mater 9:34 – 44

[43] Awd, Mustafa & Stern, Felix & Kampmann, Alexander & Kotzem, Daniel & Tenkamp, Jochen & Walther, Frank. (2018). Microstructural Characterization of the Anisotropy and Cyclic Deformation Behavior of Selective Laser Melted AlSi10Mg Structures. Metals. 8. 825

[44] N. Riikonen, A. Salminen, Tensile strength properties of stainless steel 316L lattice structures manufactured by powder bed fusion, Bachelor's Degree, Lappeenranta University of Technology, 2018

[45] Hanzl P, Zetková I, Daňa M. Uniaxial Tensile Load of Lattice Structures Produced by Metal Additive Manufacturing. Manufacturing Technology. 2019;19(2):228-231. doi: 10.21062/ujep/274.2019/a/1213-2489/MT/19/2/228

[46] Maskery, I., Aremu, A., Simonelli, M. et al. Mechanical Properties of Ti-6Al-4V Selectively Laser Melted Parts with Body-Centred-Cubic Lattices of Varying cell size. Exp Mech 55, 1261–1272 (2015). https://doi.org/10.1007/s11340-015-0021-5

[47] Brodin, Håkan & Saarimäki, Jonas. (2013). Mechanical properties of lattice truss structures made of a selective laser melted superalloy. 13th International Conference on Fracture 2013, ICF 2013.

[48] Wang, Xinglong & Wang, Cheng & Zhou, Xin & Wang, Di & Zhang, Mingkang & Gao, Yun & Wang, Lei & Zhang, Peiyu. (2020). Evaluating Lattice Mechanical Properties for Lightweight Heat-Resistant Load-Bearing Structure Design. Materials. 13. 4786. 10.3390/ma13214786

[49] Soul, Hugo & Terriault, Patrick & Brailovski, V.. (2018). The Static and Fatigue Behavior of AlSiMg Alloy Plain, Notched, and Diamond Lattice Specimens Fabricated by Laser Powder Bed Fusion. Journal of Manufacturing and Materials Processing. 2. 25. 10.3390/jmmp2020025

[50] Drücker S., Inman S., Fiedler B., Simulation and Optimization of the Load Introduction Geometry of Additively Manufactured Lattice Structure Specimens, 18th European Conference on Composite Materials (ECCM 2018), Athens, Greece, 24-28th June 2018

[51] Standard BS EN ISO 6892 – 1 : 2019 (E)

[52] Viale V., Bondioli F., Saboori A., Optimization of Inconel 718 Downskin Parameters for the Production of Metallic Parts Via Laser Powder Bed Fusion

[53] http://www.3rsystems.cz/en/3d-print/3d-print-dental/eosint-m270-metal

[54] https://www.ge.com/additive/additive-manufacturing/machines/ebm-machines/arcam-ebm-a2x

[55] https://www.easydur.com/en/3mz-tensile/

[56] D. Gu, Y.C. Hagedorn, W. Meiners, G. Meng, R.J.S. Batista, K. Wissenbach, R. Poprawe, Densification behavior, microstructure evolution, and wear performance of selective laser melting processed commercially pure titanium, Acta Mater. 60 (2012) 3849–3860

[57] B. Vrancken, L. Thijs, J.-P. Kruth, J. Van Humbeeck, Heat treatment of Ti6Al4V produced by selective laser melting: microstructure and mechanical properties, J. Alloys Compd. 541 (2012) 177–185

[58] S. Leuders, M. Thone, A. Riemer, T. Niendorf, T. Tr € oster, H.A. Richard, H.J. Maier, On the mechanical behaviour of titanium alloy TiAl6V4 manufactured by selective laser melting: fatigue resistance and crack growth performance, Int. J. Fatigue 48 (2013) 300–307

[59] https://www.researchgate.net/figure/Ti6Al4V-powder-properties-source-Arcam-AB_tbl1_271848691

[60] https://fathommfg.com/wp-content/uploads/2020/11/EOS_Aluminium_AlSi10Mg_en.pdf

[61] Gray, G. & Maudlin, Paul & Hull, Lawrence & Zuo, Ken & Chen, Shuh-Rong. (2005). Predicting material strength, damage, and fracture: The synergy between experiment and modeling. Journal of Failure Analysis and Prevention. 5. 7-17. 10.1361/15477020523725

[62] Maskery, Ian & Aboulkhair, Nesma & Aremu, Adedeji & Tuck, Christopher & Ashcroft, Ian. (2017). Compressive failure modes and energy absorption in additively manufactured double gyroid lattices. Additive Manufacturing. 16. 10.1016/j.addma.2017.04.003

[63] Takezawa, Akihiro & Yonekura, Kazuo & Koizumi, Yuichiro & Zhang, Xiaopeng & Kitamura, Mitsuru. (2018). Isotropic Ti–6Al–4V Lattice via Topology Optimization and Electron-Beam Melting. Additive Manufacturing. 22. 10.1016/j.addma.2018.06.008

[64] Bruno, J. & Rochman, Arif & Cassar, Glenn. (2017). Effect of Build Orientation of Electron Beam Melting on Microstructure and Mechanical Properties of Ti-6Al-4V. Journal of Materials Engineering and Performance. 26. 10.1007/s11665-017-2502-4

[65] Pasang, Timotius & Tavlovich, Benny & Yannay, Omry & Jakson, Ben & Fry, Mike & Tao, Yuan & Turangi, Celine & Wang, Jia-Chang & Jiang, Cho-Pei & Sato, Yuji & Tsukamoto, Masahiro & Misiolek, Wojciech. (2021). Directionally – Dependent Mechanical Properties of Ti6Al4V Manufactured by Electron Beam Melting (EBM) and Selective Laser Melting (SLM). Materials. 14. 3603. 10.3390/ma14133603

[66] Radlof, Wiebke, Christopher Benz, Horst Heyer, and Manuela Sander. 2020. "Monotonic and Fatigue Behavior of EBM Manufactured Ti-6Al-4V Solid Samples: Experimental, Analytical and Numerical Investigations", *Materials* 13, no. 20: 4642. https://doi.org/10.3390/ma13204642

[67] Maconachie, Tobias & Leary, M. & Lozanovski, Bill & Zhang, Xeuzhe & Qian, Ma & Faruque, Omar & Brandt, Milan. (2019). SLM lattice structures: Properties, performance, applications and challenges. Materials & Design. 183. 108137. 10.1016/j.matdes.2019.108137

[68] S. Raghavendra, A. Molinari, V. Fontanari, V. Luchin, G. Zappini, M. Benedetti, F. Johansson, J. Klarin, “Tensile and compression properties of variously arranged porous Ti-6Al-4V additively manufactured structures via SLM”, Procedia Structural Integrity, Volume 13, 2018, Pages 149-154, ISSN 2452-3216, https://doi.org/10.1016/j.prostr.2018.12.025